CHARACTERIZATION OF MICROSTRIP WITH SUPERSTRATE USING HERTZIAN WAVE MATRICES

By

Boutheina Kzadri

A DISSERTATION

Submitted to
Michigan State University
in partial fulfillment of the requirements
for the degree of

DOCTOR OF PHILOSOPHY

Department of Electrical Engineering

1994

ABSTRACT

CHARACTERIZATION OF MICROSTRIP WITH SUPERSTRATE USING HERTZIAN WAVE MATRICES

By

Boutheina Kzadri

Dyadic Green's function for the EM field maintained by electric currents immersed in a planar layered environment are constructed through electric Hertz potentials using wave matrices to determine the spectral amplitudes in their Sommerfeld-integral representations. Such Green's functions are appropriate for the analysis of contemporary integrated electronic and optical circuits operating at micro/mm/optical wavelengths, where the circuit components are located adjacent to a layered surround environment. This systematic new formulation accommodates general volume currents and removes any uncertainty regarding completeness of the field representation, while naturally accommodating the source-point singularity.

A full-wave analysis of a microstrip transmission line with superstrate is developed based on an integral equation description of the microstrip circuit structure. In order to obtain a complete circuit model of the microstrip transmission line with superstrate, its dispersion characteristics, current distributions and characteristic impedance are investigated via the rigorous full-wave integral equation approach. It is found that the principal mode of the microstrip with superstrate remains always a bound mode since it never leaks. Moreover, the microstrip line with superstrate

behaves similarly to the conventional microstrip in the sense that the current distributions for the principal and higher-order modes behave in the same manner.

A full-wave analysis of the characteristic impedance for the conventional microstrip using both voltage-current and power-current definitions revealed that both methods give results very close to each other. It is also established that the characteristic impedance, for the conventional microstrip and the microstrip with a superstrate layer and a substrate having the largest permittivity, will always increase with frequency.

DEDICATED TO MY HUSBAND, ATEF

AND

TO MY SON TO COME, AHMED

ACKNOWLEDGEMENTS

I would like to express my sincere thanks and appreciation to professor Dennis Nyquist for his guidance, support, and inspiration throughout the course of this research. His valuable time, kind consideration, and understanding have been an incentive for the completion of this dissertation.

Sincere gratitude is extended to the other members of my guidance committee: professor Chen, professor Rothwell, and professor Lappan for their interest and criticism.

Last, but not least, I would like to express my special gratitude to my husband Atef for his patience, love, care, and encouragement during every step I made towards the completion of this research.

TABLE OF CONTENTS

LIST OF TABLES

LIST OF FIGURES

CHAPTER 1

INTRODUCTION

The microstrip is a particularly useful transmission line medium for microwave and millimeter-wave integrated circuit applications. This dissertation presents a rigorous analysis of a new microstrip structure, namely a microstrip with a superstrate layer. The microstrip device is printed on the substrate layer and resides in the supersrtrate region as shown in Fig. 1.1. To our knowledge, this structure has not been analyzed extensively in the literature. In order to obtain a circuit model of the microstrip transmission line with superstrate layer, its propagation characteristics and characteristic impedance will be evaluated. The analysis of characteristic impedance for this particular structure is believed to be new and has not been discussed in the literature.

The rigorous analysis of printed circuit elements such as microstrips requires the use of the dyadic Green's function associated with the layered background. Therefore, the dyadic Green's functions associated with a multi-layered environment are constructed through the electric Hertz potential in a systematic manner using wave transmission matrices. Determining the Hertz potential in any region of a planar layered environment, maintained by general volume currents residing in any other layer, will be rendered to multiplication of wave matrices. This analysis will be specialized to obtain the dyadic Green's function associated with the four layered background environment of the microstrip with superstrate in Fig. 1.1. We note that

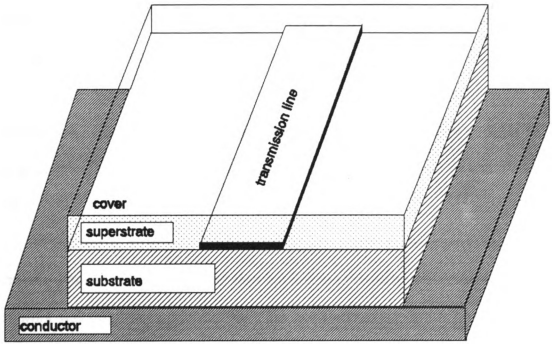

Figure 1.1: Microstrip line with supersrtate.

this otherwise extensive effort will be made relatively easy by using wave transmission matrices.

The text in this dissertation is divided into nine chapters. Chapter 2 presents a literature review of the main topics discussed in this thesis, namely, Dyadic Green's functions for planar layered environments, microstrip transmission lines and characteristic impedance. In Chapter 3, the dyadic Green's functions for the EM field maintained in any region of a planar, layered environment by general electric volume currents in any other region are constructed through electric Hertz potentials, to determine the spectral amplitudes in their Sommerfeld-integral representations. The construction of the dyadic Green's functions exploits wave transmission matrices for the tangential and normal components of potential maintained by respective currents as well as coupling matrices which couple tangential currents to normal potential components.

In Chapter 4, an electric field integral equation (EFIE) description for general microstrip circuits is developed, and then applied to microstrip transmission lines. This work was originally performed by Yuan and Nyquist [1], and is included here for completeness. However, the dyadic Green's functions associated with the layered background of a conventional microstrip environment are constructed using wave matrices as proposed in Chapter 3. Moreover, propagation modes on a single lossless microstrip transmission line are analyzed. Numerical solution to the homogeneous EFIE are implemented by the Galerkin's method of moments. Chebychev polynomials weighted by appropriate edge-condition factors are utilized as basis functions in the current expansion. The currents are obtained in a convenient quasi-closed form of rapidly convergent Chebychev polynomial series. Results of dispersion characteristics

and current distributions for the principal and higher-order modes are presented and compared to previously published data.

In order to obtain a complete equivalent transmission-line representation for the microstrip, not only its dispersion characteristics must be evaluated but also the characteristic impedance. Chapter 5 presents a full-wave analysis for the characteristic impedance of conventional microstrip transmission line. Both voltage-current and power-current definitions of characteristic impedance are utilized and compared to each other. Numerical results for both methods are presented and compared to previously published ones.

Chapter 6 presents a rigorous analysis of a microstrip structure with superstrate layer. Based on the integral-equation formulation, the microstrip line with a superstrate is studied by an approach similar to the one presented in Chapter 3 for the conventional microstrip. A rigorous full-wave solution to the integral equation is pursued again using the Galerkin's method of moments. The dispersion characteristics and current distributions of the guiding structure are analyzed for the principal and high-order modes. Extensive numerical results are presented.

Chapter 7 completes the circuit modeling of the microstrip transmission line with superstrate layer by analyzing its characteristic impedance. The voltage-current method will be used since it is less analytically involved and, as established in Chapter 5, gives results very close to those of the more accurate power-current method.

Chapter 8 exploits both an experimental method and the full-wave analysis for the dispersion characteristics and characteristic impedance of the microstrip circuit with superstrate to deduce the constitutive parameters of materials located in the superstrate layer of a four-layered microstrip background environment.

Finally, we conclude this dissertation in Chapter 9 with some general discussion on this research, along with some recommendations for future investigation on this topic.

CHAPTER 2

LITERATURE REVIEW

2.1 GREEN'S FUNCTION FOR PLANAR LAYERED MEDIA

The study of waves and fields in planarly layered media is quite a classic problem and has been studied by numerous researchers. Many books have been written on this subject. We have listed the works chronologically [2] - [9], but this list is by no means complete. The development of dyadic Green's functions for layered media is an important subject.

The components of Green's functions carry complete information regarding the general characteristics of wave propagation and coupling in a specific multilayer medium. Due to the importance of this subject, substantial research work has been published [10] - [15]. Different methods have been proposed to construct the dyadic Green's function for layered media.

The construction exposed in Kong [8] and Chew [9] is based upon either the normal electric or magnetic field components. Another approach is based on the normal components of electric and magnetic Hertz potentials as in Stoyer [10].

A method of derivation of spectral domain Green's functions for a multilayer geometry has been described by Pozar and Das [13] that uses equivalent transmission line sections to account for several layers. A similar approach is adopted by Michalski and Zheng [15].

2.2 MICROSTRIP CIRCUITS

Microstrip is a particularly useful transmission line medium for microwave and millimeter-wave integrated circuit applications. Circuits using microstrip can be implemented in many radars, some segments of point-to-point radio links, and certain portions of satellite communication systems [16]. Microstrip transmission lines are widely used in microwave integrated circuits (MIC's) for these systems. Most of the structures are also suitable for various high-speed digital applications. In addition, monolithic microwave circuits (MMC) have to be interconnected using microstrip lines and therefore such lines are important structures.

The microstrip falls into the category of the so called inhomogeneous planar transmission lines. In its basic form, it consists of a conducting strip printed on a dielectric substrate which is in turn backed by a ground plane as shown in Figure 2.1(a). This is called the open microstrip line. Some other types of planar transmission lines are shown in Figures 2.1(b)-(f) [17]. The microstrip with a cover plate and the shielded microstrip are shown in Figures 2.1(b) and (c), respectively. Figure 2.1(d) illustrates the inverted microstrip structure. The slot line and coplanar transmission lines shown in Figures 2.1(e) and (f), respectively, are also used in a number of applications.

Although the microstrip has a very simple geometric structure, the electromagnetic fields involved are actually complex. It is clear that the microstrip involves an abrupt dielectric interface between the substrate and the air above it. Therefore, the microstrip belongs to a family of inhomogeneous transmission lines. This implies that no simple TEM or waveguide-type TE and TM modes exist

independently. An accurate and thorough analysis requires quite elaborate mathematical treatments. The early work on planar transmission-line structures was based on quasi-TEM analysis [18]-[21]. Most of these papers were directed toward the evaluation of the static capacitance of the structure, from which the effective dielectric constant (ϵ_{eff}) which determines the propagation constant ($k_e = k_0\sqrt{\epsilon_{eff}}$), and the characteristic impedance are subsequently derived. A useful set of approximate relationships was derived by Wheeler [19]. Yamashita [20] presented a theoretical method to analyze microstrip lines based on a variational calculation of the line capacitance in the Fourier-transform domain.

Microstrip cannot support a pure TEM, or any other simple electromagnetic field mode. Therefore, the quasi-TEM analysis, which is approximate, is inadequate for estimating the dispersion properties of the line at higher frequencies. Hybrid mode analysis of the microstrip structure is required. There have been several approaches to the hybrid mode analysis of microstrip [1], [22]-[34]. Some of these are briefly discussed below.

Denlinger [22] presented an approximate hybrid mode solution that gives the frequency dependence of phase velocity and characteristic impedance of an open microstrip line deposited on either a dielectric or a demagnetized ferrite substrate. Getsinger [23] reported an interesting approach by proposing an alternative model for microstrip which is arranged for more straightforward analysis than the microstrip itself. It is important to note that the model is not physically realizable but it is much easier to analyze than the real microstrip because it is simply a parallel-plate line.

The most popular method used to analyze the microstrip transmission line is

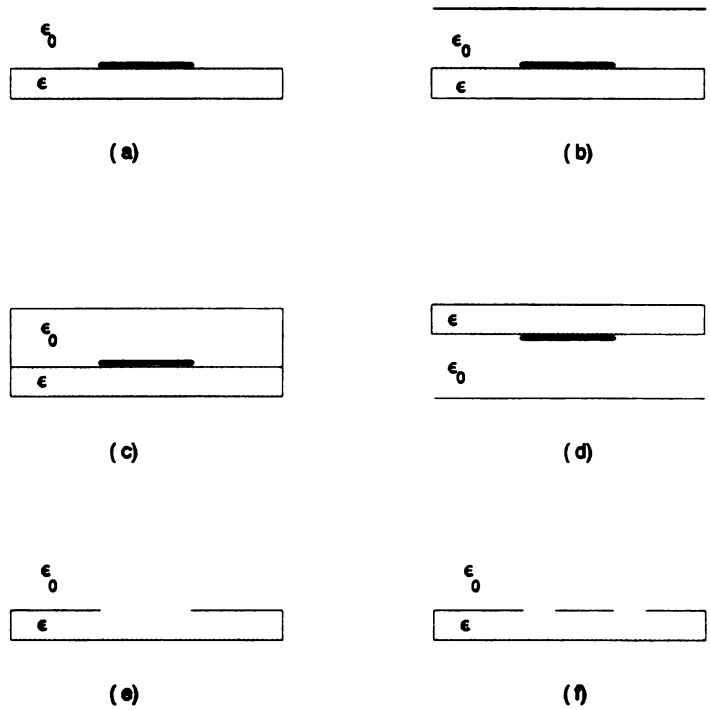

Figure 2.1: Some transmission line structures suited to microwave circuit integration.

the spectral-domain method. In this spectral or Fourier-transform method, the Green's function and boundary conditions are formulated in the spectral domain. The integral equation for the currents on the strip is also solved in the transform domain. This method is very attractive due mainly to the fact that the Green's function is relatively simplified in the spectral domain. This method appears to have originated in an early paper by Yamashita [20] and was refined by Itoh and Mittra [26]. A more recent effort by Jansen [28] gives a survey of the spectral-domain approach for microwave integrated circuits including the shielded-, covered-, and open-type microstrip. He also discussed the different aspects of this approach and considered its numerical efficiency.

The dispersion characteristics of microstrip lines have been investigated by a number of authors using a variety of methods. However, the numerical results shown in many papers were calculated using a small number of basis functions to save computation time, and the current distributions were not expressed accurately. This is the major cause for the significant disparity between computed results, as shown by Kuester and Chang [27]. The current distributions are fundamental quantities as sources for the electromagnetic fields of microstrip lines. Therefore, it is crucial to accurately represent them. In general, it is preferable to take the edge behavior of the current into account explicitly since this results in greater accuracy with fewer terms in the current expansion. Kobayashi [30] proposed closed-form expressions for the current distributions that satisfy the edge singularities. Using these expressions, the frequency-dependent characteristics for the effective relative permittivity of microstrip lines were calculated by spectral-domain analysis. In a later paper by Kobayashi [33], the spectral-domain analysis using Chebyshev polynomials as basis functions is used

to obtain the frequency dependence of current distributions and the effective relative permittivity of an open microstrip line up to $h/\lambda_0 = 1$ (normalized substrate thickness). In a paper by Fache and De Zutter [32], these characteristics were not shown in frequency ranges higher than $h/\lambda_0 = 0.2$.

2.3 CHARACTERISTIC IMPEDANCE

Accurate modeling of interconnections have gained increasing importance due to their presence in high-speed electronics and micro/millimeter-wave integrated circuits. Hence, it is necessary to obtain an equivalent transmission-line model which represents a circuit description of the microstrip structure so that it can be analyzed when connected to TEM structures such as loads and drivers. A large amount of attention was paid to evaluating the dispersion characteristics of microstrip, as seen in the previous section. In order to obtain a complete equivalent transmission line representation, not only the dispersion characteristics must be evaluated but also the characteristic impedance. There have been many different approaches to the dynamic problem of microstrip characteristic impedance and quite different functions of frequency have been predicted, extending even to opposing trends [35, 36].

The classical definition of characteristic impedance as the ratio of voltage to current at any point along a transmission line is meaningless for non-TEM structures. For a perfect TEM line, the electric field is conservative in the transverse plane, hence the voltage is uniquely defined as the negative path integral of electric field from one conductor to another along any path on the same transverse plane. However, for non-TEM structures such as microstrip lines, the path integral of electric field mentioned above is dependent on the path of integration. This matter

has been clearly discussed by Getsinger [37]. Voltage cannot be uniquely defined, and hence the above definition of characteristic impedance is ambiguous. As a result of the ambiguity in the definition of voltage, there is a wide disagreement among the microwave community about how the microstrip characteristic impedance should be defined. As an example, Bianco et al [35], defined impedances in terms of mean voltage V and center voltage V_c to yield a total of five definitions as follows:

$$
\begin{aligned}
Z_{0,1}(f) &= \frac{V}{I} \\
Z_{0,2}(f) &= \frac{V_c}{I} \\
Z_{0,3}(f) &= \frac{2P}{II*} \\
Z_{0,4}(f) &= \frac{V_c V_c}{2P} \\
Z_{0,5}(f) &= \frac{VV*}{2P}
\end{aligned}
\tag{1}
$$

where * denotes complex conjugation. The complex power P is evaluated using Poynting's theorem. These definitions lead to a variety of results. The general conclusion found by Bianco et al. is that $Z_{0,1}$ and $Z_{0,4}$ always rise with increasing frequency whereas the remaining impedances all fall with $Z_{0,3}$ exhibiting the smallest variation.

Getsinger [38] developed, using the model described in the previous section, an expression which has microstrip characteristic impedance varying inversely with the square root of ϵ_{eff}(f). In a more recent paper, Getsinger [37] defines the "apparent characteristic impedance" on the basis of accurate measurements of the reflection loss in the transfer of power between the source and the microstrip line. It was found that

the measured impedance showed a large frequency deviation. Hashimoto [39] presented rigorous, closed-form expressions for the characteristic impedance of microstrip given by the ratio of the electromagnetic power flowing along the strip to the square of the total longitudinal electric current. Pozar and Das [13] used a full-wave analysis to evaluate the characteristic impedance of several microstrip configurations by using the ratio of average voltage to the total longitudinal current. They showed that the characteristic impedance rises with frequency. As shown above, different authors choose different definitions of characteristic impedance (namely the voltage-current definition $Z = V/I$, the power-voltage definition $Z = |V|^2/2P$ and the power-current definition $Z = 2P/|I|^2$). All the three definitions of characteristic impedance lead to different results due to the ambiguity in the definition of current and voltage. However, it has been shown by Brews [40] that all three definitions of characteristic impedance become equivalent if we require the complex power P to satisfy the relation $P = I^* V/2$, which is a natural requirement upon any transmission line model. Moreover, he required that both the microstrip and the equivalent transmission line have the same propagation constant. The voltage or the current is chosen in such a way that one of them can be given a circuit interpretation but not both. In case of a single microstrip, if the current is selected as the independent variable, it can be chosen to be the total longitudinal current. If the voltage is selected as the independent variable, it can be chosen to be the strip center voltage. It is only in the low-frequency or quasi-static limit that a circuit meaning can be assigned to both the voltage and the current. Furthermore, Dezutter [41] showed that power current definition is the most appropriate model as a circuit description

since it has the most TEM-like character, as its value only starts to increase at higher frequencies as compared to the other models. Consequently, several authors adopted this method [42, 42, 44].

A recent paper by Cheng and Everard [45] presented a new method for the derivation of the characteristic impedance of an open microstrip line assuming the quasi-TEM mode of propagation. It is based on the spectral-domain approach with rectangular shaped basis functions. Finally, Slade and Webb [46] used a Finite Element Method to compute the characteristic impedance for several microstrip geometries.

CHAPTER 3

DYADIC GREEN'S FUNCTIONS FOR THE EM FIELD IN PLANAR LAYERED MEDIA BASED UPON WAVE MATRICES FOR ELECTRIC HERTZ POTENTIAL

3.1 INTRODUCTION

In this chapter, dyadic Green's functions for the EM field maintained in any region of a planar, layered environment by general electric volume currents in any other region are constructed through electric Hertz potentials, using wave matrices to determine the spectral amplitudes in their Sommerfeld-integral representations. The electromagnetics of planar layered media has received much research attention since the original treatment by Sommerfeld [2], with relatively recent efforts including those exposed in Brekhovskikh [3], Wait [4], Felsen and Marcuvitz [5], Stoyer [10], Kuester [11], Kong [8], Mosig [14], Michalski and Zheng [15] and Chew [9].

The construction exposed in this chapter is based strictly upon the electric Hertz potential, and exploits wave transmission matrices for the tangential and normal components of potential maintained by respective currents as well as coupling matrices which couple tangential currents to normal potential components. This method differs from prior ones where the fields were obtained from generating functions consisting of either the normal electric and magnetic field components as in Kong [8] and Chew [9] or the normal components of electric and magnetic Hertz potentials as in Das and Pozar [13] and Stoyer [10]. Another approach is taken by Michalski and Zheng [15] where they use a transmission line analogy to layered

media. By using wave transmission matrices here, the Green's functions are constructed systematically.

3.2 CONFIGURATION

Each of the planar layers is assumed to be linear, isotropic and locally homogeneous, with complex constitutive parameters $\epsilon_i = n_i^2 \epsilon_0$ and $\mu_i = m_i^2 \mu_0$, leading to wave number k_i and intrinsic impedance η_i in the i 'th layer. The wavenumber is $k_i = \omega\sqrt{\epsilon_i \mu_i} = n_i m_i k_0$ and $\eta_i = \sqrt{\mu_i/\epsilon_i} = m_i \eta_0 / n_i$ with k_0, η_0 the free space wavenumber and intrinsic impedance, respectively. Contrast among the various layers is described by $N_i = n_{i+1}/n_i$ and $M_i = m_{i+1}/m_i$. A coordinate system is chosen with the y-axis normal and the x,z axes tangential, respectively, to the planar interfaces at $y = y_i$, such that the i 'th layer resides within $y_i < y < y_{i-1}$ and y_i denotes the coordinate of the boundary between the i 'th and the $(i+1)$'th layer as indicated in Fig. 1. An electric volume current source is assumed to reside within the i 'th layer. As a result of multiple reflections at boundaries between the layers, two waves will exist in each of the regions, with the exception of regions 1 and N. One of these waves propagates in the positive y direction, and the other in the negative y direction. Wave amplitudes in region l above the source region are referenced to the $(l-1)$'th interface and denoted by $\tilde{a}_l^{\pm}$ while amplitudes in region l below the source region are referenced to the l 'th interface and denoted by $a_l^{\pm}$.

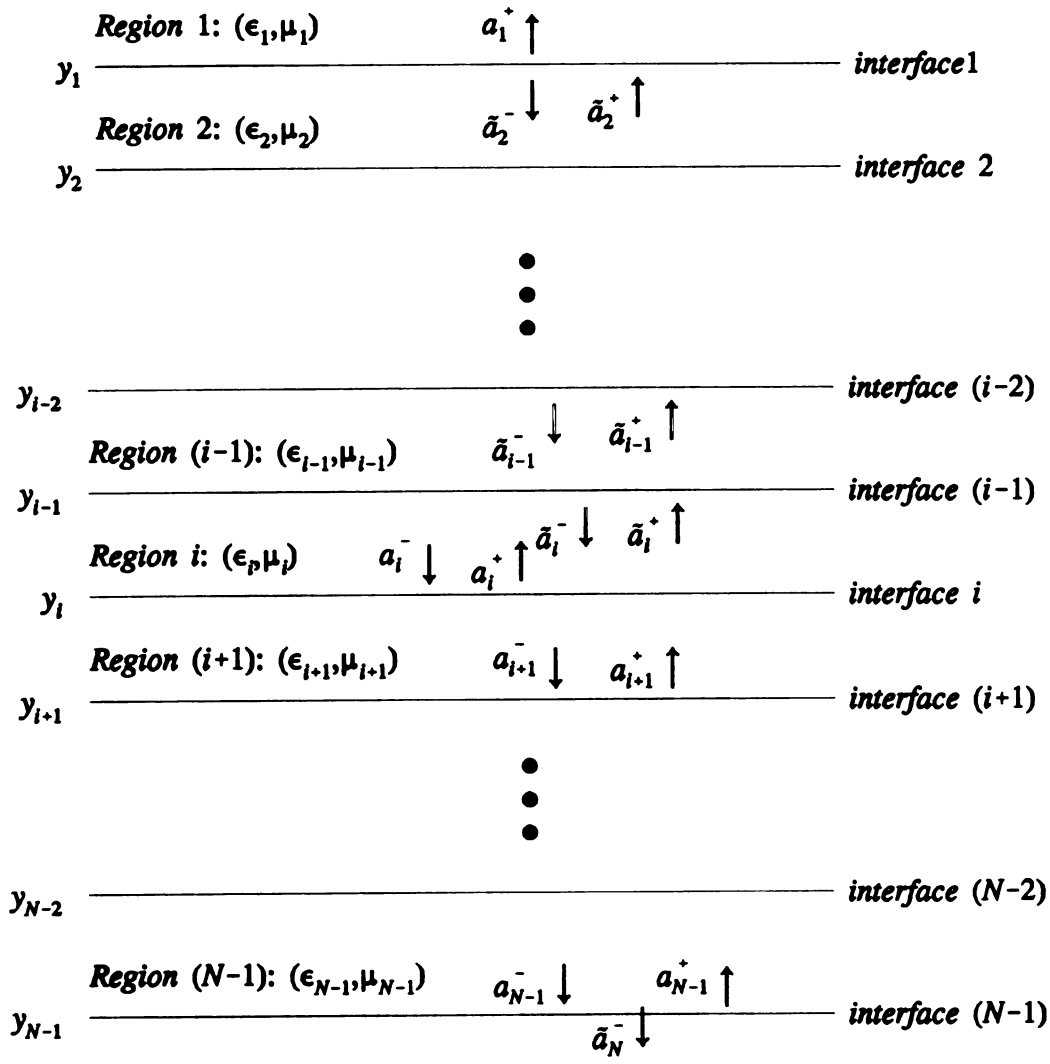

Figure 3.1: Configuration of Planar Layered Media

3.3 HERTZ POTENTIAL AND ELECTRIC FIELD

In this section, final results of the new formulation are exposed to provide an overview, with the details following in subsequent sections. The electric field in the l 'th layer can be expressed by generalization of the technique used by Bagby and Nyquist [47], as $\vec{E}_l = (k_l^2 + \nabla\nabla\cdot)\,\vec{\Pi}_{ll}$ where the Hertz potential in the l 'th layer maintained by currents in the i 'th layer is

$$\vec{\Pi}_{li}(\vec{r}) = \frac{-j\eta_i}{k_i}\int_V \ddot{G}_{li}(\vec{r}|\vec{r}')\cdot\vec{J}(\vec{r}')dv' \tag{1}$$

with $\ddot{G}_{ii} = \ddot{I}\delta_{ii}G_i^p + \ddot{G}_{ii}^s$. The first term leads to the principal wave excited in an unbounded i 'th layer, and has the sommerfeld-integral representation

$$G_i^p(\vec{r}|\vec{r}') = \iint_{-\infty}^{\infty} \frac{e^{j\vec{\lambda}\cdot(\vec{r}-\vec{r}')}\, e^{-p_i|y-y'|}}{2(2\pi)^2 p_i}\, d^2\lambda \tag{2}$$

where $p_i = \sqrt{\lambda^2 - k_i^2}$ and $\vec{\lambda} = \hat{x}\xi + \hat{z}\zeta$ is the 2-D spatial frequency transform variable, with $\lambda^2 = \xi^2 + \zeta^2$ and $d^2\lambda = d\xi d\zeta$. The branch cut for the square-root in p_i must be chosen to implement $Re\{p_i\} > 0$. This principal Green's dyad has been shown by Viola and Nyquist [48] to accommodate the electric field source-point singularity, and permits identification of Yaghjian's depolarizing dyad [49]. The scattered dyad has the form

$$\ddot{G}_{ii}^s(\vec{r}|\vec{r}') = (\hat{x}\hat{x} + \hat{z}\hat{z})G_{iic}^s + \hat{y}\left[\left(\hat{x}\frac{\partial}{\partial x} + \hat{z}\frac{\partial}{\partial z}\right)G_{iic}^s + G_{iin}^s\hat{y}\right] \tag{3}$$

with scalar component representations

$$\begin{Bmatrix} G^s_{lit}(\vec{r}|\vec{r}') \\ G^s_{lin}(\vec{r}|\vec{r}') \\ G^s_{lic}(\vec{r}|\vec{r}') \end{Bmatrix} = \iint_{-\infty}^{\infty} \begin{Bmatrix} S^t_{li}(y|y',\lambda) \\ S^n_{li}(y|y',\lambda) \\ S^c_{li}(y|y',\lambda) \end{Bmatrix} \frac{e^{j\vec{\lambda}\cdot(\vec{r}-\vec{r}')}}{2(2\pi)^2 p_i} d^2\lambda \ . \tag{4}$$

Clearly G^s_{lit} yields tangential potential components due to tangential currents, G^s_{lin} yields the normal potential due to normal current and G^s_{lic} couples tangential currents to normal potential. Scattering coefficients S^q_{li} are determined through the wave transmission and coupling matrices, and assume the generic forms

$$S^q_{li} = \sum_{k=1}^{4} B^q_{lik}(\lambda) e^{-\phi^k_{li}(y|y';\lambda)} \ldots \text{ for } q = t,n,c \ . \tag{5}$$

Expressions for the B^q_{lin} are obtained using wave matrices as described below, and the ϕ^k_{li} are simple expressions, e.g., $\phi^2_{li} = p_l(y-y_l) + p_i(y_{i-1}-y'+t_i)$ which take special forms when $l=i$ and where t_i represents the thickness of the i 'th layer.

If the differential operator is passed, with due regard (using Leibnitz's rule) for the source-point singularity (when $l=i$) of $\ddot{G}$, through the superposition integral in (1), then that field is obtained as

$$\vec{E}_l(\vec{r}) = \frac{-j\eta_l}{k_l} \int_V \ddot{G}^e_{li}(\vec{r}|\vec{r}') \cdot \vec{J}(\vec{r}') dv' \ . \tag{6}$$

The electric Green's function is identified, by the method described by Viola and Nyquist [48], as $\ddot{G}^e_{li}(\vec{r}|\vec{r}') = PV(k_l^2 + \nabla\nabla\cdot)\ddot{G}_{li}(\vec{r}|\vec{r}') + \ddot{L}\delta_{li}\delta(\vec{r}-\vec{r}')$. Notation PV

indicates that $\ddot{G}_{ii}^{e}$ should be integrated in a principle-value sense by excluding an innate "slice" principal volume at $y=y'$ to accommodate the source-point singularity of the principal-wave contribution at that point, and $\ddot{L} = -\hat{y}\hat{y}$ is an associated depolarizing dyad.

3.4 WAVE MATRICES FOR SPECTRAL HERTZ POTENTIAL

Uniformity of the planar, layered media parallel to the x-z plane prompts Fourrier transformation on those variables, leading to the transform pair

$$\left.\begin{aligned} \tilde{\Pi}_{\alpha}(\vec{\lambda},y) &= \int\int_{-\infty}^{\infty} \Pi_{\alpha}(\vec{r})\, e^{-j\vec{\lambda}\cdot\vec{r}}\, dx\, dz \\ \Pi_{\alpha}(\vec{r}) &= \frac{1}{(2\pi)^2}\int\int_{-\infty}^{\infty} \tilde{\Pi}_{\alpha}(\vec{\lambda},y)\, e^{j\vec{\lambda}\cdot\vec{r}}\, d^2\lambda \end{aligned}\right\} \quad \ldots \text{for } \alpha = x,y,z \ . \tag{7}$$

The spectral-domain Hertz potential components in the l 'th layer satisfy the transform-domain Helmoltz equation as follows

$$\left(\frac{d^2}{dy^2} - p_l^2\right)\begin{Bmatrix} \tilde{\Pi}_{l,\alpha}^{p}(\vec{\lambda},y) \\ \tilde{\Pi}_{l,\alpha}^{e}(\vec{\lambda},y) \end{Bmatrix} = \begin{Bmatrix} \dfrac{-\tilde{J}_{\alpha}(\vec{\lambda},y)}{j\omega\epsilon_l} \\ 0 \end{Bmatrix} \quad \ldots \text{for } \alpha = x,y,z \ . \tag{8}$$

We must distinguish a region l residing above the source region i, where the incident waves are travelling upward, from a region l below the source region, where downward travelling incident waves exist. Hence, all quantities associated with a downward pointing arrow are for a region l below the source region i, while those associated with an upward pointing arrow are for a region l above region i. For a

region $l \neq i$ underneath the source region, $\tilde{J}_\alpha = 0$ and appropriate homogeneous solutions to (8) are

$$\tilde{\Pi}_{l,\alpha}(\vec{\lambda},y) = a^{-}_{l,\alpha}(\lambda)\, e^{p_l(y-y_l)} + a^{+}_{l,\alpha}(\lambda)\, e^{-p_l(y-y_l)} \tag{9}$$

where the wave amplitudes are referenced to the l'th interface. For the case of upward travelling incident waves the source-free Hertz potentials are

$$\tilde{\Pi}_{l,\alpha}(\vec{\lambda},y) = \tilde{a}^{-}_{l,\alpha}(\lambda) e^{p_l(y-y_{l-1})} + \tilde{a}^{+}_{l,\alpha}(\lambda) e^{-p_l(y-y_{l-1})} . \tag{10}$$

where the wave amplitudes are referenced to the $(l-1)$'th interface. In the $l = i$ source region, the total potential is expressed as the sum of a principal wave maintained by $\tilde{J}_\alpha$ in an unbounded environment and a homogeneous solution representing waves scattered from the planar interfaces at y_i and y_{i-1} as follows

$$\tilde{\Pi}_{i,\alpha}(\vec{\lambda},y) = \tilde{\Pi}^{p}_{i,\alpha}(\vec{\lambda},y) + \tilde{\Pi}^{s}_{i,\alpha}(\vec{\lambda},y) . \tag{11}$$

The principal wave is given by

$$\tilde{\Pi}^{p}_{i,\alpha}(\vec{\lambda},y) = \int_{y_{i-1}}^{y_i} \frac{\tilde{J}_\alpha(\vec{\lambda},y')}{j\omega\epsilon_i} \frac{e^{-p_i|y-y'|}}{2p_i}\, dy' \tag{12}$$

which is a forced solution to eq. (8) as developed by Bagby and Nyquist [47].

The Sommerfeld [2] boundary conditions for electric Hertz potential are generalized to accommodate arbitrarily polarized potentials at the interfaces between media having both electric and magnetic contrast. In the spectral domain, the boundary conditions at the l'th interface require [50]

$$\left.\begin{aligned} \tilde{\Pi}_{l,\alpha}(\vec{\lambda},y) &= N_l^2 M_l^2\ \tilde{\Pi}_{l+1,\alpha}(\vec{\lambda},y) \\ \frac{\partial\tilde{\Pi}_{l,\alpha}(\vec{\lambda},y)}{\partial y} &= N_l^2 \frac{\partial\tilde{\Pi}_{l+1,\alpha}(\vec{\lambda},y)}{\partial y} \end{aligned}\right\} \quad \cdots for\ \alpha = x,z \tag{13}$$

and

$$\tilde{\Pi}_{l,y}(\vec{\lambda},y) = N_l^2\tilde{\Pi}_{l+1,y}(\vec{\lambda},y)$$

$$\left(\frac{\partial\tilde{\Pi}_{l,y}(\vec{\lambda},y)}{\partial y} - \frac{\partial\tilde{\Pi}_{l+1,y}(\vec{\lambda},y)}{\partial y}\right) = -(N_l^2 M_l^2 - 1)\left(j\xi\tilde{\Pi}_{l+1,x}(\vec{\lambda},y) + j\zeta\tilde{\Pi}_{l+1,z}(\vec{\lambda},y)\right) \tag{14}$$

where the last condition couples normal potential components to tangential ones. Applying conditions (13) and (14) at any interface leads to relations among the scattered wave amplitudes which can be described by wave matrices as detailed in Appendix A.

For a region l below the source region, a downward recursion is derived. Hence, the tangential amplitudes are related by $[a_{l,\alpha}] = [A_l^t\downarrow][a_{l+1,\alpha}]$ for $\alpha = x,z$, where the 2 x 2 matrix $[A_l^t\downarrow]$ is the tangential wave transmission matrix which chains tangential wave amplitudes in region $(l+1)$ to those in region l. The first entry in the 2x1 matrix $[a_{l,\alpha}]$ is the incident wave amplitude at the l 'th interface while the second entry is the reflected wave. Hence the above notation is a shorthand for

$$\begin{bmatrix} a_{l,\alpha}^- \\ a_{l,\alpha}^+ \end{bmatrix} = \left[A_l^t\downarrow\right]\begin{bmatrix} a_{l+1,\alpha}^- \\ a_{l+1,\alpha}^+ \end{bmatrix} \quad \cdots for\ \alpha = x,z\ . \tag{15}$$

The boundary conditions couple normal and tangential potential components such that

$$\begin{bmatrix} a_{l,y}^- \\ a_{l,y}^+ \end{bmatrix} = \left[A_l^n\downarrow\right]\begin{bmatrix} a_{l+1,y}^- \\ a_{l+1,y}^+ \end{bmatrix} + \left[C_l\downarrow\right]\left(j\xi\begin{bmatrix} a_{l+1,x}^- \\ a_{l+1,x}^+ \end{bmatrix} + j\zeta\begin{bmatrix} a_{l+1,z}^- \\ a_{l+1,z}^+ \end{bmatrix}\right). \tag{16}$$

For a region l residing above the source region, an upward recursion is derived. Hence, the wave amplitudes in region l are related to those in region $(l-1)$ as follows

$$\begin{bmatrix} \tilde{a}^{+}_{l,\alpha} \\ \tilde{a}^{-}_{l,\alpha} \end{bmatrix} = \left[A^{t}_{l-1}\uparrow\right] \begin{bmatrix} \tilde{a}^{+}_{l-1,\alpha} \\ \tilde{a}^{-}_{l-1,\alpha} \end{bmatrix} \quad \cdots for\ \alpha = x,z \tag{17}$$

and

$$\begin{bmatrix} \tilde{a}^{+}_{l,y} \\ \tilde{a}^{-}_{l,y} \end{bmatrix} = \left[A^{n}_{l-1}\uparrow\right] \begin{bmatrix} \tilde{a}^{+}_{l-1,y} \\ \tilde{a}^{-}_{l-1,y} \end{bmatrix} + \left[C_{l-1}\uparrow\right] \left(j\xi \begin{bmatrix} \tilde{a}^{+}_{l-1,x} \\ \tilde{a}^{-}_{l-1,x} \end{bmatrix} + j\zeta \begin{bmatrix} \tilde{a}^{+}_{l-1,z} \\ \tilde{a}^{-}_{l-1,z} \end{bmatrix} \right). \tag{18}$$

In eqs. (16) and (18), $[A^{n}_{l}\downarrow]$ and $[A^{n}_{l-1}\uparrow]$ are normal transmission matrices while $[C_{l}\downarrow]$ and $[C_{l-1}\uparrow]$ are the interfacial coupling matrices. $\left[A^{n}_{l}\downarrow\right]$ chains normal wave amplitudes in region $(l+1)$ to those in region l. $\left[C_{l}\downarrow\right]$ couples tangential wave amplitudes in region $(l+1)$ to normal wave amplitudes in region l. The wave matrices are identified as

$$
\begin{aligned}
\left[A_l^q{\downarrow} \right] &= \frac{1}{T_l^q{\downarrow}} \begin{bmatrix} \phi_{l+1} & R_l^q{\downarrow}\phi_{l+1}^{-1} \\ R_l^q{\downarrow}\phi_{l+1} & \phi_{l+1}^{-1} \end{bmatrix} \cdots for\, q = t,n \\
\left[A_{l-1}^q{\uparrow} \right] &= \frac{1}{T_{l-1}^q{\uparrow}} \begin{bmatrix} \phi_{l-1} & R_{l-1}^q{\uparrow}\phi_{l-1}^{-1} \\ R_{l-1}^q{\uparrow}\phi_{l-1} & \phi_{l-1}^{-1} \end{bmatrix} \cdots for\, q = t,n \\
\left[C_{l-1}{\uparrow} \right] &= \frac{1 - N_{l-1}^{-2} M_{l-1}^{-2}}{2p_l} \begin{bmatrix} -\phi_{l-1} & -\phi_{l-1}^{-1} \\ \phi_{l-1} & \phi_{l-1}^{-1} \end{bmatrix} \\
\left[C_l{\downarrow} \right] &= \frac{N_l^2 M_l^2 - 1}{2p_l} \begin{bmatrix} -\phi_{l+1} & -\phi_{l+1}^{-1} \\ \phi_{l+1} & \phi_{l+1}^{-1} \end{bmatrix}
\end{aligned}
\tag{19}
$$

where $\phi_{l+1} = \exp(p_{l+1} t_{l+1})$ and $\phi_{l-1} = \exp(p_{l-1} t_{l-1})$, with $t_{l+1} = |y_l - y_{l+1}|$ the thickness of the $(l+1)$'th layer. R_l^q and T_l^q are interfacial reflection and transmission coefficients defined in Appendix A.

3.5 DYADIC GREEN'S FUNCTION FOR LAYERED MEDIA

The wave matrix formalism allows the Green's function to be determined explicitly and in a systematic manner. First, the fields in the source layer i are evaluated, then fields in any source-free region l due to currents in region i are determined.

3.5.1. Potential in Source Layer ($l = i$)

Since only outgoing waves exist in regions 1 and N, the wave matrices can be applied to obtain relationships between the wave amplitudes in those regions and the source region i. For regions above the source region, an upward recursive scheme

is used; for layers below the source region, a downward recursive scheme is used.

A. Generalized tangential reflection coefficient

***Downward recursion*:** The tangential amplitudes at interface l are related to those in region N as follows

$$\begin{bmatrix} a_{l,\alpha}^{-} \\ a_{l,\alpha}^{+} \end{bmatrix} = \left[\prod_{k=l}^{N-1} \left[A_k^{t}\downarrow \right] \right] \begin{bmatrix} \tilde{a}_{N,\alpha}^{-} \\ 0 \end{bmatrix} \quad \cdots \textit{for } \alpha = x,z. \tag{20}$$

Hence, recursion relations for the overall reflection coefficients associated with downward travelling wave incident upon the l 'th interface are obtained as in Chew [8]

$$\mathfrak{R}_l^{t}\downarrow = \frac{R_l^{t}\downarrow + \mathfrak{R}_{l+1}^{t}\downarrow \, e^{-2p_{l+1}t_{l+1}}}{1 + R_l^{t}\downarrow \, \mathfrak{R}_{l+1}^{t}\downarrow \, e^{-2p_{l+1}t_{l+1}}} \tag{21}$$

where $a_{l,\alpha}^{+} = \mathfrak{R}_l^{t}\downarrow \, a_{l,\alpha}^{-}$ $(\alpha = x,z)$. Eq. (21) is obtained from eq. (20) by solving for the reflected wave in terms of the incident wave in region l. We first considered the case of two layers, then three, then four regions. In each case, the reflected wave is written in terms of the incident wave, thus the recursion relation (21) follows. The generalized reflection coefficient $\mathfrak{R}_l^{t}\downarrow$ associated with downward incident waves accounts for reflections from all interfaces below the region l.

***Upward recursion*:** The tangential wave amplitudes in region l at interface $(l-1)$ are related to those in region 1 as follows

$$\begin{bmatrix} \tilde{a}_{l,\alpha}^{+} \\ \tilde{a}_{l,\alpha}^{-} \end{bmatrix} = \left[\prod_{k=l-1}^{1} \left[A_k^t \uparrow \right] \right] \begin{bmatrix} a_{1,\alpha}^{+} \\ 0 \end{bmatrix} \quad \cdots \textit{for } \alpha = x,z \,. \tag{22}$$

Hence, we obtain the generalized reflection coefficient for upward travelling incident waves

$$\mathcal{R}_{l-1}^{t} \uparrow = \frac{R_{l-1}^{t} \uparrow + \mathcal{R}_{l-2}^{t} \uparrow \, e^{-2p_{l-1}t_{l-1}}}{1 + R_{l-1}^{t} \uparrow \, \mathcal{R}_{l-2}^{t} \uparrow \, e^{-2p_{l-1}t_{l-1}}} \tag{23}$$

where $\tilde{a}_{l,\alpha}^{-} = \mathcal{R}_{l-1}^{t} \uparrow \, \tilde{a}_{l,\alpha}^{+}$ $(\alpha = x,z)$. $\mathcal{R}_{l-1}^{t} \uparrow$ accounts for all reflections from all interfaces above region l.

B. Generalized normal reflection and coupling coefficients

Downward recursion: The normal wave amplitudes at interface l are related to those in region $(l+1)$ and are coupled to the incident tangential waves at interface $(l+1)$ as shown in eq. (16). We want to chain wave amplitudes in region N to those in region l. Note that the tangential wave amplitudes in region l are now available through eq. (20). Rewriting eq. (16), we have

$$\begin{bmatrix} a_{l,y}^{-} \\ a_{l,y}^{+} \end{bmatrix} = \left[A_l^n \downarrow \right] \begin{bmatrix} a_{l+1,y}^{-} \\ a_{l+1,y}^{+} \end{bmatrix} + \left[C_l \downarrow \right] \left(j\xi \begin{bmatrix} a_{l+1,x}^{-} \\ a_{l+1,x}^{+} \end{bmatrix} + j\zeta \begin{bmatrix} a_{l+1,z}^{-} \\ a_{l+1,z}^{+} \end{bmatrix} \right). \tag{24}$$

Now, we write the normal wave amplitudes in region $(l+1)$ in terms of the normal and tangential wave amplitudes in region $(l+2)$ leading to

$$\begin{bmatrix} a_{l+1,y}^{-} \\ a_{l+1,y}^{+} \end{bmatrix} = \left[A_{l+1}^n \downarrow \right] \begin{bmatrix} a_{l+2,y}^{-} \\ a_{l+2,y}^{+} \end{bmatrix} + \left[C_{l+1} \downarrow \right] \left(j\xi \begin{bmatrix} a_{l+2,x}^{-} \\ a_{l+2,x}^{+} \end{bmatrix} + j\zeta \begin{bmatrix} a_{l+2,z}^{-} \\ a_{l+2,z}^{+} \end{bmatrix} \right). \tag{25}$$

Using eq. (25) in eq. (24), we have

$$\begin{bmatrix} a_{l,y}^{-} \\ a_{l,y}^{+} \end{bmatrix} = \left[A_l^{n}\downarrow\right]\left[A_{l+1}^{n}\downarrow\right]\begin{bmatrix} a_{l+2,y}^{-} \\ a_{l+2,y}^{+} \end{bmatrix} + \left[C_l\downarrow\right]\left(j\xi \begin{bmatrix} a_{l+1,x}^{-} \\ a_{l+1,x}^{+} \end{bmatrix} + j\zeta \begin{bmatrix} a_{l+1,z}^{-} \\ a_{l+1,z}^{+} \end{bmatrix}\right) + \left[A_l^{n}\downarrow\right]\left[C_{l+1}\downarrow\right]\left(j\xi \begin{bmatrix} a_{l+2,x}^{-} \\ a_{l+2,x}^{+} \end{bmatrix} + j\zeta \begin{bmatrix} a_{l+2,z}^{-} \\ a_{l+2,z}^{+} \end{bmatrix}\right). \tag{26}$$

The tangential wave amplitudes in either region $(l+1)$ or $(l+2)$ can be written in terms of those in region l using eq. (20) as follows

$$\left.\begin{aligned} \begin{bmatrix} a_{l+1,\alpha}^{-} \\ a_{l+1,\alpha}^{+} \end{bmatrix} &= \left[A_l^{t}\downarrow\right]^{-1}\begin{bmatrix} a_{l,\alpha}^{-} \\ a_{l,\alpha}^{+} \end{bmatrix} \\ \begin{bmatrix} a_{l+2,\alpha}^{-} \\ a_{l+2,\alpha}^{+} \end{bmatrix} &= \left[A_{l+1}^{t}\downarrow\right]^{-1}\begin{bmatrix} a_{l+1,\alpha}^{-} \\ a_{l+1,\alpha}^{+} \end{bmatrix} \\ &= \left[A_{l+1}^{t}\downarrow\right]^{-1}\left[A_l^{t}\downarrow\right]^{-1}\begin{bmatrix} a_{l,\alpha}^{-} \\ a_{l,\alpha}^{+} \end{bmatrix} \end{aligned}\right\} \cdots \alpha = x,z\ . \tag{27}$$

Exploiting eq. (27), the normal wave amplitudes in region l as in eq. (26) are now given as

$$\begin{bmatrix} a_{l,y}^{-} \\ a_{l,y}^{+} \end{bmatrix} = \left[A_l^{n}\downarrow\right]\left[A_{l+1}^{n}\downarrow\right]\begin{bmatrix} a_{l+2,y}^{-} \\ a_{l+2,y}^{+} \end{bmatrix} + \left\{\left[C_l\downarrow\right]\left[A_l^{t}\downarrow\right]^{-1} + \left[A_l^{n}\downarrow\right]\left[C_{l+1}\downarrow\right]\left[A_{l+1}^{t}\downarrow\right]^{-1}\left[A_l^{t}\downarrow\right]^{-1}\right\} \times \left(j\xi \begin{bmatrix} a_{l,x}^{-} \\ a_{l,x}^{+} \end{bmatrix} + j\zeta \begin{bmatrix} a_{l,z}^{-} \\ a_{l,z}^{+} \end{bmatrix}\right). \tag{28}$$

Next, the normal wave amplitudes in region $(l+2)$ are written in terms of those in region $(l+3)$ and are coupled to tangential wave amplitudes in that region. This process is repeated until normal wave amplitudes in region N are chained to wave

amplitudes in region l. Hence, we obtain

$$\begin{bmatrix} a_{ly}^{-} \\ a_{ly}^{+} \end{bmatrix} = \left[\prod_{k=l}^{N-1} [A_k^n \downarrow] \right] \begin{bmatrix} \tilde{a}_{Ny}^{-} \\ 0 \end{bmatrix} + [C_l \downarrow] \left(j\xi \begin{bmatrix} a_{lx}^{-} \\ a_{lx}^{+} \end{bmatrix} + j\zeta \begin{bmatrix} a_{lz}^{-} \\ a_{lz}^{+} \end{bmatrix} \right) \tag{29}$$

where the overall coupling matrix $[\mathbf{C}_l \downarrow]$ from interface l to interface $(N-1)$ is given in terms of interfacial coupling and normal and tangential wave transmission matrices as follows

$$\begin{aligned} [\mathbf{C}_l \downarrow] = {} & [C_l \downarrow] [A_l^t \downarrow]^{-1} + [A_l^n \downarrow][C_{l+1} \downarrow][A_{l+1}^t \downarrow]^{-1}[A_l^t \downarrow]^{-1} \\ & + \cdots + \left(\prod_{k=l}^{N-2} [A_k^n \downarrow] \right) [C_{N-1} \downarrow] [A_{N-1}^t \downarrow]^{-1} \left(\prod_{k=N-2}^{l} [A_k^t \downarrow]^{-1} \right). \end{aligned} \tag{30}$$

Similarly, the normal wave amplitudes at interface $(l-1)$ are related to those in region 1 and are coupled to the upward incident tangential waves at the same interface leading to

$$\begin{bmatrix} \tilde{a}_{ly}^{+} \\ \tilde{a}_{ly}^{-} \end{bmatrix} = \left[\prod_{k=l-1}^{1} [A_k^n \uparrow] \right] \begin{bmatrix} a_{1y}^{+} \\ 0 \end{bmatrix} + [\mathbf{C}_{l-1} \uparrow] \left(j\xi \begin{bmatrix} \tilde{a}_{lx}^{+} \\ \tilde{a}_{lx}^{-} \end{bmatrix} + j\zeta \begin{bmatrix} \tilde{a}_{lz}^{+} \\ \tilde{a}_{lz}^{-} \end{bmatrix} \right) \tag{31}$$

where

$$\begin{aligned} [\mathbf{C}_{l-1} \uparrow] = {} & [C_{l-1} \uparrow] [A_{l-1}^t \uparrow]^{-1} + [A_{l-1}^n \uparrow][C_{l-2} \uparrow][A_{l-2}^t \uparrow]^{-1}[A_{l-1}^t \uparrow]^{-1} \\ & + \cdots + \left(\prod_{k=l-1}^{2} [A_k^n \uparrow] \right) [C_1 \uparrow] [A_1^t \uparrow]^{-1} \left(\prod_{k=2}^{l-1} [A_k^t \uparrow]^{-1} \right). \end{aligned} \tag{32}$$

Application of the above wave matrices leads to the overall normal reflection $(\mathfrak{R}_{l-1}^n \uparrow, \mathfrak{R}_l^n \downarrow)$ and coupling $(\mathbf{C}_{l-1} \uparrow, \mathbf{C}_l \downarrow)$ coefficients at the $(l-1)$'th and the l'th interface. For a region l below the source region, we use eq. (29) to solve for the reflected normal wave amplitude in region l in terms of the incident waves in the same

region and writing the tangential reflected waves as $a_{l,\alpha}^{+} = \mathfrak{R}_l^{t}\downarrow a_{l,\alpha}^{-}$ ($\alpha = x,z$) leads to

$$a_{l,y}^{+} = \mathfrak{R}_l^{n}\downarrow a_{l,y}^{-} + \mathbf{C}_l\downarrow\left(j\xi a_{l,x}^{-} + j\zeta a_{l,z}^{-}\right) . \tag{33}$$

Similarly, for a region l above the source region, we have

$$\tilde{a}_{l,y}^{-} = \mathfrak{R}_{l-1}^{n}\uparrow \tilde{a}_{l,y}^{+} + \mathbf{C}_{l-1}\uparrow\left(j\xi \tilde{a}_{l,x}^{+} + j\zeta \tilde{a}_{l,z}^{+}\right) \tag{34}$$

where $\mathfrak{R}_l^{n}\downarrow$ is the overall normal reflection coefficient for downward travelling incident waves at interface l. The latter coefficient is given by a recursion relation identical to the one for $\mathfrak{R}_l^{t}\downarrow$ with the superscript t replaced by n in that expression. The overall coupling coefficients at each interface are

$$\begin{aligned} \mathbf{C}_l\downarrow &= -\mathfrak{R}_l^{n}\downarrow (C_{11,l}\downarrow + \mathfrak{R}_l^{t}\downarrow C_{12,l}\downarrow) + (C_{21,l}\downarrow + \mathfrak{R}_l^{t}\downarrow C_{22,l}\downarrow) \\ \mathbf{C}_{l-1}\uparrow &= -\mathfrak{R}_{l-1}^{n}\uparrow (C_{11,l-1}\uparrow + \mathfrak{R}_{l-1}^{t}\uparrow C_{12,l-1}\uparrow) + (C_{21,l-1}\uparrow + \mathfrak{R}_{l-1}^{t}\uparrow C_{22,l-1}\uparrow) \end{aligned} \tag{35}$$

and $C_{11,l}\downarrow$, for example is the first entry of the coupling matrix $[\mathbf{C}_l\downarrow]$ given by eq. (30).

C. Potential in the source region

Referring to Fig. 1.1, the wave amplitudes in the source region are referenced to both i and $(i-1)$ interfaces. Hence, the scattered wave amplitudes at these interfaces are given in terms of the incident wave amplitudes as follows

$$\left.\begin{aligned} a_{i,\alpha}^{+} &= \mathfrak{R}_i^{t}\downarrow a_{i,\alpha}^{-} \\ \tilde{a}_{i,\alpha}^{-} &= \mathfrak{R}_{i-1}^{t}\uparrow \tilde{a}_{i,\alpha}^{+} \end{aligned}\right\} \quad \cdots \textit{for } \alpha = x,z \tag{36}$$

and

$$
\begin{aligned}
a_{i,y}^{+} &= \mathcal{R}_i^n \downarrow a_{i,y}^{-} + \mathbf{C}_i \downarrow \left(j\xi a_{i,x}^{-} + j\zeta a_{i,z}^{-} \right) \\
\tilde{a}_{i,y}^{-} &= \mathcal{R}_{i-1}^n \uparrow \tilde{a}_{i,y}^{+} + \mathbf{C}_{i-1} \uparrow \left(j\xi \tilde{a}_{i,x}^{+} + j\zeta \tilde{a}_{i,z}^{+} \right) .
\end{aligned}
\tag{37}
$$

The incident wave amplitudes $\tilde{a}_{i,\alpha}^{+}$ and $a_{i,\alpha}^{-}$ in the source region need to be quantified in order to find the total potential in the i 'th layer maintained by volume currents in the i 'th region; they can be obtained with the aid of Figs. 3.2 and 3.3. Direct reflection of any potential component is accommodated by Fig. 3.2, while Fig. 3.3 is applicable to coupling of tangential to normal waves.

Tangential and normal components

Referring to Fig. 3.2, the total upward travelling incident wave amplitude at interface $(i-1)$ consists of an upward travelling principal wave, $\tilde{a}_{i,\alpha}^{p+}$ maintained by source currents, augmented by the incident wave amplitude at interface i, reflected and then shifted to interface $(i-1)$ as follows

$$
\tilde{a}_{i,\alpha}^{+} = \tilde{a}_{i,\alpha}^{p+} + a_{i,\alpha}^{+} e^{-p t_i} = \tilde{a}_{i,\alpha}^{p+} + \mathcal{R}_i^q \downarrow a_{i,\alpha}^{-} e^{-p t_i}
\tag{38}
$$

with the understanding that $q=t$ when $\alpha=x,z$ and $q=n$ when $\alpha=y$. Similarly, the total downward travelling incident wave amplitude at interface i is given as

$$
a_{i,\alpha}^{-} = a_{i,\alpha}^{p-} + \tilde{a}_{i,\alpha}^{-} e^{-p t_i} = a_{i,\alpha}^{p-} + \mathcal{R}_{i-1}^q \uparrow \tilde{a}_{i,\alpha}^{+} e^{-p t_i} .
\tag{39}
$$

The $a_{i,\alpha}^{p+}$ and $\tilde{a}_{i,\alpha}^{p+}$ are the principal waves at interfaces i and $(i-1)$, respectively, maintained by source currents in region i. Replacing y by y_{i-1} in expression (12) and noting that $y>y'$ at interface $(i-1)$ leads to the expression for $\tilde{a}_{i,\alpha}^{p+}$ as

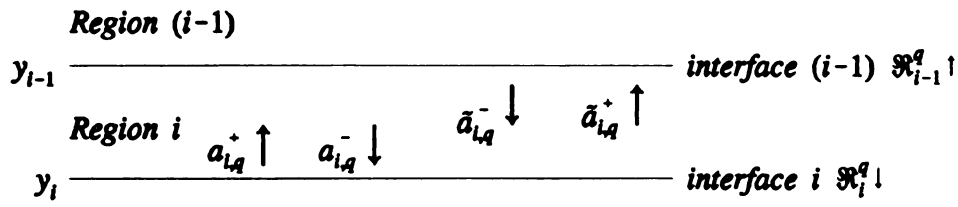

Figure 3.2 : Normal and tangential wave amplitudes.

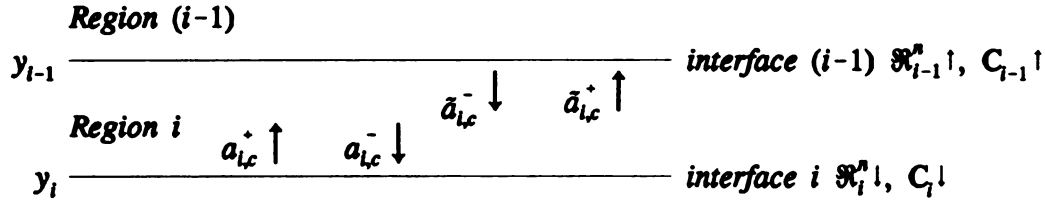

Figure 3.3: Coupled wave amplitudes.

$$\tilde{a}_{i,\alpha}^{p+} = \tilde{\Pi}_{ii,\alpha}^{p}(\vec{\lambda}, y_{i-1}) = e^{-p y_{i-1}} \int_{y_i}^{y_{i-1}} \frac{\tilde{J}_\alpha(\vec{\lambda}, y')}{j\omega\epsilon_i} \frac{e^{p y'}}{2p_i} \, dy' \,. \tag{40}$$

Similarly, to obtain the expressions for $a_{i,\alpha}^{p-}$, we replace y by y_i in expression (12) and note that $y<y'$ at interface i, leading to

$$a_{i,\alpha}^{p-} = \tilde{\Pi}_{ii,\alpha}^{p}(\vec{\lambda}, y_i) = e^{p y_i} \int_{y_i}^{y_{i-1}} \frac{\tilde{J}_\alpha(\vec{\lambda}, y')}{j\omega\epsilon_i} \frac{e^{-p y'}}{2p_i} \, dy' \,. \tag{41}$$

Solving for $a_{i,\alpha}^{-}$ and $\tilde{a}_{i,\alpha}^{+}$ from eqs. (38) and (39) leads to the unknown total incident-wave amplitudes in terms of the known principal-wave amplitudes as

$$\begin{aligned} a_{i,\alpha}^{-} &= \frac{a_{i,\alpha}^{p-} + \mathcal{R}_{i-1}^{q} \uparrow e^{-p t_i} \tilde{a}_{i,\alpha}^{p+}}{D^q} \\ \tilde{a}_{i,\alpha}^{+} &= \frac{\tilde{a}_{i,\alpha}^{p+} + \mathcal{R}_{i-1}^{q} \downarrow e^{-p t_i} a_{i,\alpha}^{p-}}{D^q} \end{aligned} \tag{42}$$

with $D^q = 1 - \mathcal{R}_i^q \downarrow \mathcal{R}_{i-1}^q \uparrow$. With the above construction, we finally obtain the scattered potential in the source layer i due to reflection only as

$$\begin{aligned} \tilde{\Pi}_{ii,\alpha}^{s}(\vec{\lambda}, y) &= a_{i,\alpha}^{+} e^{-p_i(y-y_i)} + \tilde{a}_{i,\alpha}^{-} e^{p_i(y-y_{i-1})} \\ &= \mathcal{R}_i^q \downarrow a_{i,\alpha}^{-} e^{-p_i(y-y_i)} + \mathcal{R}_{i-1}^q \uparrow \tilde{a}_{i,\alpha}^{+} e^{p_i(y-y_{i-1})} \,. \end{aligned} \tag{43}$$

Substituting the wave amplitudes $a_{i,\alpha}^{-}$ and $\tilde{a}_{i,\alpha}^{+}$ given by eq. (42) into the above Hertz potential expression and using eqs. (40) and (41) for the principal waves in region i yields

$$\tilde{\Pi}^{e}_{ii,\alpha}(\vec{\lambda},y) = \sum_{k=1}^{4} B^{q}_{iik}(\lambda) \int_{-\infty}^{\infty} \frac{\tilde{J}_{\alpha}(\vec{\lambda},y')}{j\omega\epsilon_i} \frac{e^{-\phi^{k}_{ii}}}{2p_i}\, dy' \tag{44}$$

where the B^{q}_{iik} are expressed in terms of the generalized reflection coefficients as follows

$$\left.\begin{aligned} B^{q}_{ii1} &= \frac{\Re^{q}_{i-1}\uparrow}{D^{q}} \\ B^{q}_{ii2} &= \frac{\Re^{q}_{i-1}\uparrow \Re^{q}_{i}\downarrow}{D^{q}} \\ B^{q}_{ii3} &= B^{q}_{ii2} \\ B^{q}_{ii4} &= \frac{\Re^{q}_{i}\downarrow}{D^{q}} \end{aligned}\right\} \cdots \text{for } q = t,n \tag{45}$$

and the phase shift factors ϕ^{k}_{ii} are

$$\begin{aligned} \phi^{1}_{ii} &= p_i(-y-y'+2y_{i-1}) \\ \phi^{2}_{ii} &= p_i(y-y'+2y_{i-1}-2y_i) \\ \phi^{3}_{ii} &= p_i(-y+y'+2y_{i-1}-2y_i) \\ \phi^{4}_{ii} &= p_i(y+y'-2y_i)\ . \end{aligned} \tag{46}$$

Coupling components

Referring to Fig. 3.3, the normal component of the incident wave amplitude due to coupling at interface $(i-1)$ consists of a normal reflection of the coupled component augmented by a coupling of tangential components of the incident wave amplitude at interface i with everything shifted to interface $(i-1)$. Mathematically, this is written as

$$\tilde{a}^{+}_{i,c} = \left(a^{-}_{i,c}\Re^{n}_{i}\downarrow + C_i\downarrow F^{t-}_{i}\right)e^{-p_i t_i}\ . \tag{47}$$

A similar argument leads to the coupled normal component at interface i as

$$a_{i,c}^{-} = \left(\tilde{a}_{i,c}^{+} \Re_{i-1}^{n} \uparrow + C_{i-1} \uparrow F_i^{t+}\right) e^{-p t_i} \tag{48}$$

where F_i^{t+} and F_i^{t-} are defined as

$$F_i^{t-} = j\xi a_{i,x}^{-} + j\zeta a_{i,z}^{-} \;\; ; \;\; F_i^{t+} = j\xi \tilde{a}_{i,x}^{+} + j\zeta \tilde{a}_{i,z}^{+} \, . \tag{49}$$

Solving eqs. (47) and (48) simultaneously, the coupled wave amplitudes are obtained in terms of total tangential components as follows

$$\begin{aligned} \tilde{a}_{i,c}^{+} &= \frac{F_i^{t+} C_{i-1} \uparrow \Re_i^{n} \downarrow e^{-2p t_i} + F_i^{t-} C_i \downarrow e^{-p t_i}}{D^{n}} \\ a_{i,c}^{-} &= \frac{F_i^{t-} C_i \downarrow \Re_{i-1}^{n} \uparrow e^{-2p t_i} + F_i^{t+} C_{i-1} \uparrow e^{-p t_i}}{D^{n}} \, . \end{aligned} \tag{50}$$

Since the tangential wave amplitudes are written in terms of the known principal wave amplitudes as in eq. (42), we substitute the expressions for $a_{i,x}^{-}$, $a_{i,z}^{-}$, $\tilde{a}_{i,z}^{+}$ and $\tilde{a}_{i,x}^{+}$ in eq. (50) to obtain

$$\begin{aligned} a_{i,c}^{-} &= B_{ii1}^{c} e^{-p t_i} (j\xi \tilde{a}_{i,x}^{p+} + j\zeta \tilde{a}_{i,z}^{p+}) + B_{ii3}^{c} e^{-2p t_i} (j\xi a_{i,x}^{p-} + j\zeta a_{i,z}^{p-}) \\ \tilde{a}_{i,c}^{-} &= B_{ii2}^{c} e^{-2p t_i} (j\xi \tilde{a}_{i,x}^{p+} + j\zeta \tilde{a}_{i,z}^{p+}) + B_{ii4}^{c} e^{-p t_i} (j\xi a_{i,x}^{p-} + j\zeta a_{i,z}^{p-}) \end{aligned} \tag{51}$$

where the B_{iik}^{c} ($k = 1,\cdots 4$) are identified in terms of the overall reflection and coupling coefficients as follows

$$
\begin{aligned}
B^c_{il1} &= \frac{1}{D^n D^t}\{C_i\downarrow \mathcal{R}^n_{i-1}\uparrow \mathcal{R}^t_{i-1}\uparrow e^{-2p_i t_i} + C_{i-1}\uparrow\} \\
B^c_{il2} &= \frac{1}{D^n D^t}\{C_{i-1}\uparrow \mathcal{R}^n_{i}\downarrow + \mathcal{R}^t_{i-1}\uparrow C_i\downarrow\} \\
B^c_{il3} &= \frac{1}{D^n D^t}\{C_i\downarrow \mathcal{R}^n_{i-1}\uparrow + \mathcal{R}^t_{i}\downarrow C_{i-1}\uparrow\} \\
B^c_{il4} &= \frac{1}{D^n D^t}\{C_{i-1}\uparrow \mathcal{R}^n_{i}\downarrow \mathcal{R}^t_{i}\downarrow e^{-2p_i t_i} + C_i\downarrow\} \ .
\end{aligned}
\tag{52}
$$

The normal scattered potential component must be augmented by the coupled component given by

$$
\tilde{\Pi}^s_{il,c}(\vec{\lambda},y) = \tilde{a}^+_{i,c} e^{-p_i(y-y_{i-1})} + a^-_{i,c} e^{p_i(y-y_i)} \ . \tag{53}
$$

Now, we substitute eqs. (51) into the above expression and use eqs. (40) and (41) for the principal wave amplitudes. Consequently, the expression for the coupled component of the Hertz potential becomes

$$
\tilde{\Pi}^s_{il,c}(\vec{\lambda},y) = \sum_{k=1}^{4} B^c_{ilk}(\lambda) \int_{-\infty}^{\infty} \frac{j\xi \tilde{J}_x(\vec{\lambda},y') + j\zeta \tilde{J}_z(\vec{\lambda},y')}{j\omega\epsilon_i} \frac{e^{-\phi^k_{il}(y|y',\lambda)}}{2p_i} dy' \tag{54}
$$

where $\phi^k_{il}(y|y',\vec{\lambda})$ are defined as in eq. (46).

We finally obtain the total transform domain Hertz potential in region i, which is the sum of scattered and principal waves at any point, where the principal wave is given by eq. (12). Hence, we have

$$
\tilde{\Pi}_{il,\alpha}(\vec{\lambda},y) = \tilde{\Pi}^p_{i,\alpha}(\vec{\lambda},y) + \tilde{\Pi}^s_{il,\alpha}(\vec{\lambda},y) + \delta_{\alpha y}\tilde{\Pi}^s_{il,c}(\vec{\lambda},y) \quad \cdots \alpha = x,y,z \tag{55}
$$

Next, inverse transforming the Hertz potential as in relation (7) and writting $\tilde{J}_\alpha(\vec{\lambda},y)$ in terms of space domain currents as

$$\tilde{J}_{\alpha}(\vec{\lambda},y) = \int\int_{-\infty}^{\infty} J_{\alpha}(\vec{r}') e^{-j\vec{\lambda}\cdot\vec{r}'} \, dS' \tag{56}$$

leads to expression (1), where the B_{lik}^{q} and ϕ_{li}^{k} in the Green's dyad components are identified as in relations (45), (46) and (52). Once the potential in the source region is known, the potential in the l 'th layer can be deduced from it by wave matrix multiplication as discussed in the next subsection.

3.5.2 Potential in Region l due to currents in region i

The potential in any source-free layer l can be constructed in terms of the now known wave amplitudes in the source region using wave matrices. We assume that the region l under consideration resides below the source region i such that a downward recursion is used. The Hertz potential in region l consists of only scattered waves with tangential, normal and coupling components as follows

$$\tilde{\Pi}_{li,\alpha}(\vec{\lambda},y) = \tilde{\Pi}^{s}_{li,\alpha}(\vec{\lambda},y) + \delta_{\alpha y}\tilde{\Pi}^{s}_{li,c}(\vec{\lambda},y) \quad \cdots \alpha = x,y,z \, . \tag{57}$$

We want to write the wave amplitudes $a^{+}_{l,\alpha}$ and $a^{-}_{l,\alpha}$ in region l in terms of the wave amplitudes in the source region i .

Tangential and normal components:

In this subsection, we assume that the normal components of potential are due to only normal component of primary current in region i . Referring to Fig. 3.1, the tangential and normal wave amplitudes at interface l are related to those at interface i as follows

$$\begin{bmatrix} a_{l,\alpha}^{-} \\ a_{l,\alpha}^{+} \end{bmatrix} = \left[D_l^{q\downarrow} \right] \begin{bmatrix} a_{l,\alpha}^{-} \\ a_{l,\alpha}^{+} \end{bmatrix} \quad \cdots \textit{for } \alpha = x,y,z \tag{58}$$

where the expression for $[D_l^{q\downarrow}]$ is defined as

$$\left.\begin{aligned} \left[D_l^{q\downarrow} \right] &= \left[\prod_{k=l-1}^{l} \left[A_k^{q\downarrow} \right]^{-1} \right] \\ &= \begin{bmatrix} d_{11,l}^{q\downarrow} & d_{12,l}^{q\downarrow} \\ d_{21,l}^{q\downarrow} & d_{22,l}^{q\downarrow} \end{bmatrix} \end{aligned}\right\} \cdots \textit{for } q = t,n \,. \tag{59}$$

We then obtain the unknown tangential wave amplitudes in region l in terms of the known wave amplitudes $a_{l,\alpha}^{\pm}$ as follows

$$\begin{aligned} a_{l,\alpha}^{-} &= d_{11,l}^{q\downarrow} a_{l,\alpha}^{-} + d_{12,l}^{q\downarrow} a_{l,\alpha}^{+} \\ a_{l,\alpha}^{+} &= d_{21,l}^{q\downarrow} a_{l,\alpha}^{-} + d_{22,l}^{q\downarrow} a_{l,\alpha}^{+} \,. \end{aligned} \tag{60}$$

The scattered potential in region l due to reflection only is consequently written in terms of the wave amplitudes in region i. By using eq. (60) in eq. (9) we obtain

$$\begin{aligned} \tilde{\Pi}_{ll,\alpha}^{s}(\vec{\lambda},y) = &(d_{11,l}^{q\downarrow} a_{l,\alpha}^{-} + d_{12,l}^{q\downarrow} a_{l,\alpha}^{+}) e^{p_l(y-y_l)} \\ &+ (d_{21,l}^{q\downarrow} a_{l,\alpha}^{-} + d_{22,l}^{q\downarrow} a_{l,\alpha}^{+}) e^{-p_l(y-y_l)} \end{aligned} \tag{61}$$

Substituting the wave amplitudes $a_{l,\alpha}^{\pm}$ given by eq. (42) into the above expression leads to

$$\begin{aligned} \tilde{\Pi}_{ll,\alpha}(\vec{\lambda}) = &B_{ll1}^{q} e^{p_l(y-y_l-t_l)} \tilde{a}_{l,\alpha}^{p+} + B_{ll2}^{q} e^{-p_l(y-y_l+t_l)} \tilde{a}_{l,\alpha}^{p+} \\ &+ B_{ll3}^{q} e^{p_l(y-y_l)} a_{l,\alpha}^{p-} + B_{ll4}^{q} e^{-p_l(y-y_l)} a_{l,\alpha}^{p-} \,. \end{aligned} \tag{62}$$

The coefficients B_{llk}^{q} ($k = 1,...,4$) are expressed in terms of generalized reflection

coefficients and the entries of the matrix $\left[D_l^q\downarrow\right]$ as follows

$$
\begin{aligned}
B_{li1}^q &= \frac{\Re_{i-1}^q\uparrow(d_{11,l}^q\downarrow + d_{12,l}^q\downarrow \Re_l^q\downarrow)}{D^q} \\
B_{li2}^q &= \frac{\Re_{i-1}^q\uparrow(d_{21,l}^q\downarrow + d_{22,l}^q\downarrow \Re_l^q\downarrow)}{D^q} \\
B_{li3}^q &= \frac{(d_{11,l}^q\downarrow + d_{12,l}^q\downarrow \Re_l^q\downarrow)}{D^q} \\
B_{li4}^q &= \frac{(d_{21,l}^q\downarrow + d_{22,l}^q\downarrow \Re_l^q\downarrow)}{D^q} \ .
\end{aligned}
\tag{63}
$$

Finally, we use eqs. (40) and (41) for the principal waves $a_{i,\alpha}^{p\pm}$ in eq. (62) to obtain

$$
\tilde{\Pi}_{li,\alpha}^q(\vec{\lambda},y) = \sum_{k=1}^{4} B_{lik}^q(\lambda) \int_{-\infty}^{\infty} \frac{\tilde{J}_\alpha(\vec{\lambda},y')}{j\omega\epsilon_i} \frac{e^{-\phi_{li}^k(y|y',\vec{\lambda})}}{2p_i}\, dy'
\tag{64}
$$

where the phase shift factors are

$$
\begin{aligned}
\phi_{li}^1 &= p_i(y_{i-1}-y') - p_l(y-y_l) + p_i t_i \\
\phi_{li}^2 &= p_i(y_{i-1}-y') + p_l(y-y_l) + p_i t_i \\
\phi_{li}^3 &= -p_i(y_i-y') - p_l(y-y_l) \\
\phi_{li}^4 &= -p_i(y_i-y') + p_l(y-y_l) \ .
\end{aligned}
\tag{65}
$$

Coupling component:

In this subsection, the normal components of Hertz potential in region l due to coupling to tangential currents in region i are obtained. The normal wave amplitudes at interface i are related to those in region l and are coupled to the tangential amplitudes at interface i as in eq. (29) with, region l replaced by region i and region N replaced by l, in that equation, leading to

$$\begin{bmatrix} a_{i,y}^{-} \\ a_{i,y}^{+} \end{bmatrix} = \left[\prod_{k=i}^{l-1} \left[A_k^{n} \downarrow \right] \right] \begin{bmatrix} a_{l,y}^{-} \\ a_{l,y}^{+} \end{bmatrix} + \left[C_i \downarrow \right] \left(j\xi \begin{bmatrix} a_{i,x}^{-} \\ a_{i,x}^{+} \end{bmatrix} + j\zeta \begin{bmatrix} a_{i,z}^{-} \\ a_{i,z}^{+} \end{bmatrix} \right) \tag{66}$$

where the overall coupling matrix at interface i is

$$\begin{aligned} \left[\mathbf{C}_i \downarrow \right] &= \left[C_i \downarrow \right] \left[A_i^{t} \downarrow \right]^{-1} + \left[A_i^{n} \downarrow \right] \left[C_{i+1} \downarrow \right] \left[A_{i+1}^{t} \downarrow \right]^{-1} \left[A_i^{t} \downarrow \right]^{-1} \\ &\quad + \cdots + \left(\prod_{k=i}^{l-2} \left[A_k^{n} \downarrow \right] \right) \left[C_{l-1} \downarrow \right] \left[A_{l-1}^{t} \downarrow \right]^{-1} \left(\prod_{k=l-2}^{i} \left[A_k^{t} \downarrow \right]^{-1} \right) . \end{aligned} \tag{67}$$

Isolating the normal wave amplitudes in region l leads to

$$\left[A_i^{n} \downarrow \right] \left[A_{i+1}^{n} \downarrow \right] \cdots \left[A_{l-1}^{n} \downarrow \right] \begin{bmatrix} a_{l,y}^{-} \\ a_{l,y}^{+} \end{bmatrix} = \begin{bmatrix} a_{i,y}^{-} \\ a_{i,y}^{+} \end{bmatrix} - \left[\mathbf{C}_i \downarrow \right] \left(j\xi \begin{bmatrix} a_{i,x}^{-} \\ a_{i,x}^{+} \end{bmatrix} + j\zeta \begin{bmatrix} a_{i,z}^{-} \\ a_{i,z}^{+} \end{bmatrix} \right) . \tag{68}$$

Multiplying the above matrix equation by the product of inverse transmission matrices $\left[A_{l-1}^{n} \downarrow \right]^{-1} \cdots \left[A_i^{n} \downarrow \right]^{-1}$ from the left provides

$$\begin{bmatrix} a_{l,y}^{-} \\ a_{l,y}^{+} \end{bmatrix} = \left[D_l^{n} \downarrow \right] \begin{bmatrix} a_{i,y}^{-} \\ a_{i,y}^{+} \end{bmatrix} + \left[F_{li} \downarrow \right] \left(j\xi \begin{bmatrix} a_{i,x}^{-} \\ a_{i,x}^{+} \end{bmatrix} + j\zeta \begin{bmatrix} a_{i,z}^{-} \\ a_{i,z}^{+} \end{bmatrix} \right) . \tag{69}$$

where $\left[D_l^{n} \downarrow \right]$ is defined as in eq. (59) and $\left[F_{li} \downarrow \right]$ is defined as

$$\begin{aligned} \left[F_{li} \downarrow \right] &= - \left[D_l^{n} \downarrow \right] \left[\mathbf{C}_i \downarrow \right] \\ &= \begin{bmatrix} f_{11,li} \downarrow & f_{12,li} \downarrow \\ f_{21,li} \downarrow & f_{22,li} \downarrow \end{bmatrix} . \end{aligned} \tag{70}$$

Hence, the normal wave amplitudes in region l are obtained from eq. (69) as

$$\begin{aligned} a_{l,y}^{-} &= d_{11,l}^{n} \downarrow a_{i,y}^{-} + d_{12,l}^{n} \downarrow a_{i,y}^{+} + (f_{11,li} \downarrow + f_{12,li} \downarrow \mathfrak{R}_i^{t} \downarrow)(j\xi a_{i,x}^{-} + j\zeta a_{i,z}^{-}) \\ a_{l,y}^{+} &= d_{21,l}^{n} \downarrow a_{i,y}^{-} + d_{22,l}^{n} \downarrow a_{i,y}^{+} + (f_{21,li} \downarrow + f_{22,li} \downarrow \mathfrak{R}_i^{t} \downarrow)(j\xi a_{i,x}^{-} + j\zeta a_{i,z}^{-}) . \end{aligned} \tag{71}$$

We want to find the normal wave amplitudes in region l due only to coupling with

tangential currents in the source region i. Using the fact that the normal wave components $a_{i,y}^{\pm}$ in the source region consist of normal components maintained by normal currents augmented by coupling components due to tangential currents. Hence the normal wave amplitudes in region l due to coupling with tangential currents in the source region i are

$$\begin{aligned} a_{l,c}^{-} &= d_{11,l}^{n} \downarrow a_{i,c}^{-} + d_{12,l}^{n} \downarrow a_{i,c}^{+} + (f_{11,ll} \downarrow + f_{12,ll} \downarrow \Re_i^{t} \downarrow)(j\xi a_{i,x}^{-} + j\zeta a_{i,z}^{-}) \\ a_{l,c}^{+} &= d_{21,l}^{n} \downarrow a_{i,c}^{-} + d_{22,l}^{n} \downarrow a_{i,c}^{+} + (f_{21,ll} \downarrow + f_{22,ll} \downarrow \Re_i^{t} \downarrow)(j\xi a_{i,x}^{-} + j\zeta a_{i,z}^{-}) \ . \end{aligned} \tag{72}$$

Referring to Fig. 3.3, the upward travelling coupled wave amplitude $a_{i,c}^{+}$ at interface i consists of the incident coupled wave amplitude $\tilde{a}_{i,c}^{+}$ at interface $(i-1)$ shifted to interface i as follows

$$a_{i,c}^{+} = \tilde{a}_{i,c}^{+} e^{p_i t_i} \tag{73}$$

The coupled wave amplitudes $a_{i,c}^{-}$ and $\tilde{a}_{i,c}^{+}$ were obtained previously in eq. (50) in terms of the total tangential wave amplitudes in the source region. Exploiting eqs. (50) and (73) in expression (72) leads to

$$\begin{aligned} a_{l,c}^{-} &= \left\{ d_{11,l}^{n} \downarrow \mathbf{C}_i \downarrow \Re_{i-1}^{n} \uparrow e^{-2p_i t_i} + \mathbf{C}_i \downarrow d_{12,l}^{n} \downarrow + \left(f_{11,ll} \downarrow + f_{12,ll} \downarrow \Re_i^{t} \downarrow \right) D^{n} \right\} \frac{F_i^{t-}}{D^{n}} \\ &\quad + \left\{ d_{11,l}^{n} \downarrow \mathbf{C}_{i-1} \uparrow e^{-p_i t_i} + d_{12,l}^{n} \downarrow \mathbf{C}_{i-1} \uparrow \Re_i^{n} \downarrow e^{-p_i t_i} \right\} \frac{F_i^{t+}}{D^{n}} \\ a_{l,c}^{+} &= \left\{ d_{21,l}^{n} \downarrow \mathbf{C}_i \downarrow \Re_{i-1}^{n} \uparrow e^{-2p_i t_i} + \mathbf{C}_i \downarrow d_{22,l}^{n} \downarrow + \left(f_{21,ll} \downarrow + f_{22,ll} \downarrow \Re_i^{t} \downarrow \right) D^{n} \right\} \frac{F_i^{t-}}{D^{n}} \\ &\quad + \left\{ d_{21,l}^{n} \downarrow \mathbf{C}_{i-1} \uparrow e^{-p_i t_i} + d_{22,l}^{n} \downarrow \mathbf{C}_{i-1} \uparrow \Re_i^{n} \downarrow e^{-p_i t_i} \right\} \frac{F_i^{t+}}{D^{n}} \end{aligned} \tag{74}$$

where $F_i^{t\pm}$ are defined in eq. (49).

Since the tangential wave amplitudes in region i are written in terms of the known principal wave amplitudes as in eq. (42), we substitute the expressions for $a_{i,x}^-, a_{i,z}^-, \tilde{a}_{i,z}^+$ and $\tilde{a}_{i,z}^+$ in eq. (74) to obtain

$$\begin{aligned} a_{i,c}^- &= B_{ii1}^c e^{-p f_i}\left(j\xi\,\tilde{a}_{i,x}^{p+} + j\zeta\,\tilde{a}_{i,z}^{p+}\right) + B_{ii3}^c\left(j\xi\,a_{i,x}^{p-} + j\zeta\,a_{i,z}^{p-}\right) \\ a_{i,c}^+ &= B_{ii2}^c e^{-p f_i}\left(j\xi\,\tilde{a}_{i,x}^{p+} + j\zeta\,\tilde{a}_{i,z}^{p+}\right) + B_{ii4}^c\left(j\xi\,a_{i,x}^{p-} + j\zeta\,a_{i,z}^{p-}\right) \end{aligned} \tag{75}$$

where the B_{ii}^c coefficients are defined below

$$B_{ii1}^c = \frac{\left[C_i\downarrow\left(d_{12,J}^n\downarrow + d_{11,J}^n\downarrow \Re_{i-1}^n\uparrow e^{-2p f_i}\right) + \left(f_{11,Ii}\downarrow + f_{12,Ii}\downarrow \Re_i^t\right) D^n\right] \Re_{i-1}^t\uparrow + C_{i-1}\uparrow\left(d_{11,J}^n\downarrow + d_{12,J}^n\downarrow \Re_i^n\downarrow\right)}{D^t D^n}$$

$$B_{ii2}^c = \frac{\left[C_i\downarrow\left(d_{22,J}^n\downarrow + d_{21,J}^n\downarrow \Re_{i-1}^n\uparrow e^{-2p f_i}\right) + \left(f_{21,Ii}\downarrow + f_{22,Ii}\downarrow \Re_i^t\right) D^n\right] \Re_{i-1}^t\uparrow + C_{i-1}\uparrow\left(d_{21,J}^n\downarrow + d_{22,J}^n\downarrow \Re_i^n\downarrow\right)}{D^t D^n}$$

$$B_{ii3}^c = \frac{C_i\downarrow\left(d_{12,J}^n\downarrow + d_{11,J}^n\downarrow \Re_{i-1}^n\uparrow e^{-2p f_i}\right) + \left(f_{11,Ii}\downarrow + f_{12,Ii}\downarrow \Re_i^t\right) D^n + C_{i-1}\uparrow e^{-p f_i}\left(d_{11,J}^n\downarrow + d_{12,J}^n\downarrow \Re_i^n\downarrow \Re_i^t\downarrow\right)}{D^t D^n}$$

$$B_{ii4}^c = \frac{C_i\downarrow\left(d_{22,J}^n\downarrow + d_{21,J}^n\downarrow \Re_{i-1}^n\uparrow e^{-2p f_i}\right) + \left(f_{21,Ii}\downarrow + f_{22,Ii}\downarrow \Re_i^t\right) D^n + C_{i-1}\uparrow e^{-p f_i}\left(d_{21,J}^n\downarrow + d_{22,J}^n\downarrow \Re_i^n\downarrow \Re_i^t\downarrow\right)}{D^t D^n}$$

(76)

The Hertz potential due to coupling is written in terms of the spectral amplitudes for the normal component coupled wave as

$$\tilde{\Pi}_{ii,c}^e(\vec{\lambda}, y) = a_{i,c}^- e^{p_i(y-y_i)} + a_{i,c}^+ e^{-p_i(y-y_i)} . \tag{77}$$

Using the same procedure as for tangential potentials, the Hertz potential due to coupling is given as

$$\tilde{\vec{\Pi}}^{s}_{ll,c}(\vec{\lambda},y) = \sum_{k=1}^{4} B^{c}_{llk}(\lambda) \int_{-\infty}^{\infty} \frac{j\xi \tilde{J}_x(\vec{\lambda},y') + j\zeta \tilde{J}_z(\vec{\lambda},y')}{j\omega\epsilon_i} \frac{e^{-\phi^{k}_{ll}(y|y',\vec{\lambda})}}{2p_i} dy' \qquad (78)$$

where the phase factors ϕ^{k}_{ll} are defined in eq. (65).

Applying an inverse transformation on spectral potentials given by eqs. (64) and (78) leads to the space domain Hertz potential in region l as expressed by relation (1) where the scattering coefficients S^{q}_{ll} in the expressions for the Green's functions are identified in terms of the above B^{q}_{llk} coefficients and phase factors ϕ^{q}_{ll}. For a region l above the source region, the analysis is similar to the above with the exception that an upward recursion is used to find the Hertz potential.

3.6 SUMMARY

Dyadic Green's functions for the EM field in a planar layered environment are formulated strictly in terms of the electric Hertz vector. Spectral amplitudes in their Sommerfeld-integral representations are obtained using wave matrices. The formulation based on the electric Hertz vector is complicated due to coupling of normal and tangential potential components by the boundary conditions. Wave matrices are introduced to handle the coupling in a systematic manner. This method accommodates general electric volume currents immersed in any region of planar layered environment. This approach removes any uncertainty regarding completeness of the field representation and naturally accommodates the source-point singularity.

The electric field in the l 'th layer can be expressed in terms of the Hertz vector as $\vec{E}_l = (k_l^2 + \nabla\nabla\cdot)\,\vec{\Pi}_{ll}$ where the Hertz potential in the l 'th layer maintained by

currents in the i 'th layer is

$$\vec{\Pi}_{ll}(\vec{r}) = \frac{-j\eta_i}{k_i}\int_v \ddot{G}_{ll}(\vec{r}|\vec{r}')\cdot\vec{J}(\vec{r}')dv' \tag{79}$$

with $\ddot{G}_{ll} = \ddot{I}\delta_{ll}G_i^p + \ddot{G}_{ll}^s$. The first term leads to the principal wave excited in an unbounded i 'th layer, and has the Sommerfeld-integral representation

$$G_i^p(\vec{r}|\vec{r}') = \iint_{-\infty}^{\infty} \frac{e^{j\vec{\lambda}\cdot(\vec{r}-\vec{r}')}\, e^{-p_i|y-y'|}}{2(2\pi)^2 p_i}\, d^2\lambda . \tag{80}$$

The scattered dyad has the form

$$\ddot{G}_{ll}^s(\vec{r}|\vec{r}') = (\hat{x}\hat{x}+\hat{z}\hat{z})G_{llt}^s + \hat{y}\left[\left(\hat{x}\frac{\partial}{\partial x}+\hat{z}\frac{\partial}{\partial z}\right)G_{llc}^s + G_{lln}^s\hat{y}\right] \tag{81}$$

with scalar component representations

$$\begin{Bmatrix} G_{llt}^s(\vec{r}|\vec{r}') \\ G_{lln}^s(\vec{r}|\vec{r}') \\ G_{llc}^s(\vec{r}|\vec{r}') \end{Bmatrix} = \iint_{-\infty}^{\infty} \begin{Bmatrix} S_{ll}^t(y|y',\lambda) \\ S_{ll}^n(y|y',\lambda) \\ S_{ll}^c(y|y',\lambda) \end{Bmatrix} \frac{e^{j\vec{\lambda}\cdot(\vec{r}-\vec{r}')}}{2(2\pi)^2 p_i} d^2\lambda . \tag{82}$$

Scattering coefficients S_{ll}^q were determined through the wave transmission and coupling matrices, and assume the generic forms

$$S_{ll}^q = \sum_{k=1}^{4} B_{llk}^q(\lambda) e^{-\phi_{ll}^k(y|y';\lambda)} \ldots \text{ for } q = t,n,c . \tag{83}$$

Expressions for the B_{ll} coefficients and the phase shift factors ϕ_{ll} were obtained using wave matrices as described above.

For potential in the source region, the corresponding B_{ll} coefficients and phase shift factors ϕ_{ll} are

$$\left.\begin{aligned} B^q_{il1} &= \frac{\mathcal{R}^q_{i-1}\uparrow}{D^q} \\ B^q_{il2} &= \frac{\mathcal{R}^q_{i-1}\uparrow \mathcal{R}^q_i\downarrow}{D^q} \\ B^q_{il3} &= B^q_{il2} \\ B^q_{il4} &= \frac{\mathcal{R}^q_i\downarrow}{D^q} \end{aligned}\right\} \text{for } q = t,n \qquad (84)$$

$$\begin{aligned} B^c_{il1} &= \frac{1}{D^n D^t}\{C_i\downarrow \mathcal{R}^n_{i-1}\uparrow \mathcal{R}^t_{i-1}\uparrow e^{-2p_i t_i} + C_{i-1}\uparrow\} \\ B^c_{il2} &= \frac{1}{D^n D^t}\{C_{i-1}\uparrow \mathcal{R}^n_i\downarrow + \mathcal{R}^t_{i-1}\uparrow C_i\downarrow\} \\ B^c_{il3} &= \frac{1}{D^n D^t}\{C_i\downarrow \mathcal{R}^n_{i-1}\uparrow + \mathcal{R}^t_i\downarrow C_{i-1}\uparrow\} \\ B^c_{il4} &= \frac{1}{D^n D^t}\{C_{i-1}\uparrow \mathcal{R}^n_i\downarrow \mathcal{R}^t_i\downarrow e^{-2p_i t_i} + C_i\downarrow\} \end{aligned} \qquad (85)$$

and

$$\begin{aligned} \Phi^1_{il} &= p_i(-y-y'+2y_{i-1}) \\ \Phi^2_{il} &= p_i(y-y'+2y_{i-1}-2y_i) \\ \Phi^3_{il} &= p_i(-y+y'+2y_{i-1}-2y_i) \\ \Phi^4_{il} &= p_i(y+y'-2y_i)\ . \end{aligned} \qquad (86)$$

The general reflection coefficients in region i are given in terms of interfacial reflection coefficients (defined in Appendix A) as follows

$$\begin{aligned} \mathcal{R}^q_i\downarrow &= \frac{R^q_i\downarrow + \mathcal{R}^q_{i+1}\downarrow e^{-2p_{i+1}t_{i+1}}}{1 + R^q_i\downarrow \mathcal{R}^q_{i+1}\downarrow e^{-2p_{i+1}t_{i+1}}} \\ \mathcal{R}^q_{i-1}\uparrow &= \frac{R^q_{i-1}\uparrow + \mathcal{R}^q_{i-2}\uparrow e^{-2p_{i-1}t_{i-1}}}{1 + R^q_{i-1}\uparrow \mathcal{R}^q_{i-2}\uparrow e^{-2p_{i-1}t_{i-1}}} \end{aligned} \quad \cdots \text{for } q = t,n. \qquad (87)$$

The overall coupling coefficients at interfaces i and $(i-1)$ are, respectively

$$
\begin{aligned}
\mathbf{C}_i\downarrow &= -\mathfrak{R}_i^n\downarrow(C_{11,i}\downarrow + \mathfrak{R}_i^t\downarrow C_{12,i}\downarrow) + (C_{21,i}\downarrow + \mathfrak{R}_i^t\downarrow C_{22,i}\downarrow) \\
\mathbf{C}_{i-1}\uparrow &= -\mathfrak{R}_{i-1}^n\uparrow(C_{11,i-1}\uparrow + \mathfrak{R}_{i-1}^t\uparrow C_{12,i-1}\uparrow) + (C_{21,i-1}\uparrow + \mathfrak{R}_{i-1}^t\uparrow C_{22,i-1}\uparrow)
\end{aligned}
\tag{88}
$$

where $C_{11,i}\downarrow$ is the first entry of the overall coupling matrix $[\mathbf{C}_i\downarrow]$. The coupling matrices at interfaces i and $(i-1)$ are written in terms of interfacial wave matrices as follows

$$
\begin{aligned}
[\mathbf{C}_i\downarrow] = {} & [C_i\downarrow]\left[A_i^t\downarrow\right]^{-1} + \left[A_i^n\downarrow\right][C_{i+1}\downarrow]\left[A_{i+1}^t\downarrow\right]^{-1}\left[A_i^t\downarrow\right]^{-1} \\
& + \cdots + \left(\prod_{k=i}^{N-2}\left[A_k^n\downarrow\right]\right)[C_{N-1}\downarrow]\left[A_{N-1}^t\downarrow\right]^{-1}\left(\prod_{k=N-2}^{i}\left[A_k^t\downarrow\right]^{-1}\right)
\end{aligned}
\tag{89}
$$

$$
\begin{aligned}
[\mathbf{C}_{i-1}\uparrow] = {} & [C_{i-1}\uparrow]\left[A_{i-1}^t\uparrow\right]^{-1} + \left[A_{i-1}^n\uparrow\right][C_{i-2}\uparrow]\left[A_{i-2}^t\uparrow\right]^{-1}\left[A_{i-1}^t\uparrow\right]^{-1} \\
& + \cdots + \left(\prod_{k=i-1}^{2}\left[A_k^n\uparrow\right]\right)[C_1\uparrow]\left[A_1^t\uparrow\right]^{-1}\left(\prod_{k=2}^{i-1}\left[A_k^t\uparrow\right]^{-1}\right).
\end{aligned}
\tag{90}
$$

The interfacial wave matrices are defined by eq. (19). Consequently, finding the Hertz potential in a planar layered environment is rendered to multiplication of wave matrices.

APPLICATION TO INTEGRATED-CIRCUIT ENVIRONMENT: SIMPLE MICROSTRIP STRUCTURE

4.1 INTRODUCTION

In this chapter, we apply the results obtained in chapter three to derive the electric dyadic Green's function associated with the layered background of a typical microstrip environment consisting of conductor/film/cover layers. The microstrip device is printed on the film layer and resides in the cover region as shown in Fig. 4.1. We begin by specializing the results from chapter three to obtain the EM fields in the cover layer of the tri-layered environment of Fig. 4.1, then the EM fields in the film region are derived. In a latter section, a general electric field integral equation (EFIE) description of the microstrip circuit is developed.

4.2 FIELDS IN THE COVER LAYER

The tri-layered conductor/film/cover structure, typical of the background environment in a microstrip circuit, is depicted in Fig. 4.2. The electric current source is embedded in the cover layer. The electric field in the cover region is given as in eq. (3.6) as follows

$$\vec{E}_c(\vec{r}) = \frac{-j\eta_c}{k_c}\int_V \tilde{\vec{G}}^e_{cc}(\vec{r}|\vec{r}')\cdot\vec{J}(\vec{r}')dv' \qquad (1)$$

where the electric Green's dyad is identified in terms of Hertz potential Green's dyad as

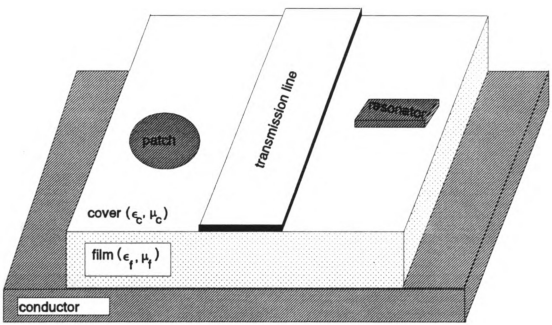

Figure 4.1: Configuration of general open microstrip integrated circuit.

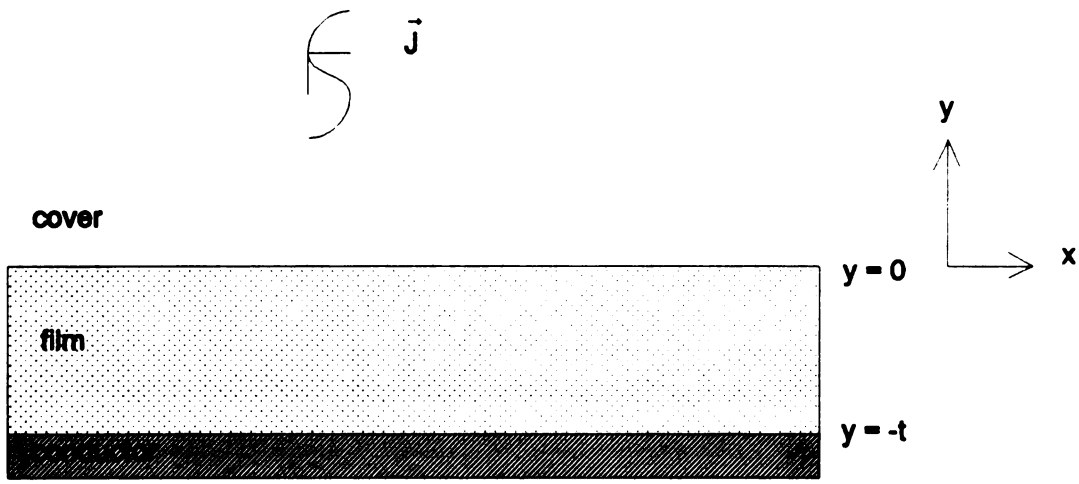

Figure 4.2: Typical background environment in a microstrip circuit.

$$\ddot{G}_{cc}^{e}(\vec{r}|\vec{r}') = PV(k_c^2+\nabla\nabla\cdot)\ddot{G}_{cc}(\vec{r}|\vec{r}') + \ddot{L}\delta(\vec{r}-\vec{r}') \ . \tag{2}$$

The Hertz potential Green's dyad decomposes into a principal part and a scattered part as follows

$$\ddot{G}_{cc} = \ddot{I}G_c^p + \ddot{G}_{cc}^s \ . \tag{3}$$

The principal Green's function is given by eq. (3.2) while the scattered Green's dyad is given by eq. (3.3). The scattered dyad has the following scalar components

$$\begin{Bmatrix} G_{cct}^s(\vec{r}|\vec{r}') \\ G_{ccn}^s(\vec{r}|\vec{r}') \\ G_{ccc}^s(\vec{r}|\vec{r}') \end{Bmatrix} = \int\int_{-\infty}^{\infty} \begin{Bmatrix} S_{cc}^t(y|y',\lambda) \\ S_{cc}^n(y|y',\lambda) \\ S_{cc}^c(y|y',\lambda) \end{Bmatrix} \frac{e^{j\vec{\lambda}\cdot(\vec{r}-\vec{r}')}}{2(2\pi)^2 p_c} d^2\lambda \ . \tag{4}$$

The scattering coefficients S_{cc}^q were determined through the wave transmission and coupling matrices, and assume the form

$$S_{cc}^q = \sum_{k=1}^{4} B_{cck}^q(\lambda) e^{-\phi_{cc}^k(y|y';\lambda)} \cdots \text{for } q = t,n,c \ . \tag{5}$$

Hence, finding the components of the Green's dyad reduces to obtaining the B_{cc} coefficients and the phase shift factors ϕ_{cc} . Since there is no interface above the source region, all quantities related to upward recursion vanish i.e. $\Re_{i-1}\uparrow = \mathbf{C}_{i-1}\uparrow = 0$. Exploiting eq. (3.45) the B_{cc} coefficients are specialized as

$$\left.\begin{matrix} B_{cc1}^q = B_{cc2}^q = B_{cc3}^q = 0 \\ B_{cc4}^q = \Re_c^q\downarrow \end{matrix}\right\} \cdots \text{for } q = t,n \ . \tag{6}$$

For coupling components, we use eq. (3.52) to obtain

$$B_{cc1}^{c} = B_{cc2}^{c} = B_{cc3}^{c} = 0$$
$$B_{cc4}^{c} = \mathbf{C}_c\downarrow \ . \tag{7}$$

Consequently, the scattering coefficients have the special form

$$S_{cc}^{q} = B_{cc4}^{q}(\lambda)\, e^{-\phi_{cc}^{4}(y|y',\lambda)} \quad \cdots \textit{for } q = t,n,c \tag{8}$$

where the phase shift factor $\phi_{cc}^{4}(y|y',\lambda)$ is defined from eq. (3.46) with $y_i = 0$ as

$$\phi_{cc}^{4}(y|y',\lambda) = p_c(y + y') \ . \tag{9}$$

Now, we need to determine the general reflection coefficient $\Re_c^q\downarrow$ and the overall coupling coefficient $\mathbf{C}_c\downarrow$. From eq. (3.21), we have

$$\Re_c^q\downarrow = \frac{R_c^q\downarrow + \Re_f^q\downarrow e^{-2p_f t_f}}{1 + R_c^q\downarrow \Re_f^q\downarrow e^{-2p_f t_f}} \quad \cdots \textit{for } q = t,n \tag{10}$$

where $t_f = t$ is the thickness of the film region. The overall reflection coefficient $\Re_f^q\downarrow$ reduces to the interfacial reflection coefficient since there is no interface below the film/conductor boundary. From Appendix A, the interfacial reflection coefficients at the cover interface are

$$R_c^t\downarrow = \frac{M_c^2 p_c - p_f}{M_c^2 p_c + p_f} \ ; \quad R_c^n\downarrow = \frac{N_c^2 p_c - p_f}{N_c^2 p_c + p_f} \tag{11}$$

where $M_c^2 = m_f^2/m_c^2$ and $N_c^2 = n_f^2/n_c^2$. Since interface f is adjacent to a perfect conductor, we have

$$R_f^t\downarrow = -1 \ ; \quad R_f^n\downarrow = 1 \ . \tag{12}$$

Hence, the overall reflection coefficients in eq. (10) reduce to

$$\Re_c^t\downarrow = \frac{R_c^t\downarrow - e^{-2p_f t}}{1 - R_c^t\downarrow e^{-2p_f t}}$$
$$\Re_c^n\downarrow = \frac{R_c^n\downarrow + e^{-2p_f t}}{1 + R_c^n\downarrow e^{-2p_f t}} . \qquad (13)$$

The overall coupling coefficient $C_c\downarrow$ is given by eq. (3.35) as follows

$$C_c\downarrow = -\Re_c^n\downarrow (C_{11,c}\downarrow + \Re_c^t\downarrow C_{12,c}\downarrow) + (C_{21,c}\downarrow + \Re_c^t\downarrow C_{22,c}\downarrow) \qquad (14)$$

where $C_{11,c}\downarrow$ is the first entry of the overall coupling matrix $[C_c\downarrow]$. The coupling matrix is given by eq. (3.30) and is specialized to this structure as

$$[C\downarrow] = [C_c\downarrow][A_c^t\downarrow]^{-1} + [A_c^n\downarrow][C_f\downarrow][A_f^t\downarrow]^{-1}[A_c^t\downarrow]^{-1} . \qquad (15)$$

Since interface f is a perfect conductor, the product of matrices $[A_c^n\downarrow][C_f\downarrow][A_f^t\downarrow]^{-1}[A_c^t\downarrow]^{-1}$ reduces to the null matrix. Hence, using eq. (3.19) , the overall coupling matrix is specialized as

$$[C_c\downarrow] = [C_c\downarrow][A_c^t\downarrow]^{-1} = \frac{1 - N_c^{-2}M_c^{-2}}{2p_c}\begin{bmatrix} -1 & -1 \\ 1 & 1 \end{bmatrix} . \qquad (16)$$

Substituting the entries of the overall coupling matrix in the expression for the overall coupling coefficient in eq. (14) leads to

$$C_c\downarrow = \frac{1 - N_c^{-2}M_c^{-2}}{2p_c}\left(1 + \Re_c^t\downarrow\right)\left(1 + \Re_c^n\downarrow\right) . \qquad (17)$$

Using eq. (11) in (13) and after some manipulations, the final expression for the generalized reflection coefficients are

$$\Re_c^{i}\downarrow = \frac{M_c^2 p_c - p_f \coth p_f t}{Z^h(\lambda)} \quad ; \quad \Re_c^{n}\downarrow = \frac{N_c^2 p_c - p_f \tanh p_f t}{Z^e(\lambda)} \tag{18}$$

where

$$\begin{aligned} Z^h(\lambda) &= M_c^2 p_c + p_f \coth p_f t \\ Z^e(\lambda) &= N_c^2 p_c + p_f \tanh p_f t \ . \end{aligned} \tag{19}$$

Substitution of eq. (18) in eq. (17) leads to the final expression for the overall coupling coefficient as

$$C_c\downarrow = \frac{2p_c\left(M_c^2 N_c^2 - 1\right)}{Z^e(\lambda) Z^h(\lambda)} \ . \tag{20}$$

Finally, the scattered Green's function components are simplified as follows

$$\begin{Bmatrix} G_{ccx}^{s}(\vec{r}|\vec{r}') \\ G_{ccn}^{s}(\vec{r}|\vec{r}') \\ G_{ccc}^{s}(\vec{r}|\vec{r}') \end{Bmatrix} = \int\int_{-\infty}^{\infty} \begin{Bmatrix} \Re_c^{i}\downarrow(\lambda) \\ \Re_c^{n}\downarrow(\lambda) \\ C_c\downarrow(\lambda) \end{Bmatrix} \frac{e^{j\vec{\lambda}\cdot(\vec{r}-\vec{r}')} e^{-p_c(y+y')}}{2(2\pi)^2 p_c} d^2\lambda \ . \tag{21}$$

Eq. (21) is a well known result [48]. Pole singularities within the integral representations of the Green's function components, as implicated in the reflection and coupling coefficients $\Re_c^{i}\downarrow(\lambda)$, $\Re_c^{n}\downarrow(\lambda)$ and $C_c\downarrow(\lambda)$, lead to the surface waves propagating in the tri-layered structure of Fig. 4.2. In fact, $Z^e(\lambda)=0$ and $Z^h(\lambda)=0$ lead to the eingenvalue equation for *TE* and *TM* surface-wave modes, respectively, supported by the layered structure of Fig. 4.2.

4.3 FIELDS IN THE FILM REGION

The electric field in the film region is given as in eq. (3.6) as follows

$$\vec{E}_f(\vec{r}) = \frac{-j\eta_c}{k_c}\int_V \vec{G}_{fc}^{e}(\vec{r}|\vec{r}')\cdot\vec{J}(\vec{r}')dv' \tag{22}$$

where the electric Green's dyad is identified in terms of Hertz potential Green's dyad as

$$\vec{G}_{fc}^{e}(\vec{r}|\vec{r}') = (k_f^2+\nabla\nabla\cdot)\vec{G}_{fc}(\vec{r}|\vec{r}') \ . \tag{23}$$

The Hertz potential Green's dyad consists of only a scattered part given by eq. (3.3), with the following scalar components

$$\begin{Bmatrix} G_{fct}^{s}(\vec{r}|\vec{r}') \\ G_{fcn}^{s}(\vec{r}|\vec{r}') \\ G_{fcc}^{s}(\vec{r}|\vec{r}') \end{Bmatrix} = \int\int_{-\infty}^{\infty} \begin{Bmatrix} S_{fc}^{t}(y|y',\lambda) \\ S_{fc}^{n}(y|y',\lambda) \\ S_{fc}^{c}(y|y',\lambda) \end{Bmatrix} \frac{e^{j\vec{\lambda}\cdot(\vec{r}-\vec{r}')}}{2(2\pi)^2 p_c} d^2\lambda \ . \tag{24}$$

The scattering coefficients S_{fc}^{q} are written in terms of the B_{fc} coefficients and the phase shift factors ϕ_{fc}. Hence, these coefficients must be determined in order to quantify the Green's function components. The results in the previous section will be used. Exploiting eq. (3.63) the tangential and normal components are

$$\left.\begin{aligned} B_{fc1}^{q} &= B_{fc2}^{q} = 0 \\ B_{fc3}^{q} &= d_{11,f}^{q}\downarrow + d_{12,f}^{q}\downarrow \Re_c^{q}\downarrow \\ B_{fc4}^{q} &= d_{21,f}^{q}\downarrow + d_{22,f}^{q}\downarrow \Re_c^{q}\downarrow \end{aligned}\right\} \cdots \textit{for } q = t,n \ . \tag{25}$$

Similarly, we specialize eq. (3.76) to obtain the coupling components as follows

$$\begin{aligned} B_{fc3}^{c} &= f_{11,fc}\downarrow + f_{12,fc}\Re_c^{i}\downarrow + d_{12,f}^{n}\downarrow \mathbf{C}_c\downarrow \\ B_{fc4}^{c} &= f_{21,fc}\downarrow + f_{22,fc}\Re_c^{i}\downarrow + d_{22,f}^{n}\downarrow \mathbf{C}_c\downarrow \ . \end{aligned} \tag{26}$$

The corresponding phase shift factors are a special case of eq. (3.65) with $y_l = 0$ and $y_l = -t$, yielding

$$\phi_{fc}^{3} = p_c y' - p_f (y + t)$$
$$\phi_{fc}^{4} = p_c y' + p_f (y + t) \ . \tag{27}$$

The matrix $\left[D_f^{q\downarrow}\right]$ is given by eq. (3.59) as

$$\left[D_f^{t\downarrow}\right] = \left[A_c^{t\downarrow}\right]^{-1} = \frac{N_c^{-2} M_c^{-2}}{1 - R_c^{t\downarrow}} \begin{bmatrix} e^{-p_f t} & -R_c^{t\downarrow} e^{-p_f t} \\ -R_c^{t\downarrow} e^{p_f t} & e^{p_f t} \end{bmatrix}$$
$$\left[D_f^{n\downarrow}\right] = \left[A_c^{n\downarrow}\right]^{-1} = \frac{N_c^{-2} N_c^{-2}}{1 - R_c^{n\downarrow}} \begin{bmatrix} e^{-p_f t} & -R_c^{n\downarrow} e^{-p_f t} \\ -R_c^{n\downarrow} e^{p_f t} & e^{p_f t} \end{bmatrix} \tag{28}$$

and the matrix $\left[F_{fc}^{\downarrow}\right]$ is given by eq. (3.70) as

$$\left[F_{fc}^{\downarrow}\right] = -\left[D_f^{n\downarrow}\right] \left[\mathbf{C}_c^{\downarrow}\right] \ . \tag{29}$$

The overall coupling matrix is given in the previous section by eq. (16). Using eqs. (16) and (28), eq. (29) becomes

$$\left[F_{fc}^{\downarrow}\right] = \frac{\left(N_c^{-4} M_c^{-2} - N_c^{-2}\right)\left(1 + R_c^{n\downarrow}\right)}{2 p_c \left(1 - R_c^{n\downarrow}\right)} \begin{bmatrix} -e^{-p_f t} & -e^{-p_f t} \\ e^{p_f t} & e^{p_f t} \end{bmatrix} \tag{30}$$

Now that the matrices $\left[D_f^{q\downarrow}\right]$ and $\left[F_{fc}^{\downarrow}\right]$ are quantified, we substitute their entries in eqs. (25) and (26) and use the expressions for the overall reflection and coupling coefficients from the previous section to obtain the final form of the tangential B_{fc} coefficients as

$$B_{fc3}^{t} = \frac{N_c^{-2} p_c}{\sinh p_f t Z^h(\lambda)}$$
$$B_{fc4}^{t} = \frac{-N_c^{-2} p_c}{\sinh p_f t Z^h(\lambda)} \tag{31}$$

and the normal B_{fc} coefficients as

$$B_{fc3}^{n} = \frac{p_c}{\cosh p_f t Z^e(\lambda)}$$
$$B_{fc4}^{n} = \frac{p_c}{\cosh p_f t Z^e(\lambda)} \; . \tag{32}$$

Similarly, the coupling components of the B_{fc} coefficients are

$$B_{fc3}^{c} = \frac{p_c N_c^{-2}\left(N_c^2 M_c^2 - 1\right)\left(1 - e^{-2p_f t}\right)e^{p_f t}}{2\sinh p_f t \cosh p_f t Z^e(\lambda) Z^h(\lambda)}$$
$$B_{fc4}^{c} = \frac{p_c N_c^{-2}\left(N_c^2 M_c^2 - 1\right)\left(1 + e^{-2p_f t}\right)e^{-p_f t}}{2\sinh p_f t \cosh p_f t Z^e(\lambda) Z^h(\lambda)} \tag{33}$$

where $Z^h(\lambda)$ and $Z^e(\lambda)$ are defined by eq. (19).

4.4 INTEGRAL EQUATION DESCRIPTION OF MICROSTRIP TRANSMISSION LINE

The general configuration of an open microstrip transmission line is depicted in Fig. 4.3. The conducting strip is embedded in the cover layer adjacent to the film/cover interface of the tri-layered conductor/film/cover environment. The y axis is normal and the x and z axes are tangential to the film/cover interface.

If excitation is provided by an incident field $\vec{E}^i(\vec{r})$ maintained by an impressed current, a surface current $\vec{K}(\vec{r})$ is induced on perfectly conducting device surface S,

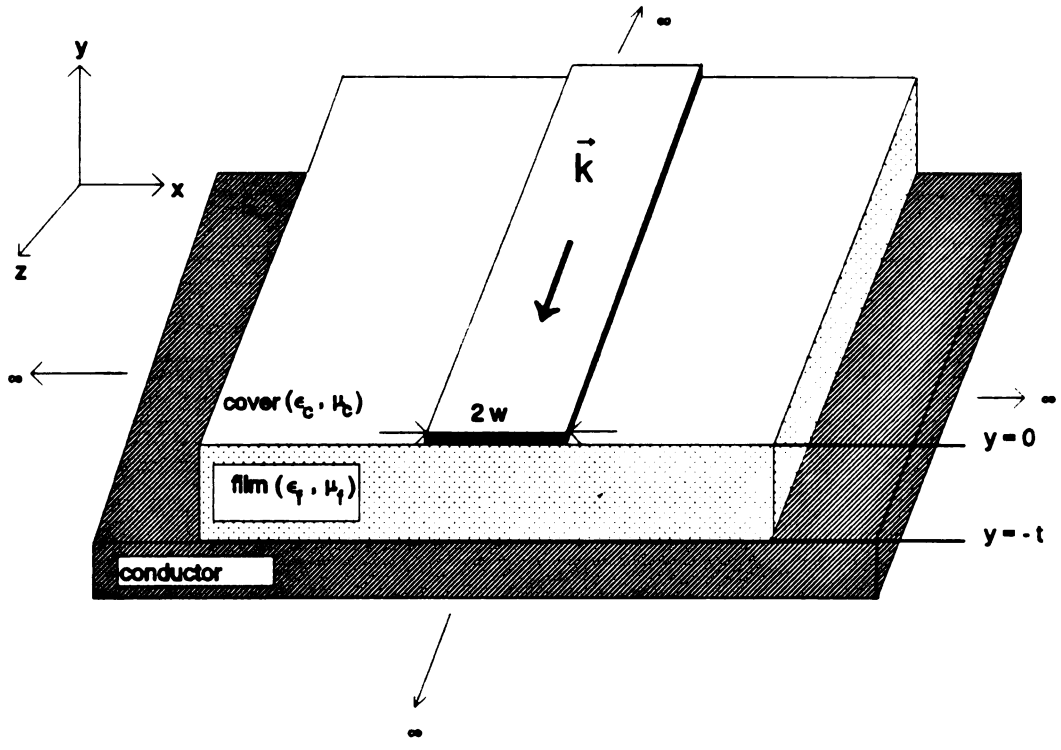

Figure 4.3: General configuration of an open microstrip transmission line

producing a scattered field $\vec{E}^s$. The boundary condition for the total tangential electric field at the conducting surface S requires that $\hat{t}\cdot(\vec{E}^i+\vec{E}^s)=0$, where $\hat{t}$ is a unit tangent vector at any point on surface S. Expressing the scattered field $\vec{E}^s$ in the form of equation (3.6) leads to the following EFIE for the unknown induced current $\vec{K}$ on the conducting strip surface

$$\hat{t}\cdot\int_S \bar{\bar{G}}^e(\vec{r}\,|\vec{r}\,')\cdot\vec{K}(\vec{r}\,')\,dS' = \frac{-jk_c}{\eta_c}\hat{t}\cdot\vec{E}^i(\vec{r}) \;\cdots\; \forall\ \vec{r}\in S\ . \tag{34}$$

The conducting strip extends infinetly along the wave-guiding z-axis, and the system is therefore z-invariant. Consequently, the axial integral is convolutional and Fourier transformation on that axial variable is suggested. Hence, EFIE (34) is axially-transformed, using the convolution and differentiation theorems, leading to

$$\hat{t}\cdot\int_C \bar{\bar{g}}^e(\vec{\rho}\,|\vec{\rho}\,';\zeta)\cdot\vec{k}(\vec{\rho}\,',\zeta)\,dl' = \frac{-jk_c}{\eta_c}\hat{t}\cdot\vec{e}^i(\vec{\rho},\zeta) \;\cdots\; \forall\ \vec{\rho}\in C \tag{35}$$

where C is the axially invariant boundary contour of the strip conductor in the transverse plane; $\vec{\rho}=\hat{x}x+\hat{y}y$ is the 2-D transverse position vector and ζ is the transform variable corresponding to z. Lower case fields and currents are transform domain quantities.

The transform-domain electric dyadic Green's function is given by

$$\begin{aligned}\bar{\bar{g}}^e(\vec{\rho}\,|\vec{\rho}\,') &= \mathcal{F}_z\{\bar{\bar{G}}^e(\vec{\rho}\,|\vec{\rho}\,';z)\}\\ &= PV(k_c^2+\tilde{\nabla}\tilde{\nabla}\cdot)\bar{\bar{g}}(\vec{\rho}\,|\vec{\rho}\,';\zeta) + \bar{\bar{L}}\delta(\vec{\rho}-\vec{\rho}\,')\end{aligned} \tag{36}$$

where $\tilde{\nabla}=\nabla_t+\hat{z}\,j\zeta$ with $\nabla_t=\hat{x}\partial/\partial x+\hat{y}\partial/\partial y$ the transverse operator. The depolarizing

dyad $\bar{L}=\hat{y}\hat{y}$ is never required since only tangential current components are present. The transform-domain Hertzian potential Green's dyad $\bar{\bar{g}}$ in eq. (36) is expressed in terms of Sommerfeld-type integrals as follows

$$\bar{\bar{g}}(\vec{\rho}\,|\,\vec{\rho}\,';\zeta)=\bar{\bar{I}}g^{p}(\vec{\rho}\,|\,\vec{\rho}\,';\zeta)+\bar{\bar{g}}^{s}(\vec{\rho}\,|\,\vec{\rho}\,';\zeta) \tag{37}$$

where

$$\bar{\bar{g}}^{s}(\vec{\rho}\,|\,\vec{\rho}\,';\zeta)=(\hat{x}\hat{x}+\hat{z}\hat{z})g_{t}^{s}(\vec{\rho}\,|\,\vec{\rho}\,';\zeta)+\hat{y}\left(\nabla_{T}g_{c}^{s}(\vec{\rho}\,|\,\vec{\rho}\,';\zeta)+g_{n}^{s}(\vec{\rho}\,|\,\vec{\rho}\,';\zeta)\hat{y}\right) \tag{38}$$

and

$$g^{p}(\vec{\rho}\,|\,\vec{\rho}\,';\zeta)=\int_{-\infty}^{\infty}\frac{e^{j\xi(x-x')}e^{-p_{c}|y-y'|}}{4\pi p_{c}}d\xi \tag{39}$$

$$\begin{Bmatrix} g_{t}^{s}(\vec{\rho}\,|\,\vec{\rho}\,';\zeta) \\ g_{n}^{s}(\vec{\rho}\,|\,\vec{\rho}\,';\zeta) \\ g_{c}^{s}(\vec{\rho}\,|\,\vec{\rho}\,';\zeta) \end{Bmatrix}=\int_{-\infty}^{\infty}\begin{Bmatrix} \mathfrak{R}^{t}\downarrow(\lambda) \\ \mathfrak{R}^{n}\downarrow(\lambda) \\ \mathbf{C}\downarrow(\lambda) \end{Bmatrix}\frac{e^{j\xi(x-x')}e^{-p_{c}(y+y')}}{4\pi p_{c}}d\xi \tag{40}$$

with $\nabla_{T}=\hat{x}\partial/\partial x+\hat{z}j\zeta$. Coefficients $\mathfrak{R}_{t}\downarrow,\mathfrak{R}_{n}\downarrow$ and $\mathbf{C}(\lambda)\downarrow$ are the same as those given in expressions (17) and (18), and are functions of ζ through λ. Note that the subscript c in the scattering coefficients and in the Green's functions, referring to the cover region, is dropped for the sake of simplicity.

Singularities in the spectral integral representation of the Green's functions lead to similar singularities in the spectral domain microstrip current $\vec{k}(\vec{\rho};\zeta)$. These singularities in the complex ζ-plane consist of simple pole singularities which correspond to discrete propagation modes and square-root branch-point singularities which lead the radiation field with a continuous spectrum.

Pole singularities of the current in the axial Fourier transform domain correspond to discrete propagation modes. For ζ near a discrete propagation-mode pole

eigenvalue ζ_p, the transform domain current can be approximated as [34]

$$\vec{k}(\vec{\rho},\zeta) \sim \frac{a_p^{\pm} \vec{k}_p^{\pm}(\vec{\rho})}{(\zeta \pm \zeta_p)^l} \tag{41}$$

where $\vec{k}_p^{\pm}(\vec{\rho})$ is the eigenmode current of a wave propagating in $\pm z$ direction on the strip. It can be shown that $l = 1$ [34], so the poles are simple. Substituting (41) in EFIE (35) leads to

$$\frac{a_p^{\pm}}{(\zeta \pm \zeta_p)} \hat{t} \cdot \int_C \vec{g}^e(\vec{\rho}\,|\,\vec{\rho}\,';\zeta) \cdot \vec{k}_p^{\pm}(\vec{\rho}\,')\, dl' = \frac{-jk_c}{\eta_c} \hat{t} \cdot \vec{e}^{\,i}(\vec{\rho},\zeta) \quad \cdots \forall \vec{\rho} \in C \,. \tag{42}$$

Since the impressed field $\vec{e}^{\,i}(\vec{\rho},\zeta)$ is regular at $\zeta = \mp\zeta_p$, the integral in the above equation must vanish at $\zeta = \mp\zeta_p$ to provide an indeterminate form [34]. Therefore $\vec{k}_p^{\pm}$ must satisfy the following homogeneous EFIE

$$\hat{t} \cdot \int_C \vec{g}^e(\vec{\rho}\,|\,\vec{\rho}\,';\zeta) \cdot \vec{k}_p^{\pm}(\vec{\rho}\,')\, dl' = 0 \quad \cdots \quad \forall \ \vec{\rho} \in C \tag{43}$$

with nontrivial solution only for $\zeta = \mp\zeta_p$. This EFIE consequently defines the discrete propagation modes and associated propagation constant $\mp\zeta_p$.

Inverse transforming the spectral current $\vec{k}$ leads to the space-domain current $\vec{K}(\vec{r})$ as

$$\vec{K}(\vec{r}) = \frac{1}{2\pi} \int_{-\infty}^{\infty} \vec{k}(\vec{\rho})\, e^{j\zeta z} d\zeta \,. \tag{44}$$

From expression (41), and for a single discrete mode, the space-domain eigenmode current is

$$\vec{K}_p(\vec{\rho},\zeta) = a_p^{\pm}\, U(\pm z)\vec{k}_p^{\pm}(\vec{\rho})\, e^{\mp j\zeta_p z} \ . \tag{45}$$

The latter expression clearly demonstrates that this a wave propagating in $\pm z$ direction along the strip with propagation phase constant ζ_p and current distribution $\vec{k}_p^{\pm}(\vec{\rho})$. The electromagnetic fields have the same z dependence through the common phase factor $e^{\mp j\zeta z}$. From here on, we assume the case for $+z$ traveling waves only.

Consider a strip conductor of infinitesimal thickness and a width of $2w$ as shown in Fig. 4.3. In this case, the EFIE is simplified as

$$\lim_{y\to 0} \hat{t}\cdot\int_C \vec{\vec{g}}^{\,e}(x,y|x',y'=0;\zeta)\cdot\vec{k}_p(x')dx' = 0 \ \cdots \ for \ -w\le x\le w \ . \tag{46}$$

The surface current for a strip of vanishing thickness has only tangential components as

$$\vec{k}(\vec{\rho}) = \hat{x}k_x(x) + \hat{z}k_z(x) \ . \tag{47}$$

Substituting eq. (47) in (46) and exploiting expression (36) for the electric Green's dyad yields a pair of integral equations by letting $\hat{t}=\hat{x}$ and $\hat{t}=\hat{z}$; they are

$$\begin{aligned}
&\lim_{y\to 0}\int_{-w}^{w} g_{xx}^{e}(x,y|x',0;\zeta)k_x(x') + g_{xz}^{e}(x,y|x',0;\zeta)k_z(x')\,dx' = 0 \\
&\lim_{y\to 0}\int_{-w}^{w} g_{zx}^{e}(x,y|x',0;\zeta)k_x(x') + g_{zz}^{e}(x,y|x',0;\zeta)k_z(x')\,dx' = 0 \\
&\qquad\qquad \cdots \ for \ -w\le x\le w \ .
\end{aligned} \tag{48}$$

The scalar components of the Green's functions are given in Appendix B as

$$g_{\alpha\beta}^{e}(x,y|x',0) = \frac{1}{2\pi}\int_{-\infty}^{\infty} C_{\alpha\beta}^{e}(\xi,\zeta)e^{j\xi(x-x')}e^{-p_0 y}\,d\xi \tag{49}$$
$$\cdots \ for \ \alpha,\beta = x,z$$

where the coefficients are functions of ξ and ζ as

$$C_{xx}^{e}(\xi,\zeta) = \frac{(N_c^2 M_c^2 - 1)\xi^2 p_c}{Z^h(\lambda) Z^e(\lambda)} + \frac{M_c^2 (k_c^2 - \xi^2)}{Z^h(\lambda)}$$

$$C_{xz}^{e}(\xi,\zeta) = C_{zx}^{e}(\xi,\zeta) = \frac{(N_c^2 M_c^2 - 1)\xi\zeta p_c}{Z^h(\lambda) Z^e(\lambda)} - \frac{M_c^2 \xi\zeta}{Z^h(\lambda)} \qquad (50)$$

$$C_{zz}^{e}(\xi,\zeta) = \frac{(N_c^2 M_c^2 - 1)\zeta^2 p_c}{Z^h(\lambda) Z^e(\lambda)} + \frac{M_c^2 (k_c^2 - \zeta^2)}{Z^h(\lambda)} \; .$$

Exchanging the spatial integration with the spectral one in eq. (48) results in the following

$$\lim_{y \to 0} \int_{-\infty}^{\infty} d\xi \, e^{p_0 y} \int_{-w}^{w} \left\{ C_{xx}^{e}(\xi,\zeta) k_x(x') + C_{xz}^{e}(\xi,\zeta) k_z(x') \right\} e^{j\xi(x-x')} dx' = 0$$

$$\lim_{y \to 0} \int_{-\infty}^{\infty} d\xi \, e^{p_0 y} \int_{-w}^{w} \left\{ C_{zx}^{e}(\xi,\zeta) k_x(x') + C_{zz}^{e}(\xi,\zeta) k_z(x') \right\} e^{j\xi(x-x')} dx' = 0 \qquad (51)$$

$$\cdots \; for \; -w \le x \le w \; .$$

A moment method solution of the above equation is pursued in the next section.

4.5 MOMENT METHOD SOLUTION

The transverse and longitudinal current components are expanded in series of Chebychev polynomials weighted by appropriate edge-condition factors as follows

$$k_x(x) = \sum_{n=0}^{N} a_{xn} e_{xn}(x)$$

$$k_z(x) = \sum_{n=0}^{N} a_{zn} e_{zn}(x) \qquad (52)$$

with

$$e_{xn}(x) = T_n(x/w) \sqrt{1 - (x/w)^2}$$

$$e_{zn}(x) = T_n(x/w) \, / \sqrt{1 - (x/w)^2} \qquad \cdots \; for \; -w \le x \le w \qquad (53)$$

where $T_n(x/w)$ is a Chebyshev polynomial of order n of the first kind and a_{xn} and a_{zn}

are unknown expansion coefficients.

Following Galerkin's method, the same basis functions are used as testing functions. Using the above current expansions in (51), and after many manipulations [50], The EFIE is finally rendered into the following matrix equation

$$\begin{bmatrix} A_{xx}^{mn} & A_{xz}^{mn} \\ A_{zx}^{mn} & A_{zz}^{mn} \end{bmatrix} \begin{bmatrix} a_{x0} \\ a_{x1} \\ \vdots \\ a_{xN} \\ a_{z0} \\ \vdots \\ a_{zN} \end{bmatrix} = 0, \qquad for\ m,n = 0,1,\cdots,N \tag{54}$$

where the matrix elements are given as

$$A_{\alpha\beta}^{mn} = \lim_{y \to 0} \int_{-\infty}^{\infty} e^{-\rho_c y} C_{\alpha\beta}(\lambda) g_{\alpha m}(\xi) f_{\beta n}(\xi)\, d\xi \qquad \cdots for\ \alpha,\beta = x,z \tag{55}$$

with

$$g_{\alpha m}(\xi) = \int_{-w}^{w} e_{\alpha m}(x) e^{j\xi x} dx \qquad \cdots for\ \alpha = x,z \tag{56}$$

and

$$f_{\beta n}(\xi) = \int_{-w}^{w} e_{\beta n}(x') e^{-j\xi x'} dx \qquad \cdots for\ \beta = x,z. \tag{57}$$

One advantage of using Chebyshev polynomials as basis functions is that it allows the spatial integrals in (56) and (57) to be evaluated in closed form.

To obtain a nontrivial solution of the matrix equation, the determinant of the $[A]$ matrix must vanish. Since the elements of A are functions of ζ, this requirement yields the propagation constant ζ_p. The corresponding expansion coefficients

are then evaluated and the eigenmode currents are obtained in quasi-closed Chebyshev polynomial series. An additional advantage of using Chebyshev polynomials is that only few terms in the series are required to accuretly represent the current.

4.6 NUMERICAL RESULTS

Table 4.1 shows a comparison of normalized propagation constants (ζ/k_o)(for a microstrip line with parameters $2w/t=1$, $\epsilon_f=8$ and $\mu_f=1$) obtained by Kobayashi et al. [33] and the present method. The influence of the number of basis functions N on the current components is also included. Table 4.1 shows that fast convergence to the exact values of ζ/k_0 is obtained even for the cases of $N=2$. The results obtained with the present method show that the results in [33] are accurate within 8 percent to 1 percent for higher frequencies. This is mainly due to the fact that in the present method the basis functions are Chebyshev polynomials of the first kind, whereas in [33] Chebyshev polynomials of the first and second kind are used as basis functions in the expansion for the current, and the resulting convergence rates differ.

Fig. 4.4 shows the value of the normalized propagation constant (ζ/k_0) as a function of frequency up to 15 GHz. We have compared the results with those obtained in [32]. The latter authors used triangular basis functions with a point-matching technique. The respective results differ by less than 2 percent.

The longitudinal current and the transverse current on the strip are shown in Figs. 4.5 and 4.6, respectively. As the longitudinal current is symmetric with respect to the center of the strip and as the transverse current is antisymmetric, only the results for the right half of the strip are displayed. The amplitude of the transverse

current changes more rapidly as a function of frequency than the longitudinal current. Moreover, the magnitude of the former is quite small compared to the latter.

4.7 SUMMARY

The conventional microstrip is analyzed as an example of an integrated circuit located adjacent to a layered surround. The dyadic Green's functions associated with the layered background of the microstrip environment are constructed using wave matrices as discussed in the previous chapter. The fields in the film region will be used in the next chapter to determine the characteristic impedance of the conventional microstrip. A Fourier transform-domain electric field integral equation (EFIE) description of general microstrip is developed, and then applied to the conventional microstrip line. The currents on the strip are needed in the analysis of characteristic impedance as discussed in the next chapter.

Table 4.1: Convergence of the propagation constant upon the number of basis functions used in the current expansion.

t / λ_0		0.005	0.05	0.1	0.2	0.3	0.4
ζ/k_0 [33]	N=1	2.3379	2.474	2.5973	2.7146	2.7623	2.7849
	N=2	2.3383	2.4753	2.5995	2.7202	2.7675	2.7897
	N=3	2.3383	2.4753	2.5995	2.7202	2.7675	2.7897
	N=4	2.3383	2.4753	2.5995	2.7202	2.7675	2.7897
ζ/k_0 present method	N=1	2.417	2.5772	2.6844	2.7662	2.7944	2.8056
	N=2	2.417	2.5773	2.6845	2.7663	2.7945	2.8069
	N=3	2.417	2.5773	2.6845	2.7663	2.7945	2.8069
	N=4	2.417	2.5773	2.6845	2.7663	2.7945	2.8069

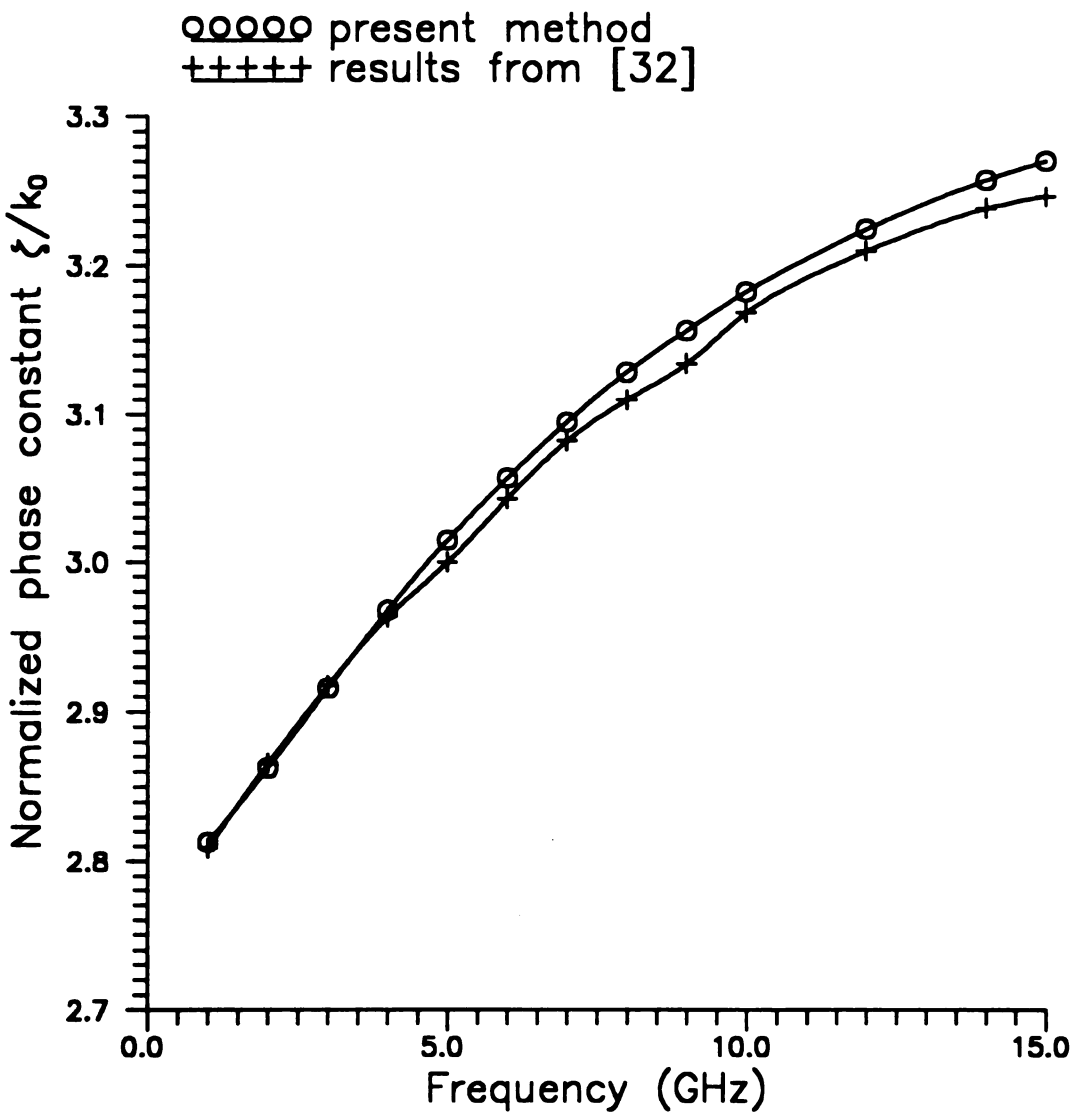

Figure 4.4: Dispersion characteristics of the principal mode for the configuration of Fig. 4.3 with w = 3.04 mm, t = 3.17 mm, and n_f = 3.42.

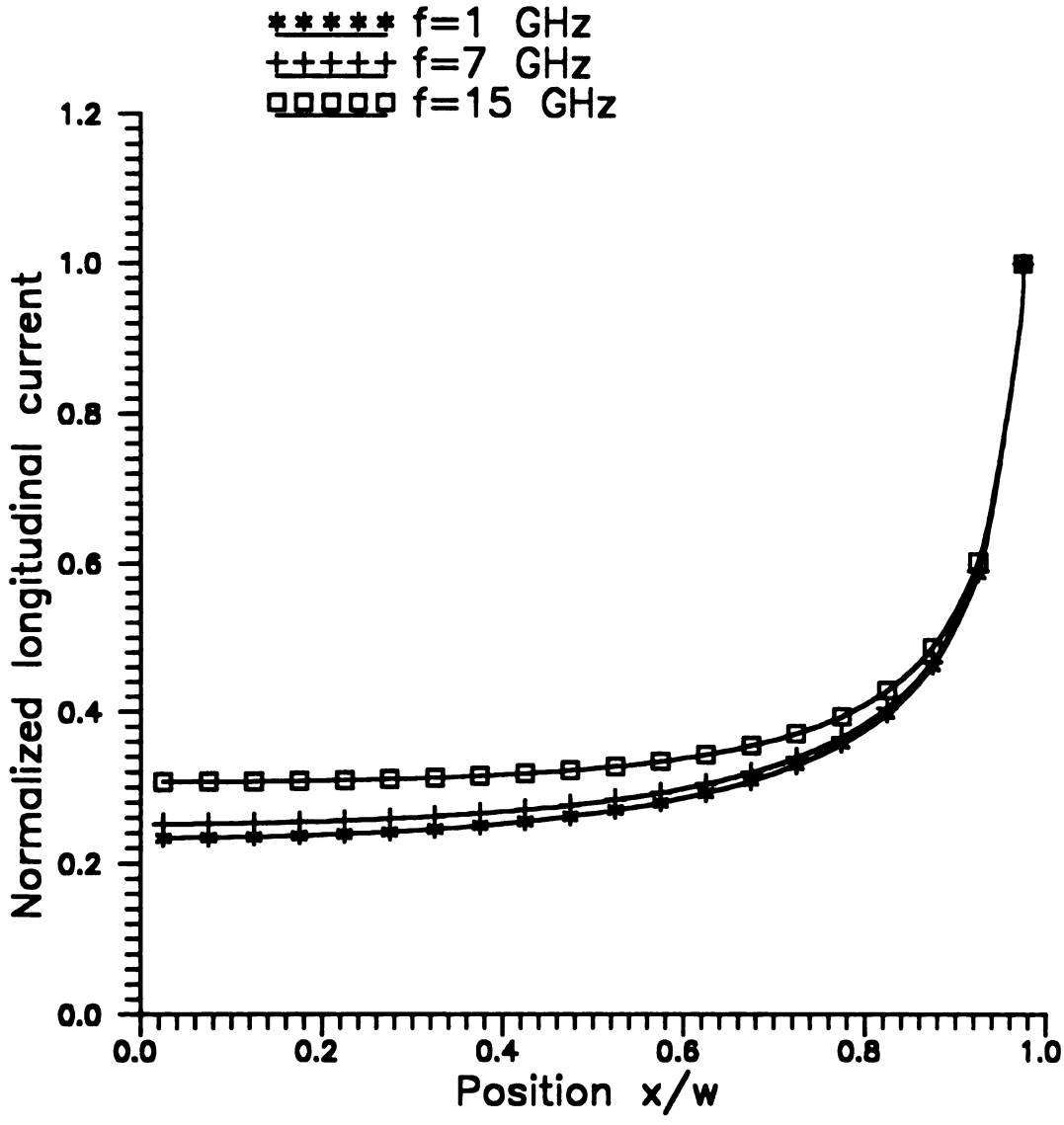

Figure 4.5: Frequency-dependent characteristics of normalized longitudinal current distribution, relevant to the example of Fig. 4.4.

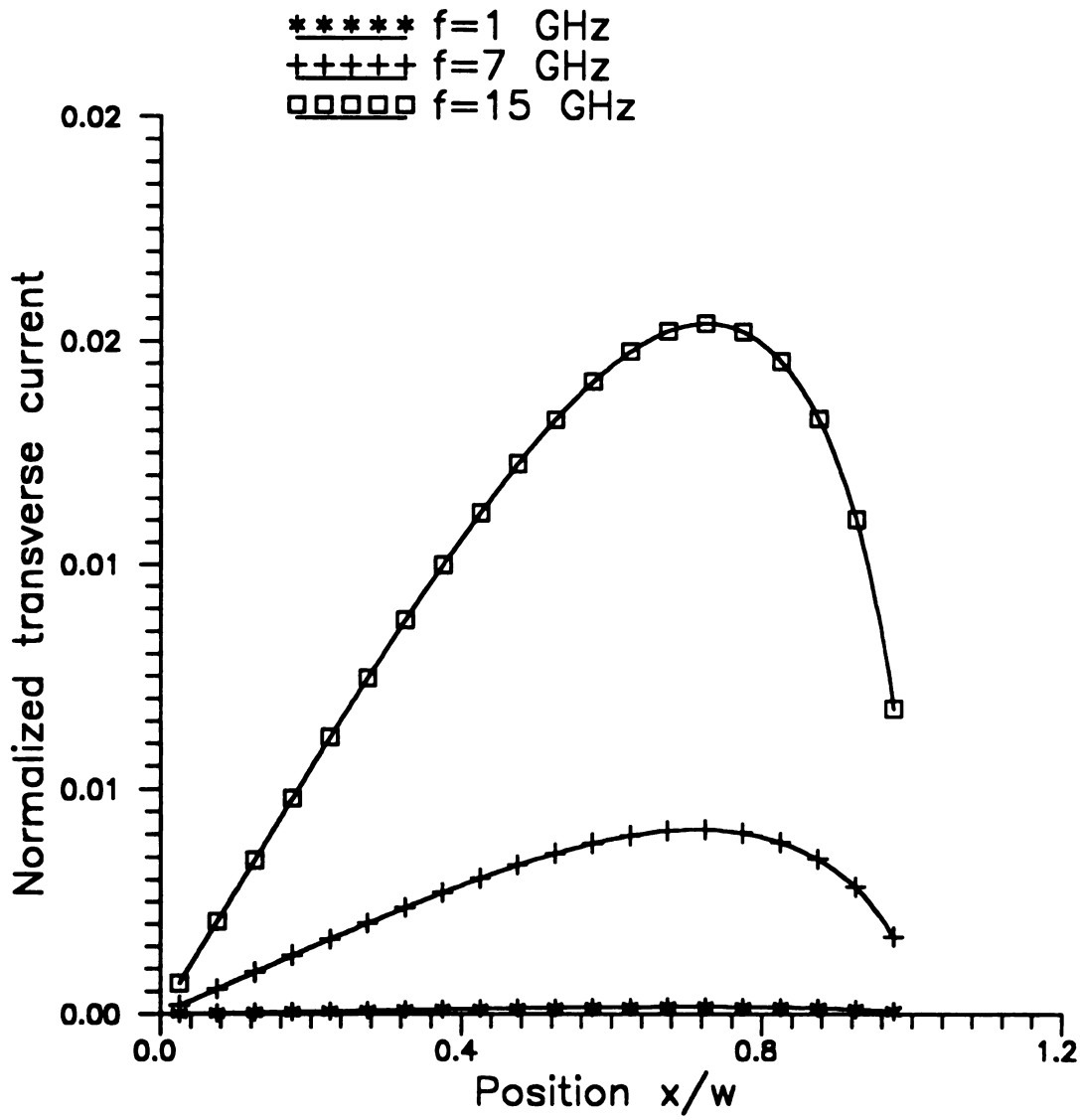

Figure 4.6: Frequency-dependent characteristics of normalized transverse current distribution, relevant to the example of Fig. 4.4.

CHAPTER 5

COMPUTATION OF CHARACTERISTIC IMPEDANCE OF MICROSTRIP TRANSMISSION LINE

5.1 INTRODUCTION

The dispersion characteristics of an open microstrip were evaluated in the previous chapter. In order to obtain a complete equivalent transmission line representation for the microstrip, not only the dispersion characteristics must be evaluated but also the characteristic impedance. As discussed in chapter two, due to the ambiguity in the definition of voltage for non-TEM structures such as the microstrip, the classical definition of characteristic impedance as the ratio of voltage to current is also ambiguous. However, it has been seen [13] that for a microstrip line, if the voltage is computed as a path integral from the ground plane to the microstrip and subsequently averaged as discussed below, this classical definition of characteristic impedance gives quite good results and it agrees with a more rigorous definition of characteristic impedance, namely the power-current method (to be discussed later). The voltage-current method is much more convenient and is less analytically involved.

The other method is based on the power-current definition of characteristic impedance ($Z = 2P/I^2$). In this power-current method, the power is computed as an integral of the poynting vector across the transverse section of the microstrip line.

5.2 VOLTAGE-CURRENT METHOD

This method has been tried for conducting planar transmission lines [13]. Consider an open microstrip line with only the principal mode propagating along the +z direction with propagation constant ζ_0. The voltage is calculated by integrating the y component of electric field along the y-axis from the ground plane to the strip conductor as follows

$$v(x) = \int_{gp}^{0} -e_{fy}(x,y)\,dy = -\int_{-t}^{0} e_{fy}(x,y)\,dy \ . \tag{1}$$

The above voltage being a function of x, its average over the microstrip region can be defined as

$$v_{av} = \frac{\int_{-w}^{w} v(x)\,dx}{2w} \tag{2}$$

or, alternatively as the weighted average

$$v_{av} = \frac{\int_{-w}^{w} v(x)\ k_z^*(x)\ dx}{\int_{-w}^{w} k_z^*(x)\ dx} \tag{3}$$

where the current density $k_z(x)$ is obtained in eqs. (4.52) and (4.53) from the MOM solution to the integral equation.

The spectral domain electric field in the film region is given as

$$\vec{e}_f(\vec{\rho}) = \frac{-j\eta_c}{k_c} \int_{-w}^{w} \vec{g}_f^{\,e}(x,y|x',0;-\zeta_0)\cdot\vec{k}(\vec{\rho}')\,dx' \tag{4}$$

With reference to Appendix B, the electric Green's dyad has the following scalar components

$$g^e_{\alpha\beta}(x,y|x',0;\zeta) = \frac{1}{2\pi}\int_{-\infty}^{\infty} B^e_{\alpha\beta}(\xi,\zeta,y)e^{j\xi(x-x')}d\xi \quad \cdots \text{for } \alpha,\beta = x,y,z\ . \tag{5}$$

Only the y-component of electric field is needed and is written as

$$e_{fy}(\vec{\rho}) = \frac{-j\eta_c}{k_c}\int_{-w}^{w}\{g^e_{yx}(x,y|x',0;-\zeta_0)k_x(x') + g^e_{yz}(x,y|x',0;-\zeta_0)k_z(x')\}dx' \tag{6}$$

where

$$\begin{aligned} B^e_{yx}(\xi,\zeta,y) &= \frac{j\xi p_f}{N_{fc}^2 Z^h(\lambda)}\frac{\cosh p_f(y+t)}{\sinh p_f t} + \frac{j\xi(k_f^2+p_f^2)(N_{fc}^2M_{fc}^2-1)}{N_{fc}^2Z^h(\lambda)Z^e(\lambda)}\frac{\cosh p_f(y+t)}{\cosh p_f t} \\ B^e_{yz}(\xi,\zeta,y) &= \frac{j\zeta p_f}{N_{fc}^2 Z^h(\lambda)}\frac{\cosh p_f(y+t)}{\sinh p_f t} + \frac{j\zeta(k_f^2+p_f^2)(N_{fc}^2M_{fc}^2-1)}{N_{fc}^2Z^h(\lambda)Z^e(\lambda)}\frac{\cosh p_f(y+t)}{\cosh p_f t}\ . \end{aligned} \tag{7}$$

Exploiting eq.(5) in relation (6) leads to

$$e_{fy}(\vec{\rho}) = \frac{-j\eta_c}{2\pi k_c}\int_{-w}^{w}\int_{-\infty}^{\infty}\{B^e_{yx}(\xi,-\zeta_0,y)k_x(x') + B^e_{yz}(\xi,-\zeta_0,y)k_z(x')\}e^{j\xi(x-x')}d\xi dx'\ . \tag{8}$$

Interchanging the spatial integration with the spectral one and recognizing that the spatial integral over the current can be interpreted as a Fourier transform on the variable x as follows

$$\begin{aligned} \int_{-w}^{w} k_x(x')e^{-j\xi x'}dx' &= \mathcal{F}\{k_x(x')\} = f_x(\xi) \\ \int_{-w}^{w} k_z(x')e^{-j\xi x'}dx &= \mathcal{F}\{k_z(x')\} = f_z(\xi) \end{aligned} \tag{9}$$

we have

$$e_{fy}(\vec{\rho}) = \frac{-j\eta_c}{2\pi k_c}\int_{-\infty}^{\infty}\{B_{yx}^{e}(\xi,-\zeta_0,y)f_x(\xi)+B_{yz}^{e}(\xi,-\zeta_0,y)f_z(\xi)\}e^{j\xi x}d\xi \ . \tag{10}$$

The current in eq. (9) is expressed as Chebyshev polynomial series given by eqs. (4.52) and (4.53). Hence, the integral in (9) can be evaluated in closed form. Referring to section 4.3, we have

$$f_\beta(\xi) = \int_{-w}^{w} k_\beta(x')e^{-j\xi x'}dx' = \sum_{n=1}^{N} a_{\beta n} f_{\beta n}(\xi) \quad \cdots for\ \beta = x,z \ . \tag{11}$$

where $f_{\beta n}(\xi)$ are evaluated in terms of Bessel functions as follows

$$\begin{aligned} f_{zn}(\xi) &= (-1)^n \pi w J_{2n}(\xi w) \\ f_{xn}(\xi) &= -j(-1)^n \frac{\pi w}{2}\left[J_{2n+1}(\xi w)+\frac{1}{2}J_{2(n+1)+1}(\xi w)+\frac{1}{2}J_{2(n-1)+1}(\xi w)\right]. \end{aligned} \tag{12}$$

Substituting the expression for the electric field into eq. (1), the average voltage in eq. (3) becomes

$$\begin{aligned} v_{av} &= \frac{-\int_{-w}^{w}\int_{-t}^{0} e_{fy}(x,y)k_z^*(x)dydx}{\int_{-w}^{w} k_z^* dx} \\ &= \frac{j\eta_c}{2\pi k_c}\frac{\int_{-w}^{w}dx\int_{-t}^{0}dy\int_{-\infty}^{\infty}\{B_{yx}^{e}(\xi,0,-\zeta_0,y)f_x(\xi)+B_{yz}^{e}(\xi,-\zeta_0,y)f_z(\xi)\}e^{j\xi x}d\xi k_z^*(x)}{\int_{-w}^{w} k_z^*(x)dx} \ . \end{aligned} \tag{13}$$

Interchanging the first spatial integration with the spectral one and using the fact that

$$\int_{-w}^{w} k_z^*(x)e^{j\xi x}dx = f_z^*(\xi) \tag{14}$$

the average voltage becomes

$$v_{av} = \frac{j\eta_c}{2\pi k_c} \frac{\int_{-t}^{0} dy \int_{-\infty}^{\infty} \{ B_{yx}^{e}(\xi,-\zeta_0,y) f_x(\xi) f_z^{*}(\xi) + B_{yz}^{e}(\xi,-\zeta_0,y) f_z(\xi) f_z^{*}(\xi) \} d\xi}{\int_{-w}^{w} k_z^{*}(x)\,dx} . \quad (15)$$

Now, the characteristic impedance is defined by

$$Z = \frac{v_{Av}}{I} \quad (16)$$

where the total longitudinal current I is given by

$$I = \int_{-w}^{w} k_z(x)\,dx . \quad (17)$$

Exploiting eqs. (15) and (17), the characteristic impedance is

$$Z = \frac{j\eta_c}{2\pi k_c} \frac{\int_{-t}^{0} dy \int_{-\infty}^{\infty} \{ B_{yx}^{e}(\xi,-\zeta_0,y) f_x(\xi) f_z^{*}(\xi) + B_{yz}^{e}(\xi,-\zeta_0,y) f_z(\xi) f_z^{*}(\xi) \} d\xi}{\int_{-w}^{w} k_z(x)\,dx \int_{-w}^{w} k_z^{*}(x)\,dx} . \quad (18)$$

The spatial integration in eq. (18) can be performed analytically to yield

$$\begin{aligned} \int_{-t}^{0} B_{yz}^{e}(\xi,-\zeta_0,y)\,dy &= \frac{-j\zeta_0}{N_c^2 Z^{h}(\lambda)} - \frac{j\zeta_0 (k_f^2 + p_f^2)(N_c^2 M_c^2 - 1)}{N_c^2 Z^{h}(\lambda) Z^{e}(\lambda) p_f} \tanh p_f t \\ &= -j\zeta_0 B^{e}(\xi,-\zeta_0) \\ \int_{-t}^{0} B_{yx}^{e}(\xi,-\zeta_0,y)\,dy &= j\xi B^{e}(\xi,-\zeta_0) \end{aligned} \quad (19)$$

where

$$B^e(\xi,-\zeta_0) = \frac{1}{N_c^2 Z^h(\lambda)} - \frac{(k_f^2+p_f^2)(N_c^2M_c^2-1)}{N_c^2 Z^h(\lambda)Z^e(\lambda)p_f}\tanh p_f t \ . \tag{20}$$

Using the fact that $k_z(x)$ is an even function of x and the orthogonality of Chebyshev polynomials, integral (18) can be readily evaluated. We obtain

$$I = \pi w a_{z0} \tag{21}$$

where a_{z0} is the first expansion coefficient in the series for the z-component of current.

Utilizing eqs. (19) and (20) in eq. (18), the final form of characteristic impedance is found as

$$Z = \frac{\eta_c}{2\pi^3 k_c w^2 |a_{z0}|^2} \int_{-\infty}^{\infty} \left[\zeta_0 B^e(\xi,-\zeta_0) f_z(\xi) f_z^*(\xi) - \xi B^e(\xi,-\zeta_0) f_x(\xi) f_z^*(\xi)\right] d\xi \ . \tag{22}$$

The integrand in the above expression is found to be an even function of ξ. Hence eq. (22) becomes

$$Z = \frac{\eta_c}{\pi^3 k_c w^2 |a_{z0}|^2} \int_{0}^{\infty} \left[\zeta_0 B^e(\xi,-\zeta_0) f_z(\xi) f_z^*(\xi) - \xi B^e(\xi,-\zeta_0) f_x(\xi) f_z^*(\xi)\right] d\xi \ . \tag{23}$$

The spectral integration in eq. (23) is evaluated numerically.

5.3 POWER-CURRENT METHOD

The characteristic impedance is defined in the power-current method, by

$$Z = \frac{2P_{av}}{I} \ . \tag{24}$$

The total longitudinal current I is available in eq. (20). The average power transported by the principal mode propagating along the microstrip is defined by the integral its poynting's vector over the transverse cross section as follows

$$\begin{aligned} P_{av} &= \frac{1}{2} Re \iint_{CS} (\vec{E}\times\vec{H}^*).\hat{z}\,dS \\ &= \frac{1}{2}\iint_{x\,y} (E_x H_y^* - E_y H_x^*)\,dx\,dy \end{aligned} \tag{25}$$

where E_α and H_α ($\alpha = x,y$) are the spatial domain fields excited by the eigenmode current. The electric fields in the cover and film layer are written in terms of the Hertz potential there as

$$\vec{E}_l(\vec{r}) = \left(k_l^2 + \nabla\nabla\cdot\right)\vec{\Pi}_l(\vec{r}) \quad \cdots for\ l = c,f\ . \tag{26}$$

The magnetic field is found from the electric field using a Maxwell equation as

$$\vec{H}_l(\vec{r}) = \frac{j}{\omega\mu_l}\nabla\times\vec{E}_l(\vec{r}) \quad \cdots for\ l = c,f. \tag{27}$$

The space-domain electric field is written as an inverse transform as follows

$$\vec{E}_l(\vec{r}) = \frac{1}{2\pi}\int_{-\infty}^{\infty} \vec{e}(\vec{\rho},\zeta)\,e^{j\zeta z}\,d\zeta \tag{28}$$

where the axially transformed field is given by

$$\vec{e}_l(\vec{\rho},\zeta) = \frac{-j\eta_c}{k_c}\int_c \vec{g}_l^{\,e}(\vec{\rho}\,|\,\vec{\rho}\,';\zeta)\cdot\vec{k}(\vec{\rho}\,',\zeta)\,dl' \quad \cdots for\ l = c,f\ . \tag{29}$$

The electric Green's function is obtained from the transform domain Hertz potential Green's function as follows

$$\vec{g}_l^{\,e}(\vec{\rho}\,|\,\vec{\rho}\,',\zeta) = (k_l^2 + \tilde{\nabla}\tilde{\nabla}\cdot)\tilde{g}_l(\vec{\rho}\,|\,\vec{\rho}\,';\zeta)\ . \tag{30}$$

The integration in eq. (28) is performed by deforming the real line contour and applying Cauchy's theorem for contour integral. The discrete propagation-mode contribution associated with pole singularities is found as

$$\vec{E}_l(\vec{r}) = j\sum_n \vec{e}_{nl}(\vec{\rho},\zeta_n)e^{-j\zeta_n z} . \tag{31}$$

For the single principal mode propagating in the $+z$ direction with propagation constant ζ_0, we have

$$\vec{E}_l(\vec{r}) = j\vec{e}_{0l}(\vec{\rho})e^{-j\zeta_0 z} . \tag{32}$$

The transverse components of the magnetic field are obtained from eqs. (25) and (30) as

$$\begin{aligned} H_x^*(\vec{r}) &= \left[\frac{-1}{\omega\mu^*}\frac{\partial e_z^*(\vec{\rho})}{\partial y} + \frac{j\zeta_0^*}{\omega\mu^*}e_y^*\right]e^{j\zeta_0 z} \\ H_y^*(\vec{r}) &= \left[\frac{-j\zeta_0^*}{\omega\mu^*}e_x^*(\vec{\rho}) + \frac{1}{\omega\mu^*}\frac{\partial e_z^*}{\partial x}\right]e^{j\zeta_0 z} . \end{aligned} \tag{33}$$

Using eqs. (32) and (33) in expression (28) and noting that $\omega\mu_l^* = k_l^*\eta_l^*$, the average power in each region is written in terms of spectral domain electric field as follows

$$P_{(av)l} = \frac{1}{2}Re\iint_{CS_l}\frac{1}{k_l^*\eta_l^*}\left[\zeta_0(e_{xl}e_{xl}^* + e_{yl}e_{yl}^*) + j(e_{xl}\frac{\partial e_{zl}^*}{\partial x} + e_{yl}\frac{\partial e_{zl}^*}{\partial y})\right]dxdy . \tag{34}$$

In the next subsection, the power flow in the film and cover regions will be calculated in detail in order to evaluate the characteristic impedance.

5.3.1 Power in the Cover Region

In the cover region, the eigenmode electric field is expressed by eq. (29) as follows

$$\vec{e}_c(\vec{\rho}) = \frac{-j\eta_c}{k_c}\int_{-w}^{w} \vec{g}_c^{\,e}(x,y|x',0;-\zeta_0)\cdot\vec{k}(x')dx' \,. \tag{35}$$

The electric Green's dyad has the following scalar components

$$g_{\alpha\beta}^{e}(x,y|x',0;\zeta) = \frac{1}{2\pi}\int_{-\infty}^{\infty} C_{\alpha\beta}^{e}(\xi,\zeta)e^{-p_c y}e^{j\xi(x-x')}d\xi \quad \cdots \textit{for } \alpha,\beta = x,y,z \,. \tag{36}$$

where the coefficients are obtained in Appendix B as follows

$$\begin{aligned}
C_{xx}^{e} &= \frac{(k_c^2-\xi^2)M_c^2}{Z^h} + \frac{p_c\xi^2(N_c^2M_c^2-1)}{Z^h(\lambda)Z^e(\lambda)} \\
C_{yx}^{e} &= \frac{-j\xi p_c M_c^2}{Z^h} + \frac{j\xi(k_c^2+p_c^2)(N_c^2M_c^2-1)}{Z^h(\lambda)Z^e(\lambda)} \\
C_{zx}^{e} &= C_{xz}^{e} = \frac{-\zeta\xi M_c^2}{Z^h} + \frac{p_c\xi\zeta(N_c^2M_c^2-1)}{Z^h(\lambda)Z^e(\lambda)} \\
C_{yz}^{e} &= \frac{-j\zeta p_c M_c^2}{Z^h} + \frac{j\zeta(k_c^2+p_c^2)(N_c^2M_c^2-1)}{Z^h(\lambda)Z^e(\lambda)} \\
C_{zz}^{e} &= \frac{(k_c^2-\zeta^2)M_c^2}{Z^h} + \frac{p_c\zeta^2(N_c^2M_c^2-1)}{Z^h(\lambda)Z^e(\lambda)} \,.
\end{aligned} \tag{37}$$

Substituting the above Green's function into eq. (33), and interchanging the spatial integration with the spectral one, the scalar field components are obtained as follows

$$e_{cx} = \frac{-j\eta_c}{2\pi k_c}\int_{-\infty}^{\infty} F_x(\xi,-\zeta_0)e^{j\xi x}e^{-p_c y}d\xi$$

$$e_{cy} = \frac{-j\eta_c}{2\pi k_c}\int_{-\infty}^{\infty} F_y(\xi,-\zeta_0)e^{j\xi x}e^{-p_c y}d\xi \qquad (38)$$

$$e_{cz} = \frac{-j\eta_c}{2\pi k_c}\int_{-\infty}^{\infty} F_z(\xi,-\zeta_0)e^{j\xi x}e^{-p_c y}d\xi$$

where

$$F_\alpha(\xi,-\zeta_0) = C^e_{\alpha x}f_x(\xi) + C^e_{\alpha z}f_z(\xi) \quad \cdots \text{for } \alpha = x,y,z\ . \qquad (39)$$

The spatial integration over the current is again denoted

$$f_\beta(\xi) = \int_{-w}^{w} k_\beta(x')e^{-j\xi x'}dx' \quad \cdots \text{for } \beta = x,z \qquad (40)$$

and has been evaluated previously in section 5.2 as given by eq. (12).

Noticing that $\partial e_z^*/\partial x = -j\xi e_z^*$ and $\partial e_z^*/\partial y = -p_c e_z^*$ and exploiting eqs. (36) in (32), the average power in the cover region is obtained as

$$P_{(av)c} = \frac{1}{2(2\pi)^2}\,Re\,\frac{\eta_c}{|k_c|^2 k_c^*}\int_{-\infty}^{\infty}dx\int_0^{\infty}dy$$

$$\left\{\zeta_0^*\left[\left(\int_{-\infty}^{\infty}F_x(\xi,-\zeta_0)e^{j\xi x}e^{-p_c y}d\xi\right)\left(\int_{-\infty}^{\infty}F_x^*(\xi',-\zeta_0)e^{j\xi' x}e^{-p_c^* y}d\xi'\right)\right.\right.$$

$$\left.\left.+\left(\int_{-\infty}^{\infty}F_y(\xi,-\zeta_0)e^{j\xi x}e^{-p_c y}d\xi\right)\left(\int_{-\infty}^{\infty}F_y^*(\xi',-\zeta_0)e^{j\xi' x}e^{-p_c^* y}d\xi'\right)\right] \qquad (41)$$

$$+\left(\int_{-\infty}^{\infty}F_x(\xi,-\zeta_0)e^{j\xi x}e^{-p_c y}d\xi\right)\left(\int_{-\infty}^{\infty}\xi' F_z^*(\xi',-\zeta_0)e^{j\xi' x}e^{-p_c^* y}d\xi'\right)$$

$$\left.-jp_c^*\left(\int_{-\infty}^{\infty}F_y(\xi,-\zeta_0)e^{j\xi x}e^{-p_c y}d\xi\right)\left(\int_{-\infty}^{\infty}F_z^*(\xi',-\zeta_0)e^{j\xi' x}e^{-p_c^* y}d\xi'\right)\right\}.$$

The integrands are all well behaved. Hence, interchanging the spatial and spectral integration is permissible and leads to

$$P_{(av)c} = \frac{1}{2(2\pi)^2} Re \frac{\eta_c}{|k_c|^2 k_c^*} \left\{ \iint_{-\infty}^{\infty} \zeta_0^* \left[F_x F_x^* + F_y F_y^* \right] d\xi \, d\xi' \int_0^{\infty} e^{-(p_c + p_c^*)y} dy \int_{-\infty}^{\infty} e^{j(\xi - \xi')x} dx \right.$$
$$+ \iint_{-\infty}^{\infty} \xi' F_x F_z^* \, d\xi d\xi' \int_0^{\infty} e^{-(p_c + p_c^*)y} dy \int_{-\infty}^{\infty} e^{j(\xi - \xi')x} dx \qquad (42)$$
$$\left. - jp_c^* \iint_{-\infty}^{\infty} F_y F_z \int_0^{\infty} e^{-(p_c + p_c^*)y} dy \int_{-\infty}^{\infty} e^{j(\xi - \xi')x} dx \right\} .$$

The spatial integrations can be evaluated analytically using

$$\int_{-\infty}^{\infty} e^{j(\xi - \xi')x} dx = 2\pi \delta(x - x')$$
$$\int_0^{\infty} e^{-(p_c + p_c^*)y} dy = \frac{1}{p_c + p_c^*} . \qquad (43)$$

Hence, the expression for the power in the cover region becomes

$$P_{(av)c} = \frac{1}{4\pi |k_c|^2} Re \left\{ \frac{\eta_c}{k_c^*} \int_{-\infty}^{\infty} \frac{\zeta_0^* (F_x F_x^* + F_y F_y^*) + \xi F_x F_z^* - jp_c^* F_y F_z^*}{p_c + p_c^*} d\xi \right\} . \qquad (44)$$

Examination of the integrand in (44) shows that it is an even function of ξ, hence the power in the cover region is finally obtained as

$$P_{(av)c} = \frac{1}{2\pi |k_c|^2} Re \left\{ \frac{\eta_c}{k_c^*} \int_0^{\infty} \frac{\zeta_0^* (F_x F_x^* + F_y F_y^*) + \xi F_x F_z^* - jp_c^* F_y F_z^*}{p_c + p_c^*} d\xi \right\} . \qquad (45)$$

The above integration is performed numerically.

5.3.2 Power in the Film Region

The power in the film region is given by eq. (34) as follows

$$P_{(avf} = \frac{1}{2} Re \int_{-\infty}^{\infty} \int_{-t}^{0} \frac{1}{k_f^* \eta_f^*} \left[\zeta_0 (e_{fx} e_{fx}^* + e_{fy} e_{fy}^*) + j (e_{fx} \frac{\partial e_{fz}^*}{\partial x} + e_{fy} \frac{\partial e_{fz}^*}{\partial y}) \right] dx dy \ . \qquad (46)$$

The spectral domain electric field in the film region is given by eq. (4). The scalar components of electric field are obtained as

$$e_{f\alpha}(x,y) = \frac{-j\eta_c}{k_c} \int_{-w}^{w} \{ g_{\alpha x}^e(x,y|x',0,-\zeta_0) k_x(x') + g_{\alpha z}^e(x,y|x',0,-\zeta_0) k_z(x') \} dx' \qquad (47)$$

$$\cdots \textit{for } \alpha = x,y,z \ .$$

The scalar components of the electric Green's dyad are given by eq. (5). Some of the coefficients were obtained in section 5.2. In this section, all the coefficients are needed and expressed as

$$\begin{aligned}
B_{xx}^e(\xi,\zeta,y) &= \frac{k_f^2 - \xi^2}{N_c^2 Z^h(\lambda)} \frac{\sinh[p_f(y+t)]}{\sinh p_f t} - \frac{\xi^2 p_f (N_c^2 M_c^2 - 1)}{N_c^2 Z^h(\lambda) Z^e(\lambda)} \frac{\sinh[p_f(y+t)]}{\cosh p_f t} \\
B_{yx}^e(\xi,\zeta,y) &= \frac{j\xi p_f}{N_c^2 Z^h(\lambda)} \frac{\cosh[p_f(y+t)]}{\sinh p_f t} + \frac{j\xi (k_f^2 + p_f^2)(N_c^2 M_c^2 - 1)}{N_c^2 Z^h(\lambda) Z^e(\lambda)} \frac{\cosh[p_f(y+t)]}{\cosh p_f t} \\
B_{zx}^e(\xi,\zeta,y) &= \frac{-\xi\zeta}{N_c^2 Z^h(\lambda)} \frac{\sinh[p_f(y+t)]}{\sinh p_f t} - \frac{\zeta \xi p_f (N_c^2 M_c^2 - 1)}{N_c^2 Z^h(\lambda) Z^e(\lambda)} \frac{\sinh[p_f(y+t)]}{\cosh p_f t} \qquad (48) \\
B_{xz}^e(\xi,\zeta,y) &= B_{zx}^e(\xi,\zeta,y) \\
B_{yz}^e(\xi,\zeta,y) &= \frac{j\zeta p_f}{N_c^2 Z^h(\lambda)} \frac{\cosh[p_f(y+t)]}{\sinh p_f t} + \frac{j\zeta (k_f^2 + p_f^2)(N_c^2 M_c^2 - 1)}{N_c^2 Z^h(\lambda) Z^e(\lambda)} \frac{\cosh[p_f(y+t)]}{\cosh p_f t} \\
B_{zz}^e(\xi,\zeta,y) &= \frac{k_f^2 - \zeta^2}{N_c^2 Z^h(\lambda)} \frac{\sinh[p_f(y+t)]}{\sinh p_f t} - \frac{\zeta^2 p_f (N_c^2 M_c^2 - 1)}{N_c^2 Z^h(\lambda) Z^e(\lambda)} \frac{\sinh[p_f(y+t)]}{\cosh p_f t} \ .
\end{aligned}$$

Substituting eq. (5) into expression (46), and interchanging the spatial integra-

tion with the spectral one, the scalar field components are obtained as follows

$$
\begin{aligned}
e_{fx}(x,y) &= \frac{-j\eta_c}{2\pi k_c}\int_{-\infty}^{\infty}\left[\frac{F_x(\xi,-\zeta_0)}{\sinh p_f t}+\frac{G_x(\xi,-\zeta_0)}{\cosh p_f t}\right]\sinh[p_f(y+t)]e^{j\xi x}d\xi \\
e_{fy}(x,y) &= \frac{-j\eta_c}{2\pi k_c}\int_{-\infty}^{\infty}\left[\frac{F_y(\xi,-\zeta_0)}{\sinh p_f t}+\frac{G_y(\xi,-\zeta_0)}{\cosh p_f t}\right]\cosh[p_f(y+t)]e^{j\xi x}d\xi \\
e_{fz}(x,y) &= \frac{-j\eta_c}{2\pi k_c}\int_{-\infty}^{\infty}\left[\frac{F_z(\xi,-\zeta_0)}{\sinh p_f t}+\frac{G_z(\xi,-\zeta_0)}{\cosh p_f t}\right]\sinh[p_f(y+t)]e^{j\xi x}d\xi
\end{aligned}
\tag{49}
$$

where

$$
\begin{aligned}
F_x(\xi,\zeta) &= \frac{(k_f^2-\xi^2)f_x(\xi)-\xi\zeta f_z(\xi)}{N_c^2 Z^h} \\
G_x(\xi,\zeta) &= \frac{-(N_c^2M_c^2-1)p_f\xi\,[\xi f_x(\xi)+\zeta f_z(\xi)]}{N_c^2 Z^e Z^h} \\
F_y(\xi,\zeta) &= \frac{j\xi p_f f_x(\xi)+j\zeta f_z(\xi)}{N_c^2 Z^h} \\
G_y(\xi,\zeta) &= \frac{j(N_c^2M_c^2-1)(p_f^2+k_f^2)[\xi f_x(\xi)+\zeta f_z(\xi)]}{N_c^2 Z^e Z^h} \\
F_z(\xi,\zeta) &= \frac{-\zeta\xi f_x(\xi)+(k_f^2-\zeta^2)f_z(\xi)}{N_c^2 Z^h} \\
G_z(\xi,\zeta) &= \frac{-(N_c^2M_c^2-1)p_f\zeta\,[\xi f_x(\xi)+\zeta f_z(\xi)]}{N_c^2 Z^e Z^h}
\end{aligned}
\tag{50}
$$

and $f_x(\xi)$ and $f_z(\xi)$ are those given by eqs. (11) and (12).

Similar to the case of the power in the cover region, the fields are well behaved functions, hence interchanging the spectral integration with the spatial ones is allowed after exploiting eq. (47) in relation (44). Again, the integration with respect to x gives rise to a δ-distribution. The integrals with respect to y fall into six catego-

ries

$$
\begin{aligned}
Y_1 &= \int_{-t}^{0} \frac{\sinh p_f(y+t)\sinh p_f^*(y+t)}{\sinh p_f t \sinh p_f^* t}\,dy \\
Y_2 &= \int_{-t}^{0} \frac{\sinh p_f(y+t)\sinh p_f^*(y+t)}{\sinh p_f t \cosh p_f^* t}\,dy \\
Y_3 &= \int_{-t}^{0} \frac{\sinh p_f(y+t)\sinh p_f^*(y+t)}{\cosh p_f t \cosh p_f^* t}\,dy \\
Z_1 &= \int_{-t}^{0} \frac{\cosh p_f(y+t)\cosh p_f^*(y+t)}{\sinh p_f t \sinh p_f^* t}\,dy \\
Z_2 &= \int_{-t}^{0} \frac{\cosh p_f(y+t)\cosh p_f^*(y+t)}{\cosh p_f t \cosh p_f^* t}\,dy \\
Z_3 &= \int_{-t}^{0} \frac{\cosh p_f(y+t)\cosh p_f^*(y+t)}{\sinh p_f t \cosh p_f^* t}\,dy \,.
\end{aligned}
\tag{51}
$$

Each of the above integrals can be evaluated analytically. Hence the power in the film region is obtained as

$$
\begin{aligned}
P_{(avg)f} = \frac{|\eta_c|^2}{2(2\pi)\,|k_c|^2}\, Re \int_{-\infty}^{\infty} \frac{1}{k_f^*\,\eta_f^*} \Big\{ \zeta_0^* \Big[& F_x F_x^* Y_1 + F_x G_x^* Y_2 + G_x F_x^* Y_2^* + G_x G_x^* Y_3 \\
& + F_y F_y^* Z_1 + F_y G_y^* Z_3 + F_y^* G_y Z_3^* + G_y G_y^* Z_2 \Big] \\
& + \xi \Big[F_x F_z^* Y_1 + F_x G_z^* Y_2 + G_x F_z^* Y_2^* + G_x G_z^* Y_3 \Big] \\
& + j p_f^* \Big[F_y F_z^* Z_1 + F_y G_z^* Z_3 + G_y F_z^* Z_3^* + G_y G_z^* Z_2 \Big] \Big\}\, d\xi \,.
\end{aligned}
\tag{52}
$$

The integrand in eq. (52) is an even function of ξ. Therefore the power in the film region is finally obtained as

$$P_{(av)f} = \frac{|\eta_c|^2}{(2\pi)|k_c|^2} Re \int_0^\infty \frac{1}{k_f^* \eta_f^*} \{\zeta_0^* [F_x F_x^* Y_1 + F_x G_x^* Y_2 + G_x F_x^* Y_2^* + G_x G_x^* Y_3 + F_y F_y^* Z_1 + F_y G_y^* Z_3 + F_y^* G_y Z_3^* + G_y G_y^* Z_2] + \xi [F_x F_z^* Y_1 + F_x G_z^* Y_2 + G_x F_z^* Y_2^* + G_x G_z^* Y_3] + jp_f^* [F_y F_z^* Z_1 + F_y G_z^* Z_3 + G_y F_z^* Z_3^* + G_y G_z^* Z_2]\} d\xi \ . \quad (53)$$

The above integration is again performed numerically.

The characteristic impedance for the principal mode of a single microstrip line is obtained from eqs. (24), (45) and (53) as

$$Z = \frac{2}{\pi^2 w^2 a_{z0}^2} (P_{(av)c} + P_{(av)f}) \quad (54)$$

5.4 NUMERICAL RESULTS

Figure 5.1 shows the frequency dependence of the characteristic impedance for the same open microstrip transmission line studied in Chapter 4. At each frequency, the characteristic impedance for the microstrip line can be evaluated after a characteristic value of ζ_0 has been found. The voltage-current method is adopted. It is clear from Fig. 5.1 that exploiting both the transverse and longitudinal current components in the expression for the characteristic impedance gives results very close to those obtained using only the longitudinal component of current. Hence, neglecting the transverse component to evaluate the characteristic impedance is justified.

In Figure 5.2, the power-current method is compared with the voltage-current one. It is clear that the power-current method has the most TEM-like character [41], since the characteristic impedance is relatively constant at low frequencies and only starts to increase at higher frequencies, as compared with the voltage-current results.

They both coincide at very low frequencies as expected.

Figure 5.3 shows the characteristic impedance a function of microstrip width for both the power-current and the voltage-current method. As expected, the characteristic impedance decreases with an increase in the width $2w$ of the microstrip. This is because for the very wide microstrip line, nearly all of the field is confined to the substrate dielectric, the structure resembles a parallel-plate structure. In the case of very narrow microstrip, the field is almost equally shared by the cover and the substrate.

Figure 5.4 shows the characteristic impedance as a function of frequency for a microstrip of width $2w = 3.04\,mm$, substrate height $t = 3.17\,mm$, and $\epsilon_r = 11.7$. Our results are compared to those obtained by Dezutter [41] for both the power-current and the voltage-current method. Our results agree with those in [41] in the sense that the power-current method demonstrates a TEM-like behavior as the characteristic impedance only starts to increase at higher frequencies. Our results were obtained using only two terms in the Chebyshev series expansion for the current whereas in [41], a large number of triangular basis functions were required. This illustrates the advantage of using Chebyshev polynomials as basis functions against triangular basis functions used by the latter authors.

Finally, our results are compared to those presented by Pozar [13] for the characteristic impedance versus microstrip width for a microstrip line of substrate thickness $t = 1.27\,mm$ and $\epsilon_r = 10.2$. This comparison is shown in Figure 5.5. Our results differ by 3% from the results in [13]. This is mainly due to inaccurate modeling of the currents in the latter effort.

5.5 SUMMARY

A full-wave analysis for the characteristic impedance using both voltage-current and power-current definitions is presented. It is shown that the voltage-current method gives results very close to those of the more rigorous power-current method. Hence, the voltage-current method will be adopted later since it is less analytically involved than the power-current method. The dependence of characteristic impedance upon frequency was a controversial issue since quite different functions of frequency have been predicted. It is established in this chapter that, for the conventional microstrip, the characteristic impedance will always increase with frequency.

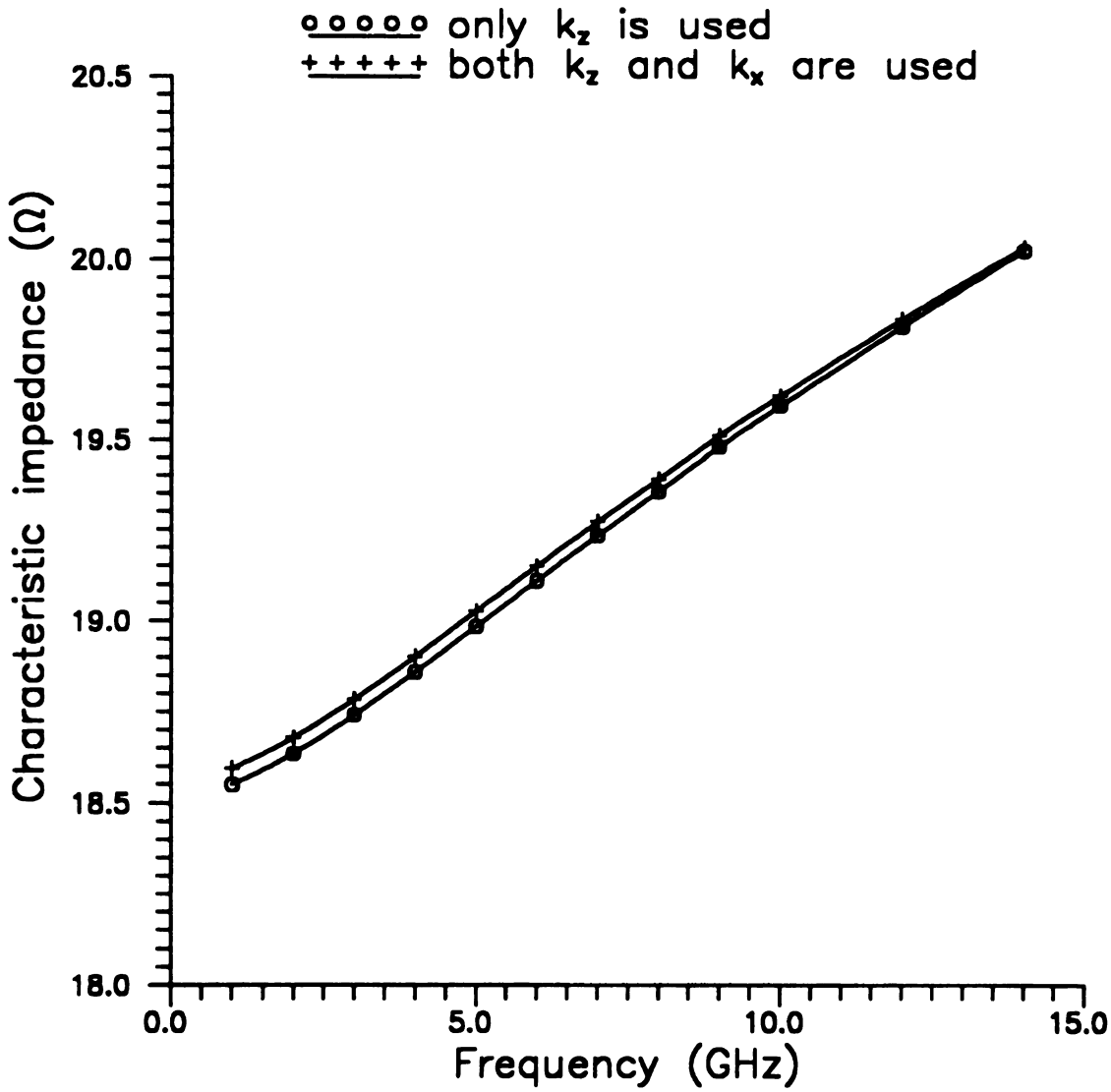

Figure 5.1: Characteristic impedance versus frequency using the voltage-current method (w = 1.5 mm, t = 0.635 mm, and ϵ_r = 9.8).

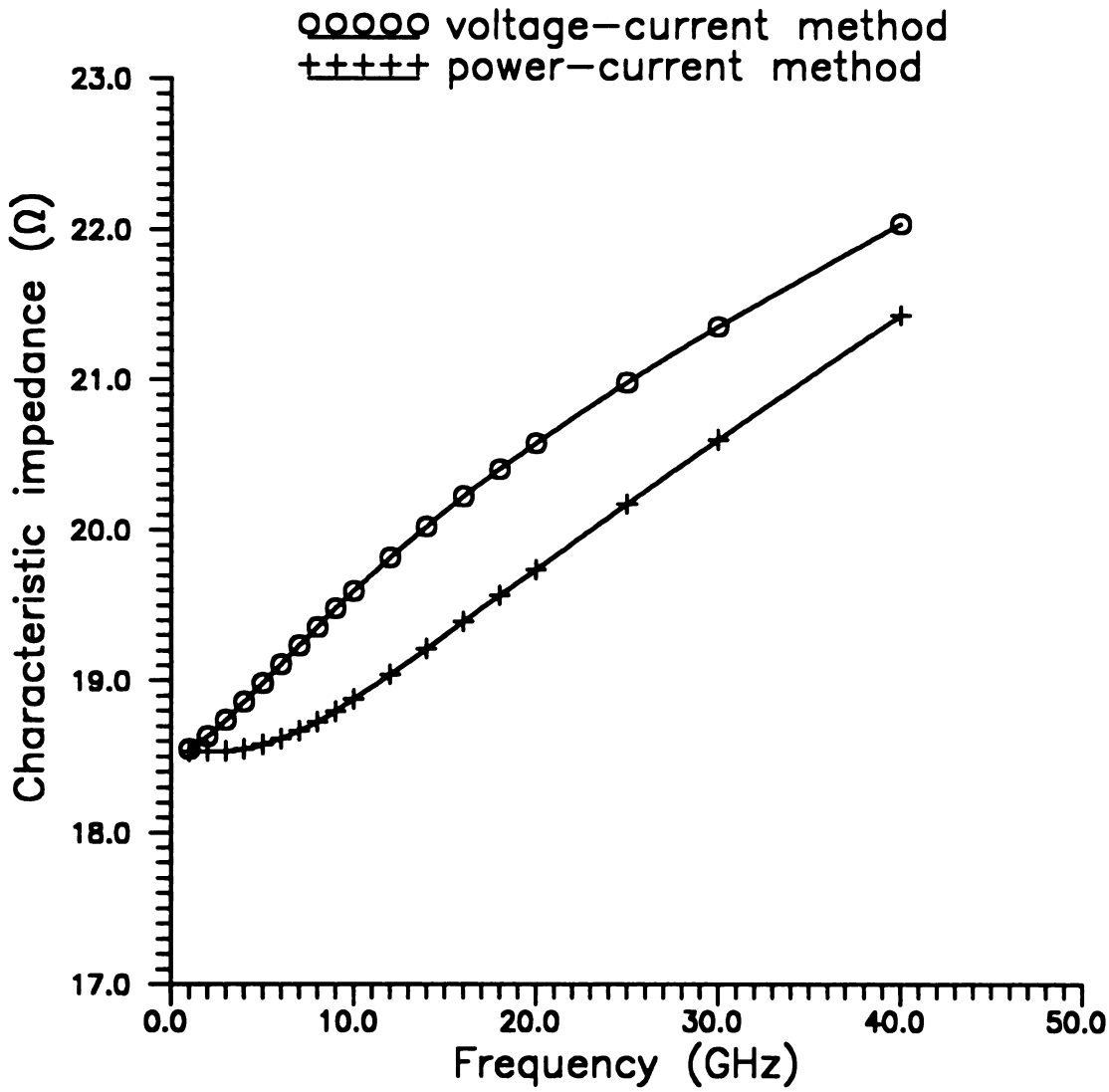

Figure 5.2: Characteristic impedance versus frequency for two different methods (w = 1.5 mm, t = 0.635 mm, and ϵ_r = 9.8).

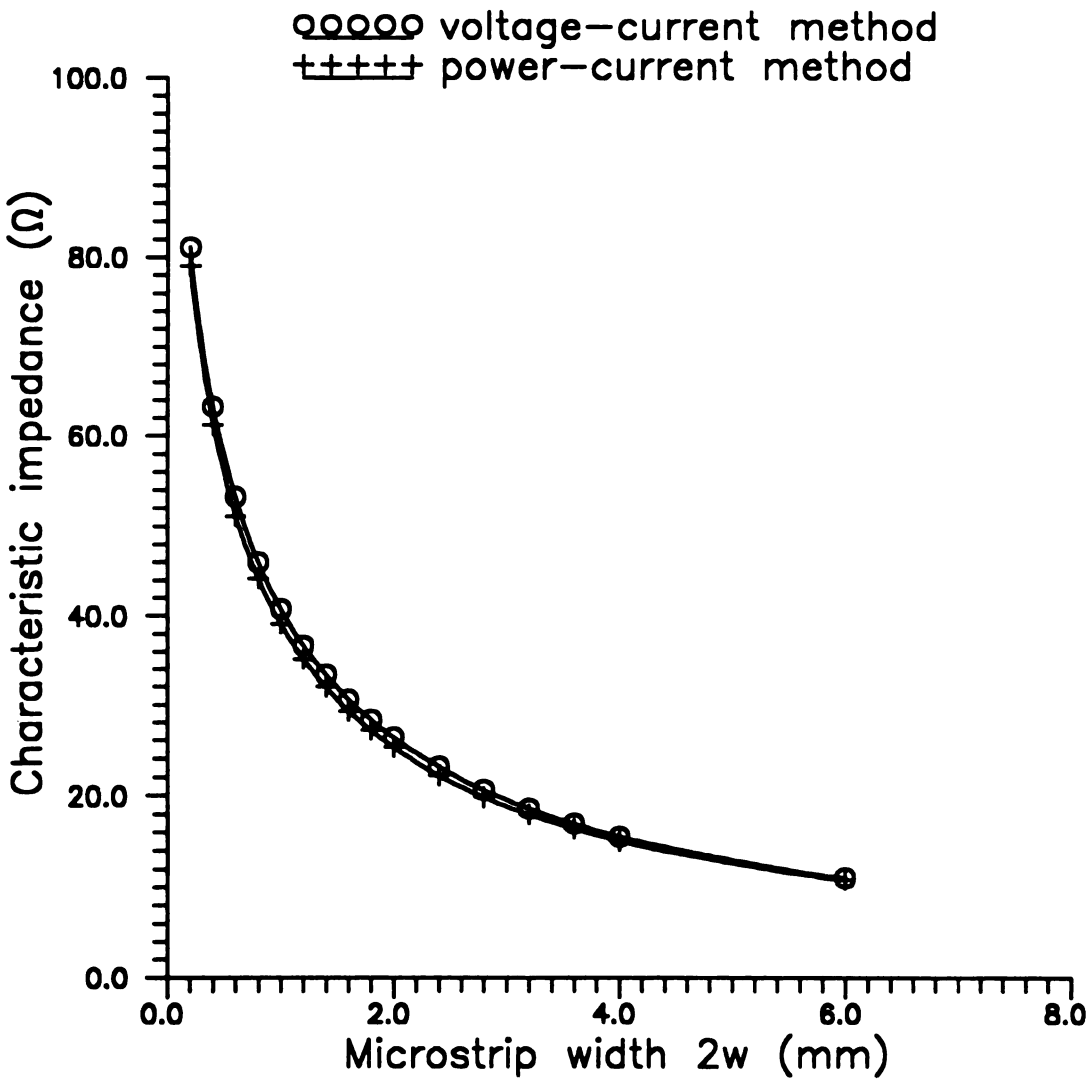

Figure 5.3: Characteristic impedance as a function of microstrip width at 10 GHz (t = 0.635 mm, and ϵ_r = 9.8).

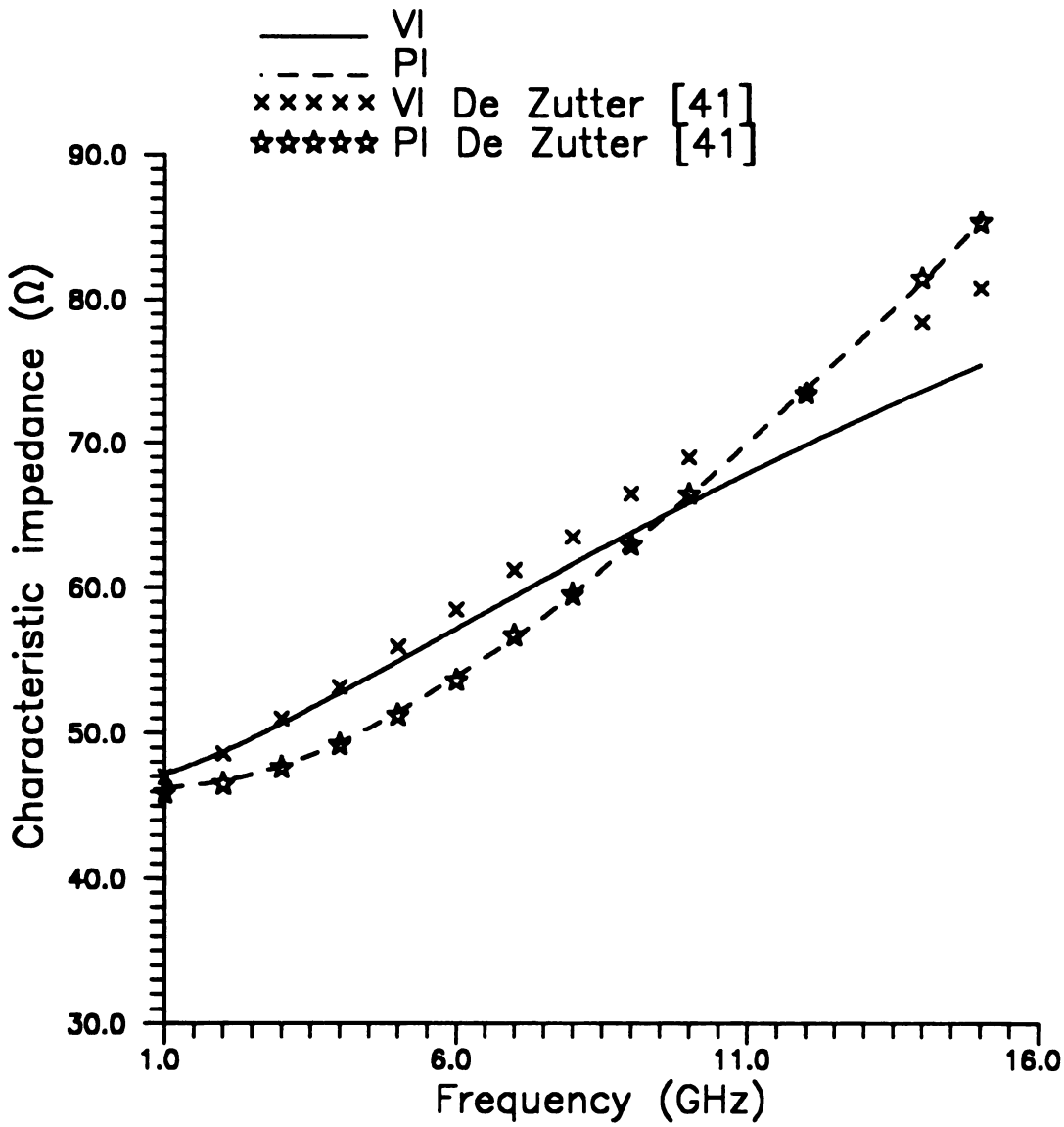

Figure 5.4: Comparison of characteristic impedance with published results (w = 1.52 mm, t = 3.17 mm, ϵ_r = 11.7).

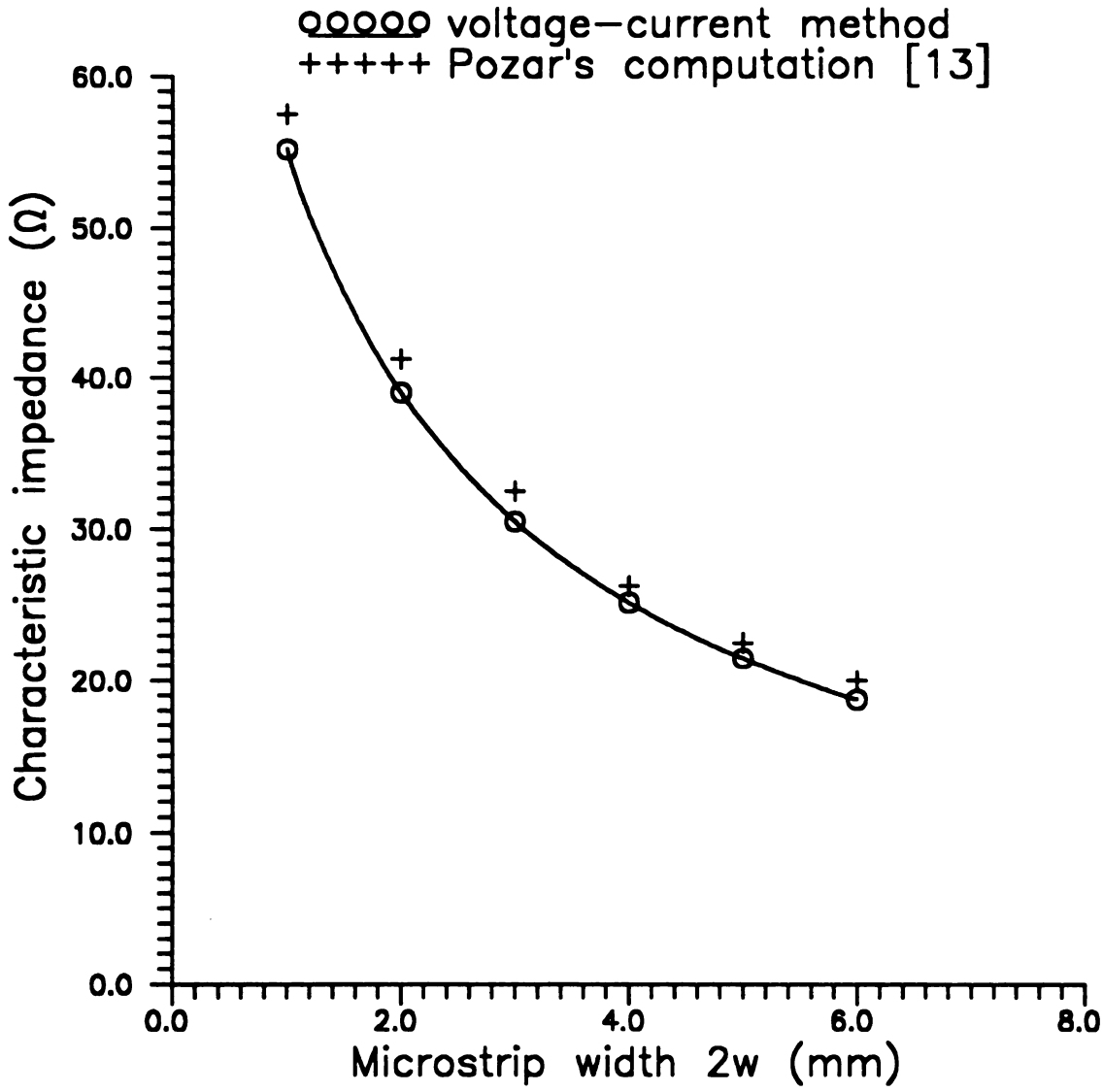

Figure 5.5: Comparison of characteristic impedance versus microstrip width with Pozar's results at 3 GHz. (t = 1.27 mm, ϵ_r = 10.2).

CHAPTER 6

ANALYSIS OF MICROSTRIP STRUCTURE WITH SUPERSTRATE LAYER

6.1 INTRODUCTION

The rigorous analysis of printed circuit elements such as microstrips requires the use of the dyadic Green's function associated with the layered background. In this chapter, a microstrip structure with a superstrate layer is analyzed. The microstrip device is printed on the substrate layer and resides in the superstrate region as shown in Fig. 6.1. Hence, for the geometry of Fig. 6.1 the dyadic Green's function is needed. We begin by specializing the results from chapter three to obtain the EM fields in the superstrate and in the substrate regions of the layered environment of Fig. 6.2. We note that this otherwise extensive effort was made relatively easy by using wave transmission matrices. Moreover, to our knowledge, the microstrip with a superstrate has not been extensively analyzed in the literature.

Based on the integral-equation formulation, we study the microstrip line with a superstrate by an approach similar to that used for an open microstrip. A rigorous full-wave solution to the integral equation is pursued again using the Galerkin's method of moments. The dispersion characteristics and current distributions of the guiding structure will be analyzed.

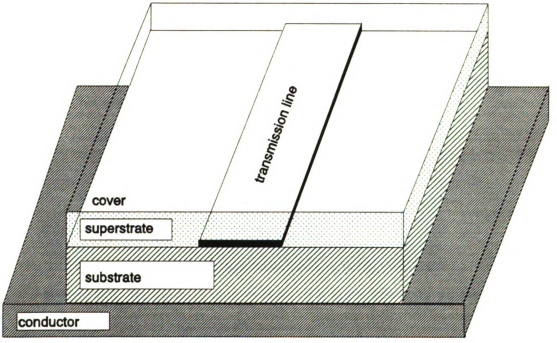

Figure 6.1: Microstrip with a superstrate layer

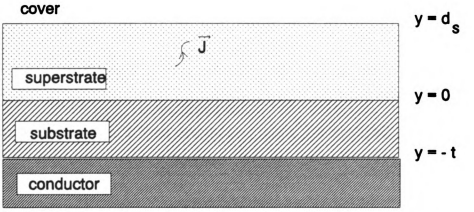

Figure 6.2: Background environment of a microstrip with superstrate.

6.2 FIELDS IN THE SUPERSTRATE LAYER

The four-layered conductor/substrate/superstrate/cover structure is depicted in Fig. 6.2. The superstrate region resides between interface c and interface s. The electric current source is embedded in the superstrate region. The electric field in the superstrate layer is formulated as follows

$$\vec{E}_s(\vec{r}) = \frac{-j\eta_s}{k_s}\int_V \ddot{G}_{ss}^{e}(\vec{r}|\vec{r}')\cdot \vec{J}(\vec{r}')dv' \tag{1}$$

where the electric Green's dyad is identified in terms of a Hertz potential Green's dyad as

$$\ddot{G}_{ss}^{e}(\vec{r}|\vec{r}') = PV(k_s^2+\nabla\nabla\cdot)\ddot{G}_{ss}(\vec{r}|\vec{r}') + \ddot{L}\delta(\vec{r}-\vec{r}') \ . \tag{2}$$

The Hertz potential Green's dyad decomposes into a principal part and a scattered part as follows

$$\ddot{G}_{ss} = \ddot{I}G_s^p + \ddot{G}_{ss}^{s} \ . \tag{3}$$

The principal Green's function is written as

$$G_s^p(\vec{r}|\vec{r}') = \int\int_{-\infty}^{\infty} \frac{e^{j\vec{\lambda}\cdot(\vec{r}-\vec{r}')}\ e^{-p_s|y-y'|}}{2(2\pi)^2 p_s}\ d^2\lambda \tag{4}$$

while the scattered Green's function is formulated as

$$\ddot{G}_{ss}^{s}(\vec{r}|\vec{r}') = (\hat{x}\hat{x}+\hat{z}\hat{z})G_{ssx}^{s} + \hat{y}\left[\left(\hat{x}\frac{\partial}{\partial x}+\hat{z}\frac{\partial}{\partial z}\right)G_{ssc}^{s} + G_{ssn}^{s}\hat{y}\right] . \tag{5}$$

The scattered dyad has the following scalar components

$$\begin{Bmatrix} G^s_{sst}(\vec{r}|\vec{r}') \\ G^s_{ssn}(\vec{r}|\vec{r}') \\ G^s_{ssc}(\vec{r}|\vec{r}') \end{Bmatrix} = \iint_{-\infty}^{\infty} \begin{Bmatrix} S^t_{ss}(y|y',\lambda) \\ S^n_{ss}(y|y',\lambda) \\ S^c_{ss}(y|y',\lambda) \end{Bmatrix} \frac{e^{j\vec{\lambda}\cdot(\vec{r}-\vec{r}')}}{2(2\pi)^2 p_s} d^2\lambda \ . \tag{6}$$

The scattering coefficients S^q_{ss} can be determined through wave transmission and coupling matrices as in chapter three, and assume the form

$$S^q_{ss} = \sum_{k=1}^{4} B^q_{sst}(\lambda) e^{-\phi^k_{ss}(y|y';\lambda)} \quad \cdots \textit{for } q = t,n,c \ . \tag{7}$$

Exploiting eq. (3.45), the B_{ss} coefficients are specialized as

$$\left.\begin{aligned} B^q_{ss1} &= \frac{\Re^q_c\uparrow}{D^q} \\ B^q_{ss2} &= \frac{\Re^q_c\uparrow \Re^q_s\downarrow}{D^q} \\ B^q_{ss3} &= B^q_{ss2} \\ B^q_{ss4} &= \frac{\Re^q_s\downarrow}{D^q} \end{aligned}\right\} \cdots \textit{for } q = t,n \ . \tag{8}$$

For coupling components, we use eq. (3.52) to obtain

$$\begin{aligned} B^c_{ss1} &= \frac{1}{D^n D^t} \{C_s\downarrow \Re^n_c\uparrow \Re^t_c\uparrow e^{-2p_s d_s} + C_c\uparrow\} \\ B^c_{ss2} &= \frac{1}{D^n D^t} \{C_c\uparrow \Re^n_s\downarrow + \Re^t_c\uparrow C_s\downarrow\} \\ B^c_{ss3} &= \frac{1}{D^n D^t} \{C_s\downarrow \Re^n_c\uparrow + \Re^t_s\downarrow C_c\uparrow\} \\ B^c_{ss4} &= \frac{1}{D^n D^t} \{C_c\uparrow \Re^n_s\downarrow \Re^t_s\downarrow e^{-2p_s d_s} + C_s\downarrow\} \end{aligned} \tag{9}$$

where

$$D^q = 1 - \Re^q_s\downarrow \Re^q_c\uparrow e^{-2p_s d_s} \ . \tag{10}$$

The phase shift factors $\phi_{ss}^{k}(y|y',\lambda)$ are defined in eq. (3.46) as follows

$$\begin{aligned}
\phi_{ss}^{1} &= p_s(-y-y'+2y_c) \\
\phi_{ss}^{2} &= p_s(y-y'+2y_c-2y_s) \\
\phi_{ss}^{3} &= p_s(-y+y'+2y_c-2y_s) \\
\phi_{ss}^{4} &= p_s(y+y'-2y_s) \ .
\end{aligned} \tag{11}$$

Using the fact that interface c is at $y=d_s$ and interface s is at $y=0$, the phase shift factors become

$$\begin{aligned}
\phi_{ss}^{1} &= p_s(-y-y'+2d_s) \\
\phi_{ss}^{2} &= p_s(y-y'+2d_s) \\
\phi_{ss}^{3} &= p_s(-y+y'+2d_s) \\
\phi_{ss}^{4} &= p_s(y+y') \ .
\end{aligned} \tag{12}$$

Now the general reflection coefficients $\Re_c\uparrow$ and $\Re_s\downarrow$, and the overall coupling coefficients $\mathbf{C}_c\uparrow$ and $\mathbf{C}_s\downarrow$ need to be determined. From eq. (3.21), we have

$$\Re_s^q\downarrow = \frac{R_s^q\downarrow + \Re_f^q\downarrow e^{-2p_f t_f}}{1+R_s^q\downarrow \Re_f^q\downarrow e^{-2p_f t_f}} \quad \cdots \textit{for } q=t,n \tag{13}$$

where $t_f=t$ is the thickness of the substrate region. The overall reflection coefficient $\Re_f^q\downarrow$ reduces to the interfacial reflection coefficient $R_f^q\downarrow$ since there is no interface below the substrate/conductor boundary. Moreover, interface f is adjacent to a perfect conductor leading to

$$R_f^t\downarrow = -1 \ ; \ R_f^n\downarrow = 1 \ . \tag{14}$$

Hence, the overall reflection coefficients at interface s in eq. (13) reduce to

$$\begin{aligned} \mathcal{R}_s^t\downarrow &= \frac{R_s^t\downarrow - e^{-2p_f t}}{1 - R_s^t\downarrow e^{-2p_f t}} \\ \mathcal{R}_s^n\downarrow &= \frac{R_s^n\downarrow + e^{-2p_f t}}{1 + R_s^n\downarrow e^{-2p_f t}} \end{aligned} \tag{15}$$

where the interfacial reflection coefficients are given in Appendix A as

$$R_s^t\downarrow = \frac{M_s^2 p_s - p_f}{M_s^2 p_s + p_f} \; ; \quad R_s^n\downarrow = \frac{N_s^2 p_s - p_f}{N_s^2 p_s + p_f} \; . \tag{16}$$

Similarly, the overall reflection coefficient $\mathcal{R}_c^q\uparrow$ reduces to the interfacial reflection coefficient $R_c^q\uparrow$ since there is no interface above the superstrate/cover boundary. From Appendix A, the interfacial reflection coefficients at the cover interface are

$$R_c^t\uparrow = \frac{p_s - M_c^2 p_c}{M_c^2 p_c + p_s} \; ; \quad R_c^n\uparrow = \frac{p_s - N_c^2 p_c}{N_c^2 p_c + p_s} \; . \tag{17}$$

The overall coupling coefficients $\mathbf{C}_s\downarrow$ and $\mathbf{C}_c\uparrow$ at interface s and interface c, respectively, are given by eq. (3.35) as follows

$$\begin{aligned} \mathbf{C}_s\downarrow &= -\mathcal{R}_s^n\downarrow (C_{11,s}\downarrow + \mathcal{R}_s^t\downarrow C_{12,s}\downarrow) + (C_{21,s}\downarrow + \mathcal{R}_s^t\downarrow C_{22,s}\downarrow) \\ \mathbf{C}_c\uparrow &= -\mathcal{R}_c^n\uparrow (C_{11,c}\uparrow + \mathcal{R}_c^t\uparrow C_{12,c}\uparrow) + (C_{21,c}\uparrow + \mathcal{R}_c^t\uparrow C_{22,c}\uparrow) \end{aligned} \tag{18}$$

where $C_{11,c}\uparrow$ for example, is the first entry of the overall coupling matrix for upward

travelling incident wave at interface c. The overall coupling matrices are given by eq. (3.32) and are specialized to this structure as

$$\begin{aligned}[\mathbf{C}_s\downarrow] &= [C_s\downarrow]\left[A_s^t\downarrow\right]^{-1} + \left[A_s^n\downarrow\right][C_f\downarrow]\left[A_f^t\downarrow\right]^{-1}\left[A_s^t\downarrow\right]^{-1} \\ [\mathbf{C}_c\uparrow] &= [C_c\uparrow]\left[A_c^t\uparrow\right]^{-1} .\end{aligned} \tag{19}$$

Since interface f is a perfect conductor, the product of matrices $\left[A_s^n\downarrow\right][C_f\downarrow]\left[A_f^t\downarrow\right]^{-1}\left[A_s^t\downarrow\right]^{-1}$ reduces to the null matrix. Hence, using eq. (3.19) the overall coupling matrices are specialized as

$$\begin{aligned}[\mathbf{C}_s\downarrow] &= [C_s\downarrow]\left[A_c^t\downarrow\right]^{-1} \\ &= \frac{1-N_s^{-2}M_s^{-2}}{2p_s}\begin{bmatrix}-1 & -1\\ 1 & 1\end{bmatrix}\end{aligned} \tag{20}$$

and

$$[\mathbf{C}_c\uparrow] = \frac{N_c^2M_c^2-1}{2p_s}\begin{bmatrix}-1 & -1\\ 1 & 1\end{bmatrix}. \tag{21}$$

Substituting the entries of the overall coupling matrices in the expressions for the overall coupling coefficients in eq. (18) leads to

$$\begin{aligned}\mathbf{C}_s\downarrow &= \frac{(1-N_s^{-2}M_s^{-2})}{2p_s}(1+\Re_s^t\downarrow)(1+\Re_s^n\downarrow) \\ \mathbf{C}_c\uparrow &= \frac{(N_c^2M_c^2-1)}{2p_s}(1+\Re_c^t\uparrow)(1+\Re_c^n\uparrow) .\end{aligned} \tag{22}$$

Exploiting the expressions for the overall reflection coefficients at interface s given by eq. (15) and knowing that the overall reflection coefficient at interface c reduces

to the interfacial one, eq. (22) becomes

$$C_s\downarrow = \frac{(1-N_s^{-2}M_s^{-2})(1+R_s^t\downarrow)(1+R_s^n\downarrow)(1-e^{-2p_f t})(1+e^{-2p_f t})}{2p_s(1-R_s^t\downarrow e^{-2p_f t})(1+R_s^n\downarrow e^{-2p_f t})}$$
$$C_c\uparrow = \frac{(N_c^2M_c^2-1)}{2p_s}(1+R_c^t\uparrow)(1+R_c^n\uparrow)\ . \tag{23}$$

Substitution of eq. (16) and (17) in eqs. (15) and (23) leads to the final expressions for the B_{ss} coefficients. For tangential and normal components, we have

$$B_{ss1}^t = \frac{(p_s - M_c^2p_c)(M_s^2p_s + p_f\coth p_f t)}{Z^h}$$
$$B_{ss2}^t = \frac{(p_s - M_c^2p_c)(M_s^2p_s - p_f\coth p_f t)}{Z^h}$$
$$B_{ss3}^t = B_{ss2}^t \tag{24}$$
$$B_{ss4}^t = \frac{(p_s + M_c^2p_c)(M_s^2p_s - p_f\coth p_f t)}{Z^h}$$

and

$$B_{ss1}^n = \frac{(p_s - N_c^2p_c)(M_s^2p_s + p_f\tanh p_f t)}{Z^e}$$
$$B_{ss2}^n = \frac{(p_s - N_c^2p_c)(M_s^2p_s - p_f\tanh p_f t)}{Z^e}$$
$$B_{ss3}^n = B_{ss2}^n \tag{25}$$
$$B_{ss4}^n = \frac{(p_s + N_c^2p_c)(M_s^2p_s - p_f\tanh p_f t)}{Z^e}$$

where

$$Z^e = (N_c^2p_s + p_f\tanh p_f t)(p_s + N_c^2p_c) - (p_s - N_c^2p_c)(N_s^2p_s - p_f\tanh p_f t)e^{-2p_s d_s}$$
$$Z^h = (M_c^2p_s + p_f\coth p_f t)(p_s + M_c^2p_c) - (p_s - M_c^2p_c)(M_s^2p_s - p_f\coth p_f t)e^{-2p_s d_s}\ . \tag{26}$$

For coupling components, we have

$$B_{ss1}^{c} = \frac{2p_s}{Z^e Z^h}\Big\{(N_s^2M_s^2-1)(p_s-M_c^2p_c)(p_s-N_c^2p_c)e^{-2p_fd_s}$$
$$+(N_c^2M_c^2-1)(M_s^2p_s+p_f\coth p_ft)(N_s^2p_s+p_f\tanh p_ft)\Big\}$$
$$B_{ss2}^{c} = \frac{2p_s}{Z^e Z^h}\Big\{(N_s^2M_s^2-1)(p_s-M_c^2p_c)(p_s+N_c^2p_c)$$
$$+(N_c^2M_c^2-1)(M_s^2p_s+p_f\coth p_ft)(N_s^2p_s-p_f\tanh p_ft)\Big\} \quad (27)$$
$$B_{ss3}^{c} = \frac{2p_s}{Z^e Z^h}\Big\{(N_s^2M_s^2-1)(p_s+M_c^2p_c)(p_s-N_c^2p_c)$$
$$+(N_c^2M_c^2-1)(M_s^2p_s-p_f\coth p_ft)(N_s^2p_s+p_f\tanh p_ft)\Big\}$$
$$B_{ss4}^{c} = \frac{2p_s}{Z^e Z^h}\Big\{(N_s^2M_s^2-1)(p_s+M_c^2p_c)(p_s+N_c^2p_c)$$
$$+(N_c^2M_c^2-1)(M_s^2p_s-p_f\coth p_ft)(N_s^2p_s-p_f\tanh p_ft)\Big\}$$

Pole singularities within the integral representations of the Green's function components are implicated in the scattering coefficients given by eq. (7). In fact, setting $Z^e(\lambda)=0$ and $Z^h(\lambda)=0$ leads to the eingenvalue equations for *TM* and *TE* surface-wave modes, respectively, supported by the layered structure of Fig. 6.2.

6.3 FIELDS IN THE SUBSTRATE LAYER

The electric field in the substrate region maintained by currents in the superstrate layer is given as follows

$$\vec{E}_f(\vec{r}) = \frac{-j\eta_s}{k_s}\int_V \ddot{G}_{fs}^{e}(\vec{r}|\vec{r}')\cdot\vec{J}(\vec{r}')dv' \quad (28)$$

where the electric Green's dyad is again identified in terms of a Hertz potential Green's dyad as

$$\tilde{\bar{G}}^{e}_{fs}(\vec{r}|\vec{r}') = (k_f^2 + \nabla\nabla\cdot)\tilde{G}_{fs}(\vec{r}|\vec{r}') \ . \tag{29}$$

The Hertz potential Green's dyad consists of only a scattered part given by eq. (3.3) with the following scalar components

$$\begin{Bmatrix} G^{s}_{fsx}(\vec{r}|\vec{r}') \\ G^{s}_{fsn}(\vec{r}|\vec{r}') \\ G^{s}_{fsc}(\vec{r}|\vec{r}') \end{Bmatrix} = \int\int_{-\infty}^{\infty} \begin{Bmatrix} S^{t}_{fs}(y|y',\lambda) \\ S^{n}_{fs}(y|y',\lambda) \\ S^{c}_{fs}(y|y',\lambda) \end{Bmatrix} \frac{e^{j\vec{\lambda}\cdot(\vec{r}-\vec{r}')}}{2(2\pi)^2 p_s} d^2\lambda \ . \tag{30}$$

The scattering coefficients S^{q}_{fs} are written in terms of the B_{fs} coefficients and the phase shift factors ϕ_{fs}. Hence, these coefficients must be determined in order to quantify the Green's function components. The substrate region resides between interface s and interface f. The phase shift factors are a special case of eq. (3.65) with $y_i = 0$, $y_{i-1} = d_s$, $y_l = -t$ and $t_i = d_s$ yielding

$$\begin{aligned} \phi^{1}_{ss} &= p_s(-y'+2d_s) - p_f(y+t) \\ \phi^{2}_{ss} &= p_s(-y'+2d_s) + p_f(y+t) \\ \phi^{3}_{ss} &= p_s y' - p_f(y+t) \\ \phi^{4}_{ss} &= p_s y' + p_f(y+t) \ . \end{aligned} \tag{31}$$

Exploiting eq. (3.63) the tangential and normal components of the B_{fs} coefficients are

$$\begin{aligned} B^{q}_{fs1} &= B^{q}_{fs3}\ \Re^{q}_{c}\uparrow \\ B^{q}_{fs} &= B^{q}_{fs4}\ \Re^{q}_{c}\uparrow \\ B^{q}_{fs3} &= \frac{1}{D^q}\{d^{q}_{11,f}\downarrow + d^{q}_{12,f}\downarrow\ \Re^{q}_{s}\downarrow\} \\ B^{q}_{fs4} &= \frac{1}{D^q}\{d^{q}_{21,f}\downarrow + d^{q}_{22,f}\downarrow\ \Re^{q}_{s}\downarrow\} \end{aligned} \tag{32}$$

where D^q is defined in relation (10) and $d^q_{11,f}\downarrow$ is the first entry of the 2×2 matrix

$\left[D^q_f\downarrow\right]$ given by eq. (3.59) as follows

$$\left[D^t_f\downarrow\right]=\left[A^t_s\downarrow\right]^{-1}=\frac{N_s^{-2}M_s^{-2}}{1-R^t_s\downarrow}\begin{bmatrix} e^{-p_f t} & -R^t_s\downarrow e^{-p_f t} \\ -R^t_s\downarrow e^{p_f t} & e^{p_f t} \end{bmatrix}$$
$$\left[D^n_f\downarrow\right]=\left[A^n_s\downarrow\right]^{-1}=\frac{N_s^{-2}}{1-R^n_s\downarrow}\begin{bmatrix} e^{-p_f t} & -R^n_s\downarrow e^{-p_f t} \\ -R^n_s\downarrow e^{p_f t} & e^{p_f t} \end{bmatrix}. \tag{33}$$

Similarly, the coupling components are obtained by specializing eq. (3.76) as follows

$$B^c_{fs1}=\frac{1}{D^t D^n}\Big\{\Big[C_s\downarrow\left(d^n_{12,f}\downarrow+d^n_{11,f}\downarrow\Re^n_c\uparrow e^{-2p_f d_s}\right)+\left(f_{11,fs}\downarrow+f_{12,fs}\downarrow\Re^t_s\downarrow\right)D^n\Big]\Re^t_c\uparrow$$
$$+C_c\uparrow\left(d^n_{11,f}\downarrow+d^n_{12,f}\downarrow\Re^n_s\downarrow\right)\Big\}$$
$$B^c_{fs2}=\frac{1}{D^t D^n}\Big\{\Big[C_s\downarrow\left(d^n_{22,f}\downarrow+d^n_{21,f}\downarrow\Re^n_c\uparrow e^{-2p_f d_s}\right)+\left(f_{21,fs}\downarrow+f_{22,fs}\downarrow\Re^t_s\downarrow\right)D^n\Big]\Re^t_c\uparrow$$
$$+C_c\uparrow\left(d^n_{21,f}\downarrow+d^n_{22,f}\downarrow\Re^n_s\downarrow\right)\Big\}$$
$$B^c_{fs3}=\frac{1}{D^t D^n}\Big\{C_s\downarrow\left(d^n_{12,f}\downarrow+d^n_{11,f}\downarrow\Re^n_c\uparrow e^{-2p_f d_s}\right)+\left(f_{11,fs}\downarrow+f_{12,fs}\downarrow\Re^t_s\downarrow\right)D^n$$
$$+C_c\uparrow e^{-p_f d_s}\left(d^n_{11,f}\downarrow+d^n_{12,f}\downarrow\Re^n_s\downarrow\Re^t_s\downarrow\right)\Big\}$$
$$B^c_{fs4}=\frac{1}{D^t D^n}\Big\{C_s\downarrow\left(d^n_{22,f}\downarrow+d^n_{21,f}\downarrow\Re^n_c\uparrow e^{-2p_f d_s}\right)+\left(f_{21,fs}\downarrow+f_{22,fs}\downarrow\Re^t_s\downarrow\right)D^n$$
$$+C_c\uparrow e^{-p_f d_s}\left(d^n_{21,f}\downarrow+d^n_{22,f}\downarrow\Re^n_s\downarrow\Re^t_s\downarrow\right)\Big\}. \tag{34}$$

where $f_{11,fs}$ is the first entry of the matrix $\left[F_{fs}\downarrow\right]$ given by eq. (3.70) as follows

$$[F_{fs}\downarrow] = -[D_f^n\downarrow][C_s\downarrow] \,. \tag{35}$$

The overall coupling matrix was obtained in the previous section and is given by eq. (19). Exploiting eqs. (19) and (33), eq. (35) becomes

$$[F_{fs}\downarrow] = \frac{N_s^{-2}(N_s^{-2}M_s^{-2}-1)(1+R_s^n\downarrow)}{2p_s(1-R_s^n\downarrow)} \begin{bmatrix} -e^{-p_f f} & -e^{-p_f f} \\ e^{p_f f} & e^{p_f f} \end{bmatrix} . \tag{36}$$

Now that the matrices $[D_f^q\downarrow]$ and $[F_{fs}\downarrow]$ are quantified, we substitute their entries in eq. (31) and (34) and use the expressions for the overall coupling and reflection coefficients as in eq. (14) and (23). The B_{fs} coefficients are obtained in terms of interfacial reflection coefficients as follows

$$\begin{aligned} B_{fs1}^q &= R_c^q\uparrow B_{fs3}^q \\ B_{fs2}^q &= R_c^q\uparrow B_{fs4}^q \qquad \cdots \textit{for } q = t,n \end{aligned} \tag{37}$$

$$\begin{aligned} B_{fs3}^t &= \frac{N_s^{-2}M_s^{-2}e^{-p_f f}(1+R_s^t\downarrow)}{\left(1-R_s^t\downarrow e^{-2p_f f}-R_c^t\uparrow\left(R_s^t\downarrow - e^{-2p_f f}\right)e^{-2p_s d_s}\right)} \\ B_{fs3}^n &= \frac{N_s^{-2}e^{-p_f f}(1+R_s^n\downarrow)}{\left(1+R_s^n\downarrow e^{-2p_f f}-R_c^n\uparrow\left(R_s^n\downarrow + e^{-2p_f f}\right)e^{-2p_s d_s}\right)} \,; \end{aligned} \tag{38}$$

$$\begin{aligned} B_{fs4}^t &= -B_{fs3}^t \\ B_{fs4}^n &= B_{fs3}^n \,. \end{aligned} \tag{39}$$

Similarly, the coupling components of the B_{fs} coefficients are

$$B_{fs1}^{c} = \Big\{ R_c^{t}\uparrow (1 - N_s^{-2} M_s^{-2})(1 + R_s^{n}\downarrow)(1 + R_s^{t}\downarrow)(1 - e^{-2p_f f})(1 + R_c^{n}\uparrow e^{-2p_s d_s}) + (N_c^2 M_c^2 - 1)(1 + R_c^{t}\uparrow)(1 + R_c^{n}\uparrow)(1 + R_s^{n}\downarrow)(1 - R_s^{t}\downarrow e^{-2p_f f}) \Big\} \times N_s^{-2} e^{-p_f f} \Big/ 2p_s (1 + R_s^{n}\downarrow e^{-2p_f f} - R_c^{n}\uparrow (R_s^{n}\downarrow + e^{-2p_f f}) e^{-2p_s d_s})(1 - R_s^{t}\downarrow e^{-2p_f f} - R_c^{t}\uparrow (R_s^{t}\downarrow - e^{-2p_f f}) e^{-2p_s d_s}) \; ; \tag{40}$$

$$B_{fs2}^{c} = B_{fs1}^{c} \tag{41}$$

$$B_{fs3}^{c} = \Big\{ (1 - N_s^{-2} M_s^{-2})(1 + R_s^{n}\downarrow)(1 + R_s^{t}\downarrow)(1 - e^{-2p_f f})(1 + R_c^{n}\uparrow e^{-2p_s d_s}) + (N_c^2 M_c^2 - 1)(1 + R_c^{t}\uparrow)(1 + R_c^{n}\uparrow)(1 + R_s^{n}\downarrow)(R_s^{t}\downarrow - e^{-2p_f f}) e^{-2p_s d_s} \Big\} \times N_s^{-2} e^{-p_f f} \Big/ 2p_s (1 + R_s^{n}\downarrow e^{-2p_f f} - R_c^{n}\uparrow (R_s^{n}\downarrow + e^{-2p_f f}) e^{-2p_s d_s})(1 - R_s^{t}\downarrow e^{-2p_f f} - R_c^{t}\uparrow (R_s^{t}\downarrow - e^{-2p_f f}) e^{-2p_s d_s}) \; ; \tag{42}$$

$$B_{fs4}^{c} = B_{fs3}^{c} \; . \tag{43}$$

The scattering coefficients in the expression for the Green's function components in eq. (30) can be obtained as follows

$$S_{fs}^{q}(y|y';\lambda) = \sum_{k=1}^{4} B_{fsk}^{q} e^{-\phi_{fs}^{k}} \quad \text{... for } q = t,n,c. \tag{44}$$

Exploiting eqs. (37) through (43) and after some manipulations, the above expressions for the scattering coefficients become

$$\begin{aligned} S_{fs}^{t}(y|y';\lambda) &= 2B_{fs3}^{t} \sinh p_f (y+t) \left[R_c^{t}\uparrow e^{-p_s(2d_s - y')} + e^{-p_s y'} \right] \\ S_{fs}^{n}(y|y';\lambda) &= 2B_{fs3}^{n} \cosh p_f (y+t) \left[R_c^{n}\uparrow e^{-p_s(2d_s - y')} + e^{-p_s y'} \right] \\ S_{fs}^{c}(y|y';\lambda) &= 2\cosh p_f (y+t) \left[B_{fs1}^{c} e^{-p_s(2d_s - y')} + B_{fs3}^{c} e^{-p_s y'} \right] . \end{aligned} \tag{45}$$

The final expressions for the $B^{q}_{fs3}(q=t,n,c)$ and B^{c}_{fs1} coefficients are obtained by substituting the relation for the interfacial reflection coefficients at interface s in eqs. (38), (40) and (42). We obtain

$$B^{t}_{fs3} = \frac{N_s^{-2} p_s (M_c^2 p_c + p_s)}{\sinh p_f t \; Z^h}$$
$$B^{n}_{fs3} = \frac{p_s (N_c^2 p_c + p_s)}{\cosh p_f t \; Z^e} \tag{46}$$

$$B^{c}_{fs1} = \left\{ N_s^{-2}(N_s^2 M_s^2 - 1) p_s (p_s - M_c^2 p_c)(p_s + N_c^2 p_c + (p_s - N_c^2 p_c) e^{-2p_s d_s}) + (N_c^2 M_c^2 - 1) 2 p_s^2 (M_s^2 p_s + p_f \coth p_f t) \right\} \frac{1}{\cosh p_f t Z^e Z^h}$$
$$B^{c}_{fs3} = \left\{ N_s^{-2}(N_s^2 M_s^2 - 1) p_s (p_s + M_c^2 p_c)(p_s + N_c^2 p_c + (p_s - N_c^2 p_c) e^{-2p_s d_s}) + (N_c^2 M_c^2 - 1) 2 p_s^2 (M_s^2 p_s - p_f \coth p_f t) e^{-2p_s d_s} \right\} \frac{1}{\cosh p_f t Z^e Z^h} \tag{47}$$

where $Z^e(\lambda)$ and $Z^h(\lambda)$ are defined in expression (26). We have to note that, by letting the cover and the superstrate have the same permittivity, the Hertz potential Green's functions found above reduce to the ones obtained in chapter four.

6.4 INTEGRAL EQUATION DESCRIPTION OF MICROSTRIP TRANSMISSION LINE

In this section, we will study the microstrip structure with a superstrate layer. The general configuration of this microstrip transmission line is depicted in Fig. 6.3. The conducting strip is embedded in the superstrate layer adjacent to the substrate/superstrate interface of the four layered conductor/substrate/superstrate/cover environment. The y axis is normal and the x and z axes are tangential to the substrate/superstrate interface.

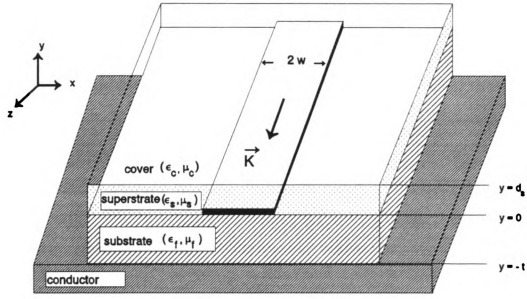

Figure 6.3: Configuration of microstrip transmission line with superstrate

A homogeneous transform-domain EFIE for the eigencurrent on the strip was developed in chapter four, which, for the present case reduces to

$$\lim_{y\to 0}\ \hat{t}\cdot\int_C \bar{\bar{g}}^e(x,y|x',y'=0;\zeta)\cdot\vec{k}_p^{\pm}(x')dx' = 0 \ \cdots \ for\ -w\le x\le w\ . \tag{48}$$

with nontrivial solutions only for $\zeta = \mp\zeta_p$. $\vec{k}_p^{\pm}(x)$ is the current distribution of the p'th propagation mode on the strip and $\pm\zeta_p$ is the associated propagation constant. The space-domain eingenmode currents are

$$\vec{K}_p^{\pm}(\vec{\rho},z) = \vec{k}_p^{\pm}(\vec{\rho})e^{\mp j\zeta_p z}\ . \tag{49}$$

This a current wave propagating in $\pm z$ direction along the strip. Since the current distributions for $\pm z$ directed waves are essentially the same, we restrict our discussion to the case of $+z$ directed current.

The transform-domain electric Green's dyad is given by

$$\begin{aligned}\bar{\bar{g}}^e(\vec{\rho}\,|\,\vec{\rho}') &= \mathcal{F}_z\{\bar{\bar{G}}^e(\vec{\rho}\,|\,\vec{\rho}';z)\}\\ &= PV(k_s^2+\tilde{\nabla}\tilde{\nabla}\cdot)\bar{\bar{g}}(\vec{\rho}\,|\,\vec{\rho}';\zeta) + \bar{\bar{L}}\delta(\vec{\rho}-\vec{\rho}')\ .\end{aligned} \tag{50}$$

The transform-domain Green's dyad $\bar{\bar{g}}$ in eq. (48) is expressed in terms of Sommerfeld-type integrals as follows

$$\bar{\bar{g}}(\vec{\rho}\,|\,\vec{\rho}';\zeta) = \bar{\bar{I}}g^p(\vec{\rho}\,|\,\vec{\rho}';\zeta) + \bar{\bar{g}}^s(\vec{\rho}\,|\,\vec{\rho}';\zeta) \tag{51}$$

where

$$\bar{\bar{g}}^s(\vec{\rho}\,|\,\vec{\rho}';\zeta) = (\hat{x}\hat{x}+\hat{z}\hat{z})g_t^s(\vec{\rho}\,|\,\vec{\rho}';\zeta) + \hat{y}\left(\nabla_T g_c^s(\vec{\rho}\,|\,\vec{\rho}';\zeta) + g_n^s(\vec{\rho}\,|\,\vec{\rho}';\zeta)\hat{y}\right) \tag{52}$$

with $\nabla_T = \hat{x}\dfrac{\partial}{\partial x} + \hat{z}\dfrac{\partial}{\partial z}$ and

$$g^p(\vec{\rho}\,|\,\vec{\rho}\,';\zeta) = \int_{-\infty}^{\infty} \frac{e^{j\xi(x-x')}\, e^{-p_s|y-y'|}}{4\pi p_s}\, d\xi \ . \tag{53}$$

The scattered Green's dyad has the following components

$$\begin{Bmatrix} g_t^s(\vec{\rho}\,|\,\vec{\rho}\,';\zeta) \\ g_n^s(\vec{\rho}\,|\,\vec{\rho}\,';\zeta) \\ g_c^s(\vec{\rho}\,|\,\vec{\rho}\,';\zeta) \end{Bmatrix} = \int_{-\infty}^{\infty} \begin{Bmatrix} S^t(y|y';\lambda) \\ S^n(y|y';\lambda) \\ S^c(y|y';\lambda) \end{Bmatrix} \frac{e^{j\xi(x-x')}}{4\pi p_s}\, d\xi \ . \tag{54}$$

The scattering coefficients S^q are functions of ξ, through $\lambda^2 = \xi^2 + \zeta^2$ and are defined in previous sections. We note that the subscripts referring to the superstrate is dropped for the sake of simplicity.

The surface current for a strip of vanishing thickness has only tangential components as

$$\vec{k}(\vec{\rho}) = \hat{x}k_x(x) + \hat{z}k_z(x) \ . \tag{55}$$

Due to the symmetry of the problem, there are two categories of modes for the microstrip, even modes and odd modes, defined according to the symmetry of the z component current as

$$\left.\begin{aligned} k_x(-x) &= -k_x(x) \\ k_z(-x) &= k_z(x) \end{aligned}\right\} \cdots \textit{even mode}$$

$$\left.\begin{aligned} k_x(-x) &= k_x(x) \\ k_z(-x) &= -k_z(x) \end{aligned}\right\} \cdots \textit{odd mode} \ . \tag{56}$$

Substituting eq. (55) in (48) yields a pair of integral equations by letting $\hat{t} = \hat{x}$ and $\hat{t} = \hat{z}$; they are

$$\lim_{y\to 0}\int_{-w}^{w}\left\{g_{xx}^{e}(x,y|x',0;\zeta)k_x(x') + g_{xz}^{e}(x,y|x',0;\zeta)k_z(x')\right\}dx' = 0$$
$$\lim_{y\to 0}\int_{-w}^{w}\left\{g_{zx}^{e}(x,y|x',0;\zeta)k_x(x') + g_{zz}^{e}(x,y|x',0;\zeta)k_z(x')\right\}dx' = 0 \qquad (57)$$
$$\cdots \text{for } -w \le x \le w \ .$$

The scalar components of the electric Green's functions can be found as in Appendix B as

$$g_{\alpha\beta}^{e}(x,y|x',0) = \frac{1}{2\pi}\int_{-\infty}^{\infty}\left(C_{\alpha\beta}^{+}(\xi,\zeta)e^{-p_s y} + C_{\alpha\beta}^{-}(\xi,\zeta)e^{p_s y}\right)e^{j\xi(x-x')}\,d\xi \qquad (58)$$
$$\cdots \text{for } \alpha,\beta = x,z$$

where the coefficients are functions of ξ and ζ as

$$C_{xx}^{+} = \frac{(k_s^2-\xi^2)M_s^2(p_s+M_c^2p_c)}{Z^h(\lambda)} + \frac{\xi^2 p_s A^{+}(\lambda)}{Z^e Z^h}$$
$$C_{xx}^{-} = \frac{(k_s^2-\xi^2)M_s^2(p_s-M_c^2p_c)}{Z^h(\lambda)} - \frac{\xi^2 p_s A^{-}(\lambda)}{Z^e Z^h}\ ; \qquad (59)$$

$$C_{xz}^{+} = \frac{-\xi\zeta M_s^2(p_s+M_c^2p_c)}{Z^h(\lambda)} + \frac{\xi\zeta p_s A^{+}(\lambda)}{Z^e Z^h}$$
$$C_{xz}^{-} = \frac{-\xi\zeta M_c^2(p_s-M_s^2p_c)}{Z^h(\lambda)} - \frac{\xi\zeta p_s A^{-}(\lambda)}{Z^e Z^h}\ ; \qquad (60)$$

$$C_{zz}^{+} = \frac{(k_s^2-\zeta^2)M_s^2(p_s+M_c^2p_c)}{Z^h(\lambda)} + \frac{\zeta^2 p_s A^{+}(\lambda)}{Z^e Z^h}$$
$$C_{zz}^{-} = \frac{(k_s^2-\zeta^2)M_s^2(p_s-M_c^2p_c)}{Z^h(\lambda)} - \frac{\zeta^2 p_s A^{-}(\lambda)}{Z^e Z^h} \qquad (61)$$

with

$$
\begin{aligned}
A^{+}(\lambda) &= (N_s^2 M_s^2 - 1)(p_s + N_c^2 p_c)\left[e^{-2p_s d_s}(p_s - M_c^2 p_c) + (p_s + M_c^2 p_c)\right] \\
&\quad + 2M_s^2 p_s e^{-2p_s d_s}(N_c^2 M_c^2 - 1)(N_s^2 p_s - p_f \tanh p_f t) \\
A^{-}(\lambda) &= (N_s^2 M_s^2 - 1)(p_s - N_c^2 p_c)\left[e^{-2p_s d_s}(p_s - M_c^2 p_c) + (p_s + M_c^2 p_c)\right] \\
&\quad + 2M_s^2 p_s (N_c^2 M_c^2 - 1)(N_s^2 p_s + p_f \tanh p_f t) \ .
\end{aligned}
\tag{62}
$$

Substituting eq. (58) into (57), and interchanging the spatial and spectral integration, leads to

$$
\begin{aligned}
&\lim_{y \to 0} \int_{-\infty}^{\infty} d\xi \int_{-w}^{w} \left\{\left(C_{xx}^{+} e^{-p_s y} + C_{xx}^{-} e^{p_s y}\right) k_x(x') + \left(C_{xz}^{+} e^{-p_s y} + C_{xz}^{-} e^{p_s y}\right) k_z(x')\right\} e^{j\xi(x-x')} dx' = 0 \\
&\lim_{y \to 0} \int_{-\infty}^{\infty} d\xi \int_{-w}^{w} \left\{\left(C_{zx}^{+} e^{-p_s y} + C_{zx}^{-} e^{p_s y}\right) k_x(x') + \left(C_{zz}^{+} e^{-p_s y} + C_{zz}^{-} e^{p_s y}\right) k_z(x')\right\} e^{j\xi(x-x')} dx' = 0 \\
&\qquad\qquad \cdots \textit{for} \ -w \le x \le w \ .
\end{aligned}
\tag{63}
$$

A moment-method solution of the above coupled equations is pursued next.

6.5 MOMENT METHOD SOLUTION

The transverse and longitudinal current components are expanded in series of Chebyshev polynomials weighted by appropriate edge-condition factors as follows

$$
\begin{aligned}
k_x(x) &= \sum_{n=0}^{N} a_{xn} e_{xn}(x) \\
k_z(x) &= \sum_{n=0}^{N} a_{zn} e_{zn}(x)
\end{aligned}
\tag{64}
$$

with

$$
\begin{aligned}
e_{xn}(x) &= T_n(x/w) \ \sqrt{1 - (x/w)^2} \\
e_{zn}(x) &= T_n(x/w) \ / \sqrt{1 - (x/w)^2}
\end{aligned}
\tag{65}
$$

where $T_n(x/w)$ is the Chebyshev polynomial of order n of the first kind and a_{xn} and a_{zn} are unknown expansion coefficients.

Exploiting the current expansions in (64) gives

$$\begin{aligned}
&\lim_{y\to 0}\int_{-\infty}^{\infty} e^{j\xi x}d\xi \int_{-w}^{w}\left\{\left(C_{xx}^{+}e^{-p_0 y}+C_{xx}^{-}e^{p_0 y}\right)\sum_{n=0}^{N}a_{xn}f_{xn}(\xi)\right.\\
&\qquad\left.+\left(C_{xz}^{+}e^{-p_0 y}+C_{xz}^{-}e^{p_0 y}\right)\sum_{n=0}^{N}a_{zn}f_{zn}(\xi)\right\}dx'=0\\
&\lim_{y\to 0}\int_{-\infty}^{\infty} e^{j\xi x}d\xi \int_{-w}^{w}\left\{\left(C_{zx}^{+}e^{-p_0 y}+C_{zx}^{-}e^{p_0 y}\right)\sum_{n=0}^{N}a_{xn}f_{xn}(\xi)\right.\\
&\qquad\left.+\left(C_{zz}^{+}e^{-p_0 y}+C_{zz}^{-}e^{p_0 y}\right)\sum_{n=0}^{N}a_{zn}f_{zn}(\xi)\right\}dx'=0\\
&\qquad\qquad\cdots \textit{for } -w\le x\le w
\end{aligned}\tag{66}$$

where

$$f_{\beta n}(\xi)=\int_{-w}^{w}e_{\beta n}(x')e^{-j\xi x'}dx' \qquad \cdots \textit{for } \alpha=x,z. \tag{67}$$

Following Galerkin's method, the same basis functions are used as testing functions. We define the testing operator as

$$\int_{-w}^{w}dx\,e_{\alpha m}(x)\{\cdots\} \qquad \textit{for } \cdots\alpha=x,z\ . \tag{68}$$

Then applying this operator to (66), we have

$$\begin{aligned}
&\lim_{y\to 0}\sum_{n=0}^{N}\int_{-\infty}^{\infty}g_{xm}(\xi)d\xi \int_{-w}^{w}\left[\left(C_{xx}^{+}e^{-p_0 y}+C_{xx}^{-}e^{p_0 y}\right)a_{xn}f_{xn}(\xi)\right.\\
&\qquad\left.+\left(C_{xz}^{+}e^{-p_0 y}+C_{xz}^{-}e^{p_0 y}\right)a_{zn}f_{zn}(\xi)\right]dx'=0\\
&\lim_{y\to 0}\sum_{n=0}^{N}\int_{-\infty}^{\infty}g_{zm}(\xi)d\xi \int_{-w}^{w}\left[\left(C_{zx}^{+}e^{-p_0 y}+C_{zx}^{-}e^{p_0 y}\right)a_{xn}f_{xn}(\xi)\right.\\
&\qquad\left.+\left(C_{zz}^{+}e^{-p_0 y}+C_{zz}^{-}e^{p_0 y}\right)a_{zn}f_{zn}(\xi)\right]dx'=0\\
&\qquad\qquad\cdots \textit{for } -w\le x\le w
\end{aligned}\tag{69}$$

where

$$g_{\alpha m}(\xi) = \int_{-w}^{w} e_{\alpha m}(x) e^{j\xi x} dx \ . \tag{70}$$

If we let

$$A_{\alpha\beta}^{mn} = \lim_{y \to 0} \int_{-\infty}^{\infty} \left(C_{\alpha\beta}^{+} e^{-p_\beta y} + C_{\alpha\beta}^{-} e^{p_\beta y} \right) g_{\alpha m}(\xi) f_{\beta n}(\xi) d\xi \quad \cdots \alpha, \beta = x, z \tag{71}$$

then eq. (69) becomes

$$\begin{aligned} \sum_{n=0}^{N} \left(A_{xx}^{mn} a_{xn} + A_{xz}^{mn} a_{zn} \right) &= 0 \\ \sum_{n=0}^{N} \left(A_{zx}^{mn} a_{xn} + A_{zz}^{mn} a_{zn} \right) &= 0 \ . \end{aligned} \tag{72}$$

The above is a system of linear equations for unknown expansion coefficients $a_{\alpha n}$. It can be written in a convenient matrix form as

$$\begin{bmatrix} A_{xx}^{mn} & A_{xz}^{mn} \\ A_{zx}^{mn} & A_{zz}^{mn} \end{bmatrix} \begin{bmatrix} a_{x0} \\ a_{x1} \\ \vdots \\ a_{xN} \\ a_{z0} \\ \vdots \\ a_{zN} \end{bmatrix} = 0, \qquad \cdots \textit{for } m, n = 0, 1, \cdots, N \ . \tag{73}$$

To obtain a nontrivial solution of the matrix equation, the determinant of the $[A]$ matrix must vanish. Since the elements of $[A]$ are functions of ζ, this requirement yields the propagation constant ζ_p. The corresponding expansion coefficients are then evaluated and the eigenmode currents are obtained in quasi-

closed Chebyshev polynomial series.

One advantage of using Chebyshev polynomials as basis functions is that it allows spatial integrals in (67) and (70) to be evaluated in closed form. Chebyshev polynomials of even order are even functions while those of odd order are odd functions. Hence, for even modes, the transverse current is represented by Chebyshev polynomials of odd order while the longitudinal current is represented by Chebyshev polynomials of even order; vice-versa for the odd mode. Therefore, four types of integrals emerge and can be evaluated as follows

$$\int_0^w \frac{T_{2n}(x/w)}{\sqrt{1-(x/w)^2}}\cos(\xi x)\,dx = (-1)^n \frac{\pi w}{2} J_{2n}(\xi w) \tag{74}$$

$$\int_0^w \frac{T_{2n+1}(x/w)}{\sqrt{1-(x/w)^2}}\sin(\xi x)\,dx = (-1)^n \frac{\pi w}{2} J_{2n+1}(\xi w) \tag{75}$$

$$\int_0^w T_{2n}(x/w)\sqrt{1-(x/w)^2}\cos(\xi x)\,dx = (-1)^n \frac{\pi w}{4}\left[J_{2n}(\xi w) + \frac{1}{2}J_{2(n+1)}(\xi w) + \frac{1}{2}J_{2(n-1)}(\xi w)\right] \tag{76}$$

$$\int_0^w T_{2n}(x/w)\sqrt{1-(x/w)^2}\sin(\xi x)\,dx = (-1)^n \frac{\pi w}{4}\left[J_{2n+1}(\xi w) + \frac{1}{2}J_{2(n+1)+1}(\xi w) + \frac{1}{2}J_{2(n-1)+1}(\xi w)\right] \tag{77}$$

where $J_n(x)$ is the Bessel function of the first kind.

The matrix elements in eq.(71) are inverse Fourier transform integrals. For

bound propagation modes, the real axis is taken as inverse integration contour in the complex ξ-plane. The surface-wave poles implicated in the coefficients $C^{\pm}_{\alpha,\beta}(\xi)$ through $Z^{e}(\xi)$ and $Z^{h}(\xi)$, are on or near the imaginary axis in the proper half plane, and are not implicated in the integrals.

An important issue that merits examination in this MOM solution is the convergence problem of the integrals representing the MOM matrix. By examining the asymptotic behavior of the integrands as ξ approaches infinity, it was shown that the integrals converge regardless of the value of y. Hence, interchanging the limit $y \to 0$ with the integration is justified in eq. (71).

6.6 NUMERICAL RESULTS

Numerical results are obtained for the typical configuration shown in Fig. 6.3 with various physical parameters. We first consider a microstrip line with parameters $2w = 3.0mm$, $t = d_s = 0.635mm$, $n_c = 1.0$, $n_f = 3.13$ and $n_s = 1.4$. An additional advantage of using Chebyshev polynomials as basis functions is that only a few terms in the series are required to accurately represent the current. Figure 6.4 shows the convergence of the normalized propagation constant ζ/k_0, as a function of the number of terms used in the series expansion for the current. It can be seen that fast convergence to the exact value of ζ/k_0 is obtained even for the case of $N = 2$.

Figure 6.5 presents plots of the normalized propagation constant ζ/k_0 versus frequency, obtained by solving eq. (72). As expected, the EH_0 mode is purely bound at all frequencies. The dashed line is the dispersion curve of the TM_0 background

surface-wave mode, that is the solution to $Z^e(\lambda)=0$ for $\lambda=\lambda_p$. For bound modes, the propagation constant satisfies $\lambda_p<\zeta<k_f$. Hence, λ_p provides a cutoff condition with corresponding cutoff frequency. Higher-order modes become leaky when the frequency is below cutoff. Background surface-wave and/or space radiation is then excited.

Figure 6.6 shows the dispersion curve of the principal mode for various superstrate permittivities and fixed superstrate height. It can be seen that as the superstrate permittivity becomes larger so does the propagation constant. This is as expected, since for bound modes and for this particular structure, the propagation constant satisfies $k_s<\zeta<k_f$. Hence, as the superstrate permittivity grows, the fields in that region have more influence on the propagation constant.

Figure 6.7 illustrates the dispersion curve for the principal mode with a fixed superstrate permittivity and normalized superstrate height as parameter. It can be seen that as the superstrate thickness gets larger, the propagation constant increases. This can be explained by the fact that as the superstrate thickness grows, the propagation constant is more influenced by the fields in the substrate than by the fields in the supersrate.

The longitudinal and the transverse currents on the strip for the principal mode are shown in Figures 6.8 and 6.9, respectively. Only the results for the right half of the strip $0\le x\le w$ are displayed. As expected, the longitudinal current is even with respect to the center of the strip and the transverse current is odd. In Figures 6.8 and 6.9, the current distributions for the microstrip of Fig. 6.3 is compared with the

current distributions of the conventional microstrip structure of Fig. 4.3, both operating at two different frequencies. It can be seen that for both structures, the change in longitudinal current is relatively small as a function of frequency, and the transverse current significantly increases with increasing frequency.

Now, we turn our attention to the microstrip of fig. 6.3 having air as substrate and cover. Figure 6.10 shows the dispersion curve of the principal EH_0 mode and the next higher-order mode. It can be seen that the principal mode never leaks as the curve for the propagation constant stays always above the curve for the background TM_0 surface-wave pole λ_p. Figure 6.11 shows the dispersion curve for the principal mode with the superstrate refractive index as parameter. As the superstrate refractive index gets larger, so does the propagation constant. Moreover, the propagation constant displays a significant change as a function of frequency for larger superstrate refractive indices (for $n_s = 2.5$ and $n_s = 3.13$). The normalized propagation constant starts from a value very close to the substrate refractive index $n_f = 1$. This is due to the fact that most of the field is concentrated underneath the strip in the substrate region. Figure 6.12 illustrates the normalized propagation constant versus frequency up to 40 GHz with superstrate thickness as parameter. As the superstrate gets thicker, the propagation constant increases. This can be explained by the fact that the propagation constant is more influenced by the fields in the superstrate and consequently approaches its refractive index of $n_f = 3.13$.

Figures 6.13 and 6.14 show the longitudinal and transverse current distributions, respectively, of the principal EH_0 mode. As expected, the longitudinal

current is even with respect to the center of the strip whereas the transverse component is odd. Moreover, the transverse current is quite small compared to the longitudinal component. Figures 6.15 and 6.16 show the current distributions of the first higher-order EH_1 mode for two different frequencies. The longitudinal current is now odd with respect to the center of the strip while the transverse current is even. Unlike the principle mode, the magnitude of the transverse current for the EH_1 mode decreases as the frequency increases. Moreover, the relative amplitude of the transverse components are significant compared with the longitudinal one.

6.7 SUMMARY

A rigorous analysis of a microstrip transmission line with a superstrate layer has been presented. The dispersion characteristics and current distributions of the guiding structure were analyzed for the principal and higher-order modes. It is found that the principal mode of such structure never leaks. It was shown by Oliner et al [51,52] that a leaky dominant mode is present at higher frequencies on conventional microstrip line. Hence, the microstrip with superstrate can be used as an improvement to the conventional microstrip.

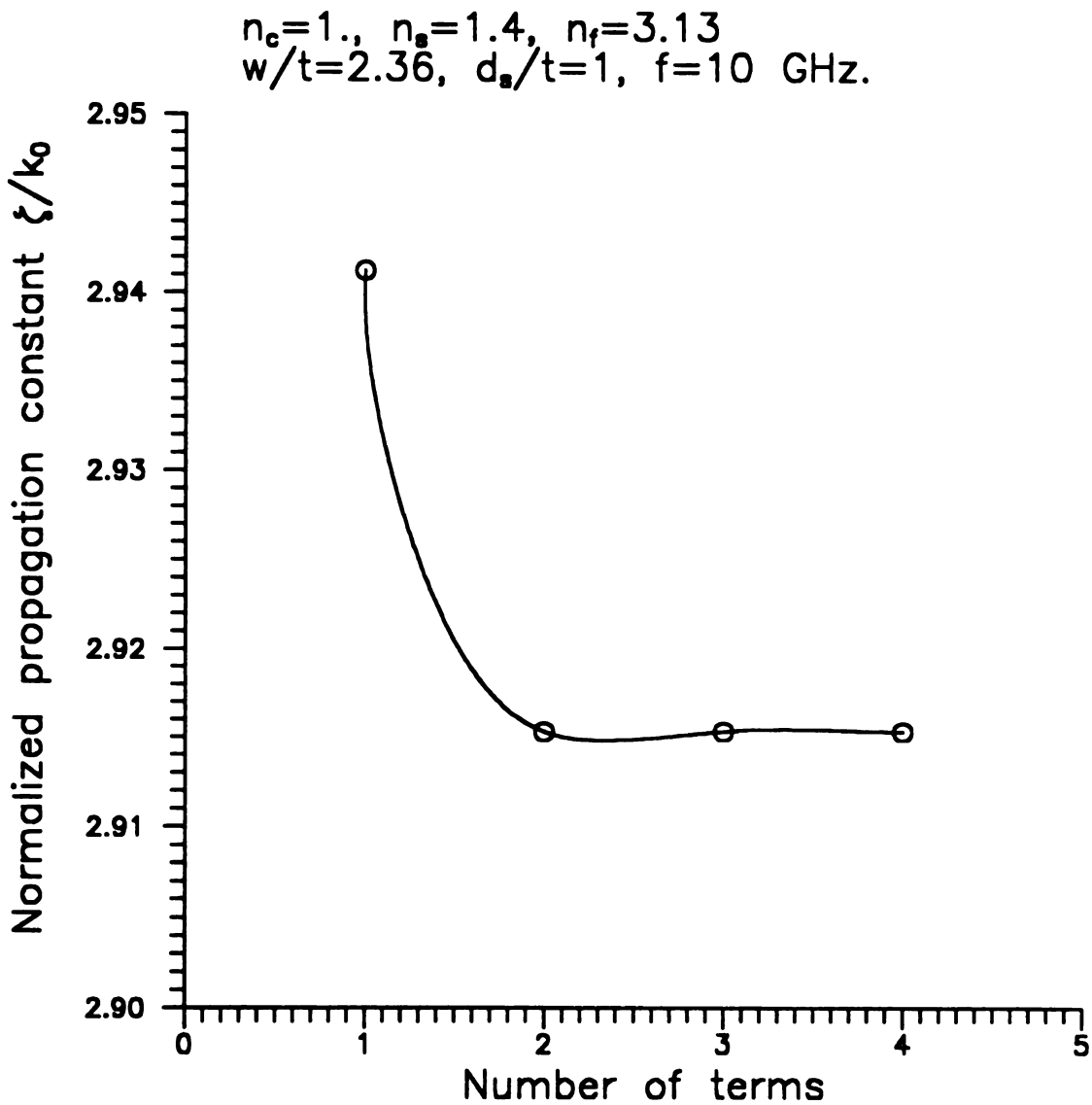

Figure 6.4: Convergence of the normalized propagation constant as a function of number of terms used in the Chebyshev series expansion for the current.

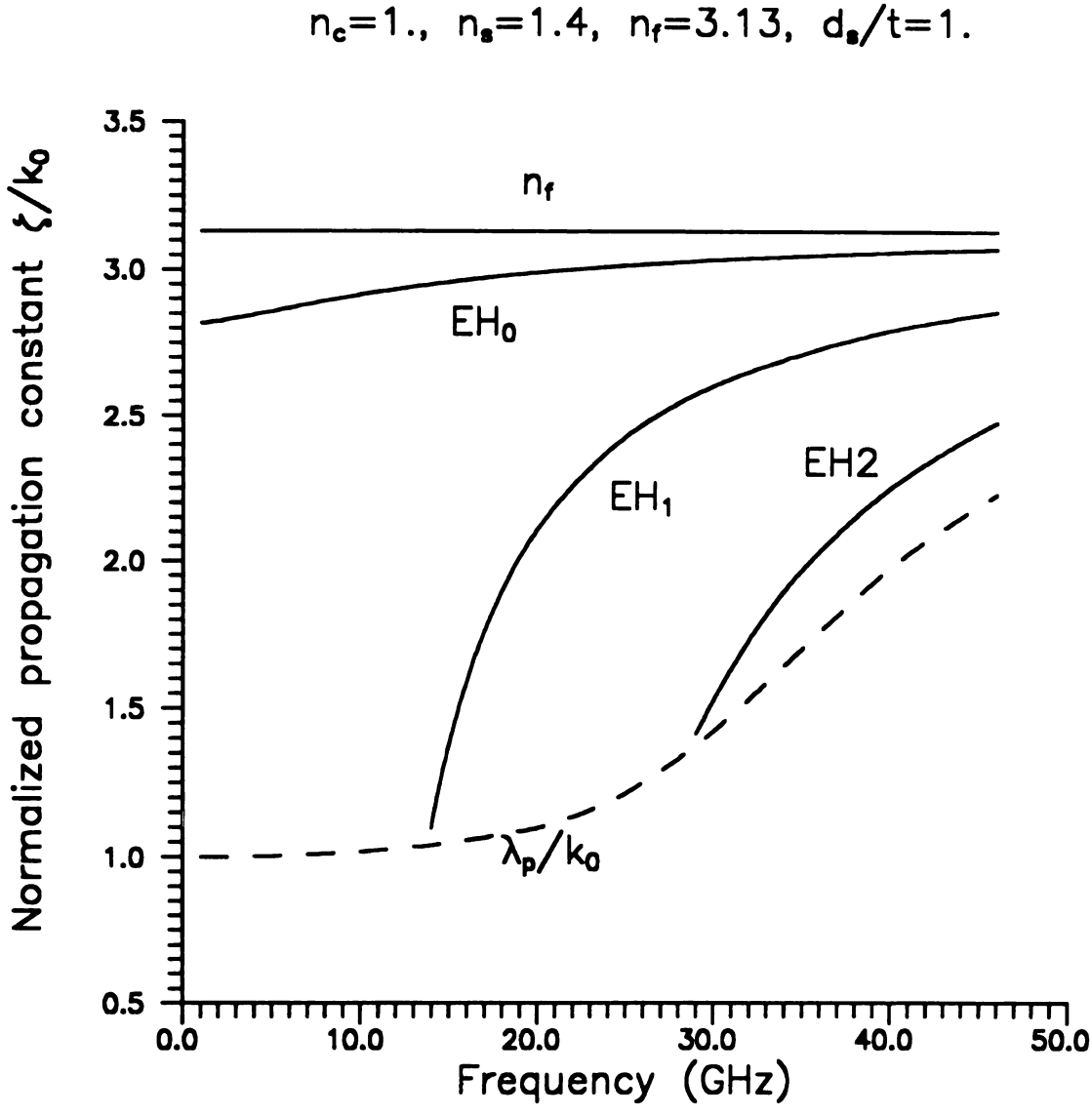

Figure 6.5: Dispersion characteristics of the principal and the first two higher-order modes of the microstriop line with superstrate.

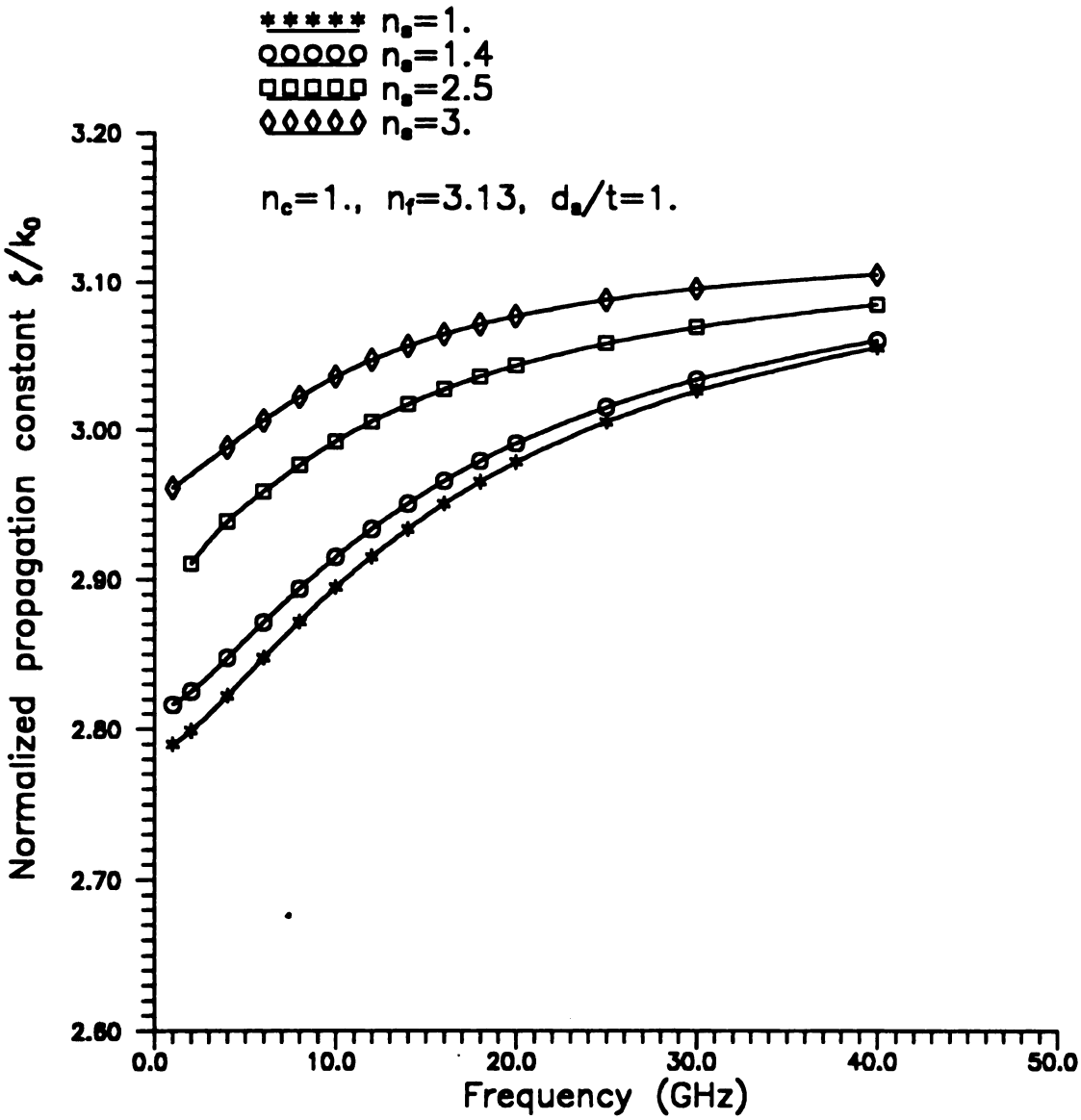

Figure 6.6: Dispersion characteristics of the principal mode with superstrate refractive index as parameter.

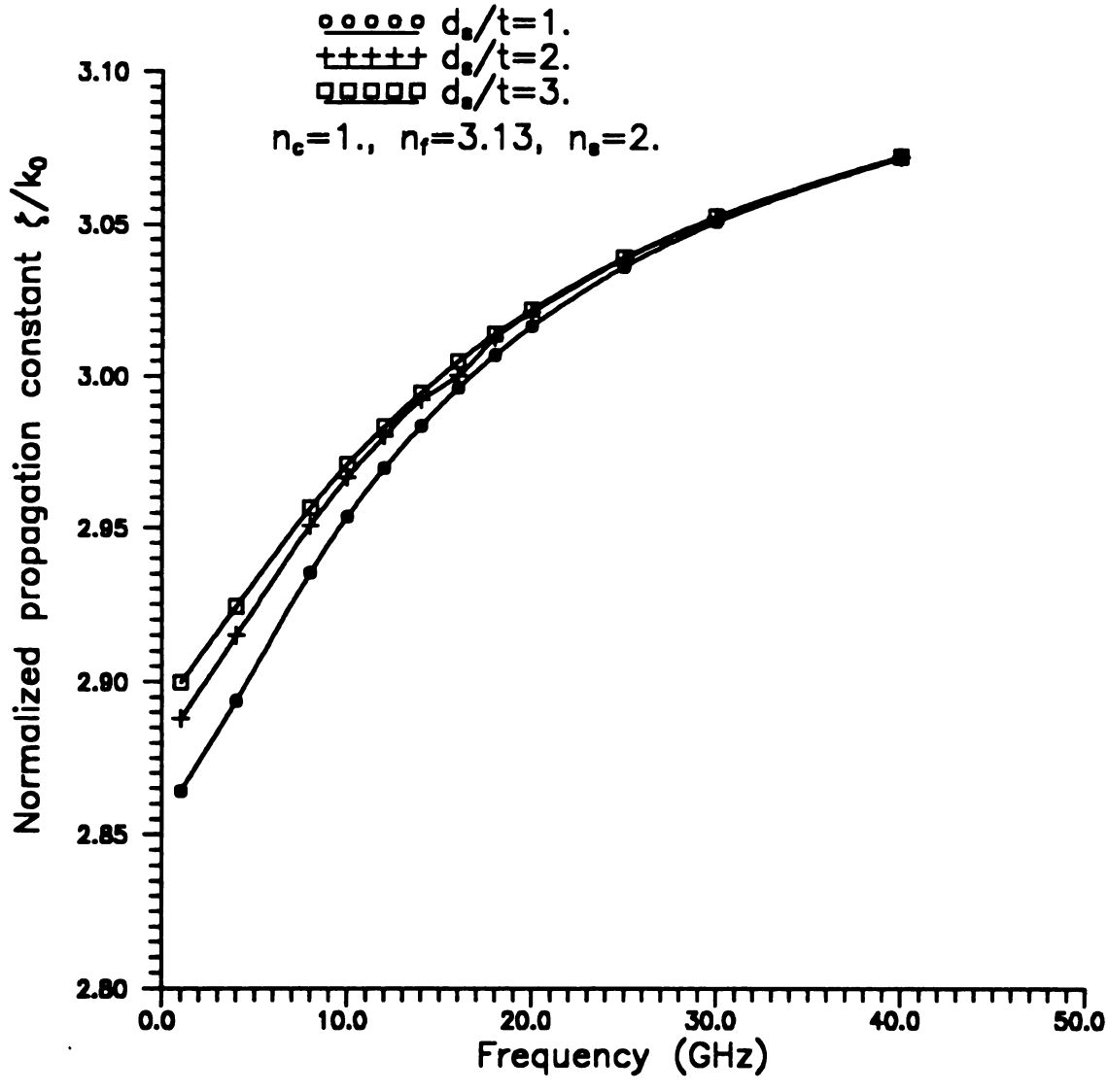

Figure 6.7: Dispersion characteristics of the principal mode with superstrate thickness as parameter.

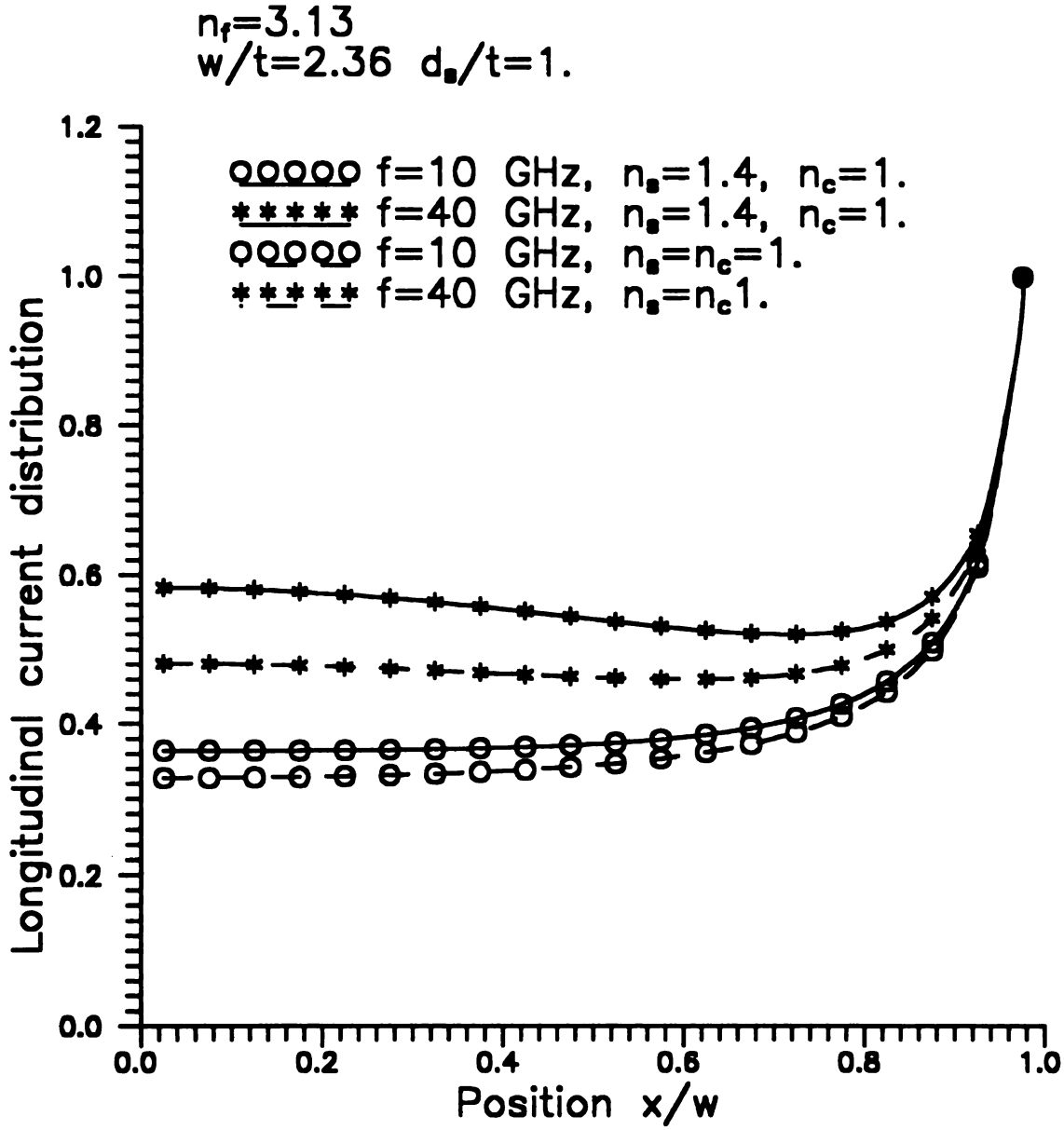

Figure 6.8: Comparison between the longitudinal current distributions of the principal mode for the conventional microstrip and those for the microstrip with superstrate operating at two frequencies.

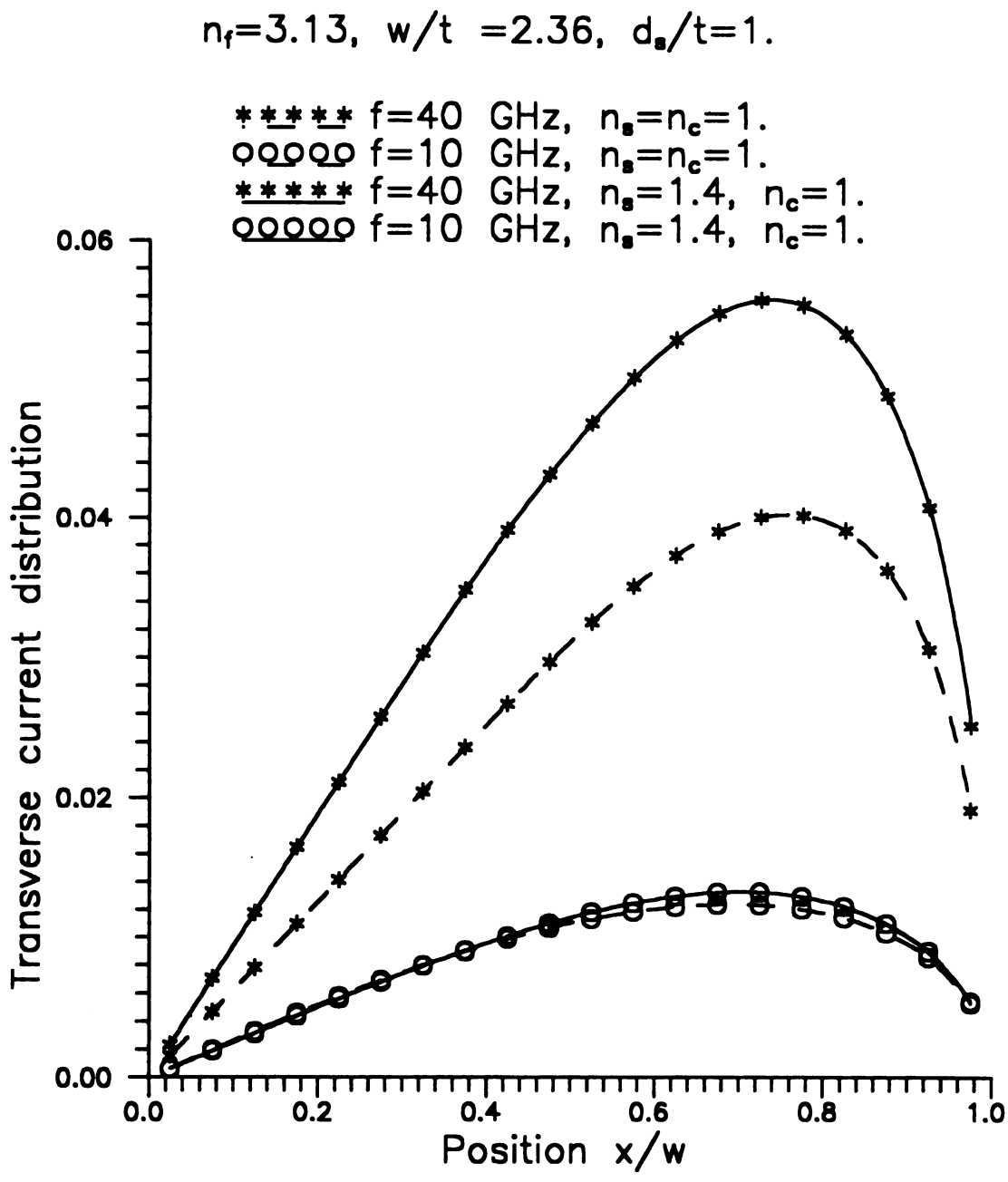

Figure 6.9: Comparison between the transverse current distributions of the principal mode for the conventional microstrip and those for the microstrip with superstrate operating at two frequencies.

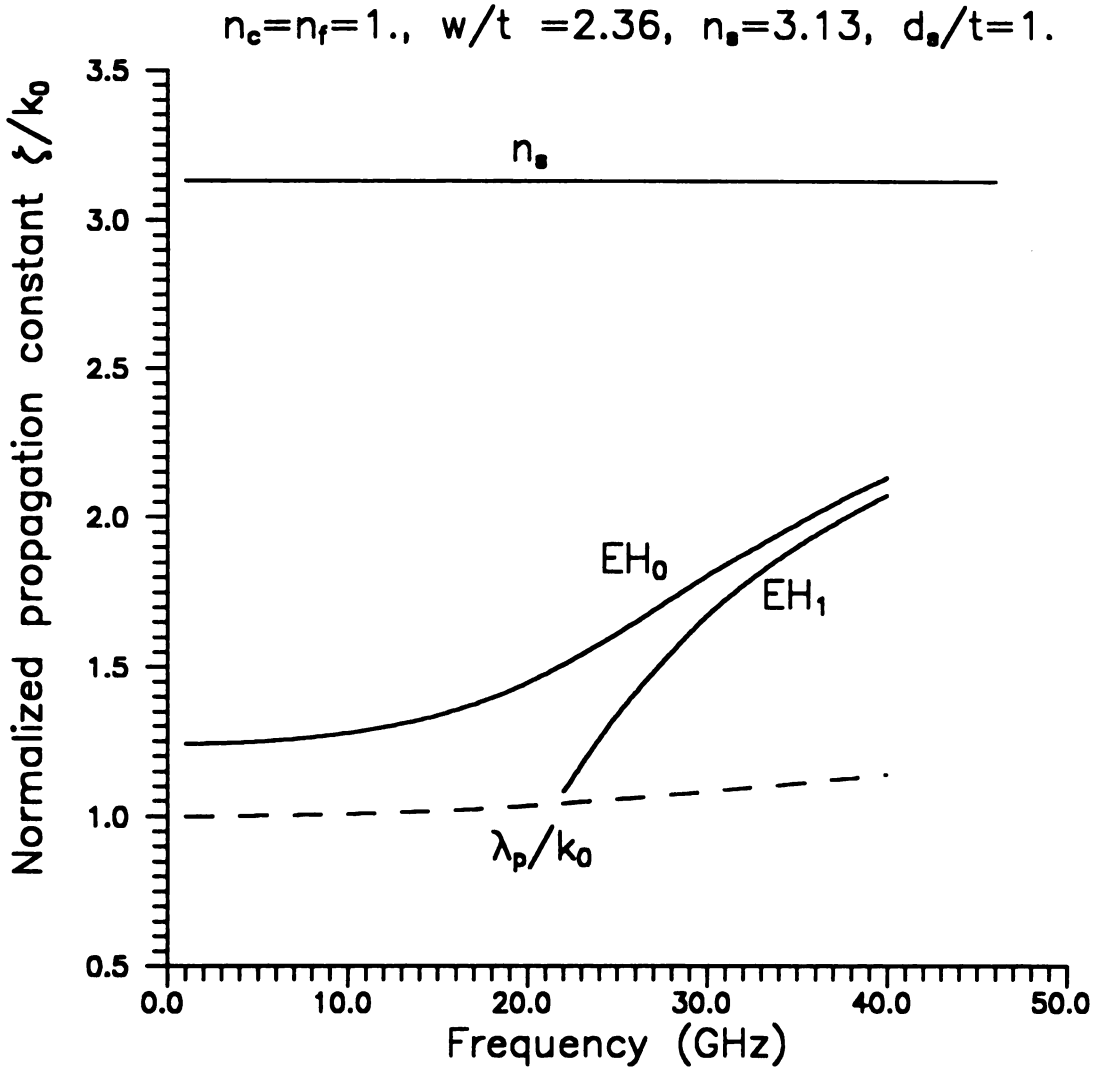

Figure 6.10: Dispersion characteristics of the principal and the first higher-order modes of the microstriop line with superstrate.

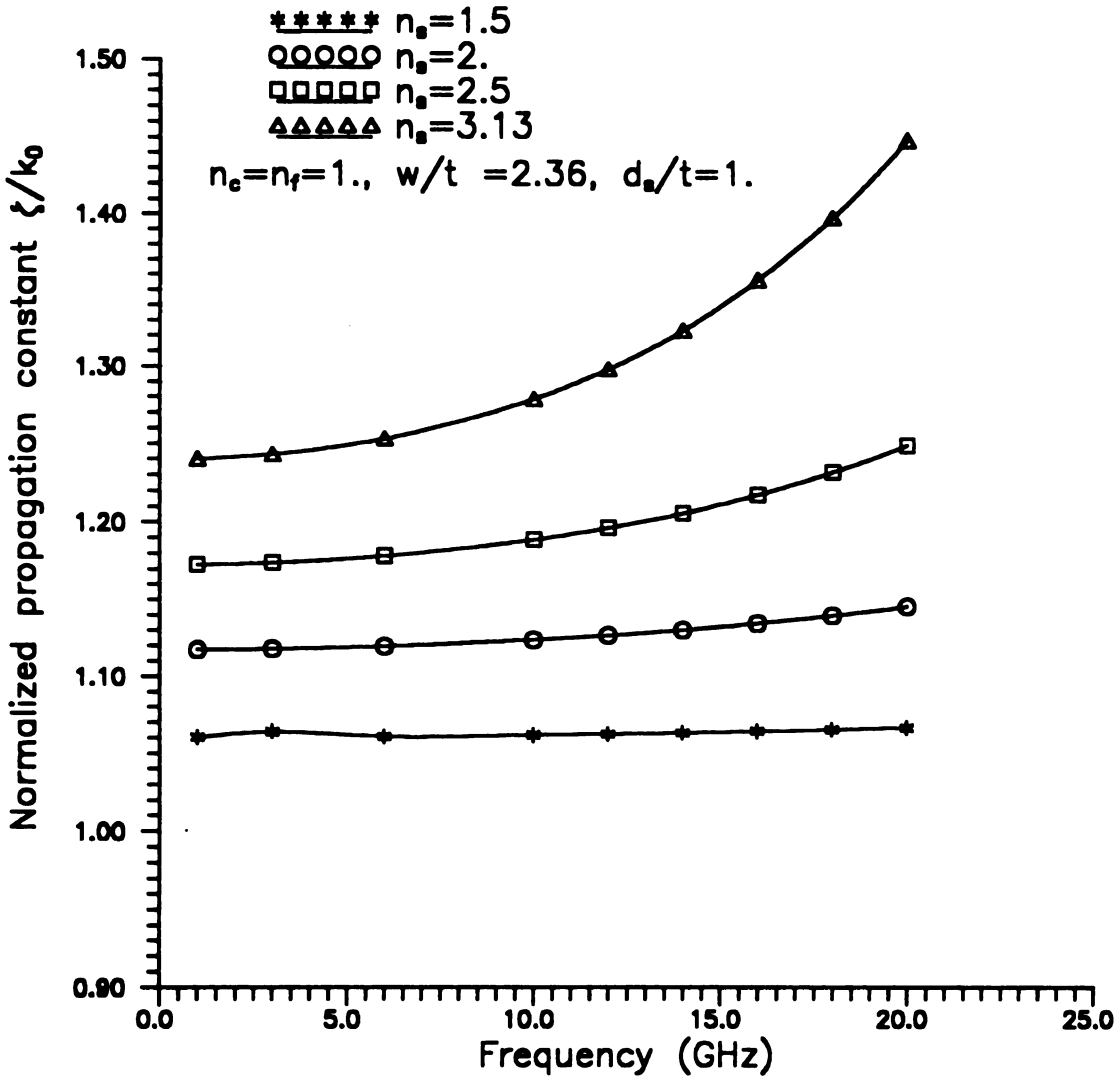

Figure 6.11: Dispersion characteristics of the principal mode with superstrate refractive index as parameter.

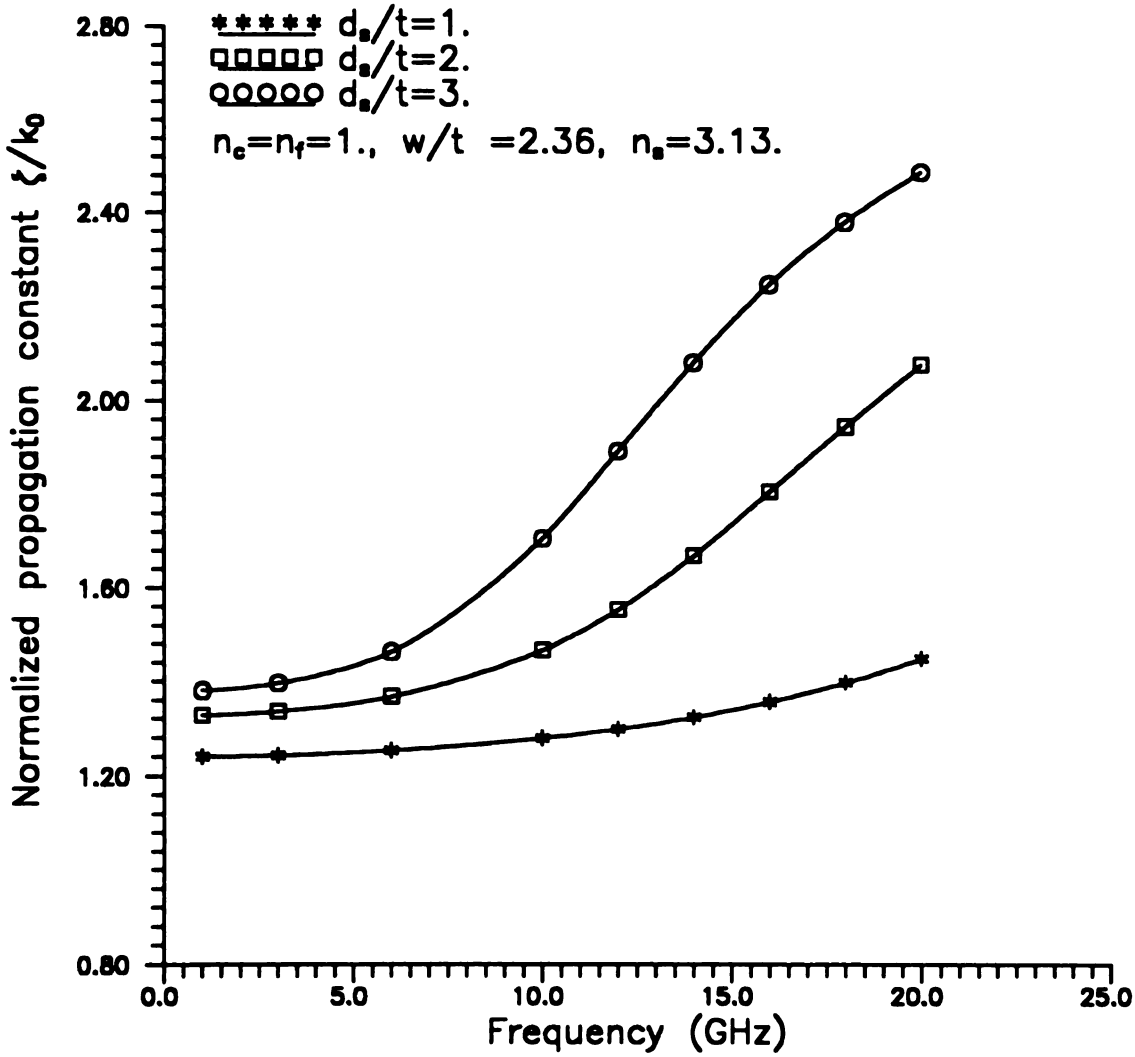

Figure 6.12: Dispersion characteristics of the principal mode with superstrate thickness as parameter.

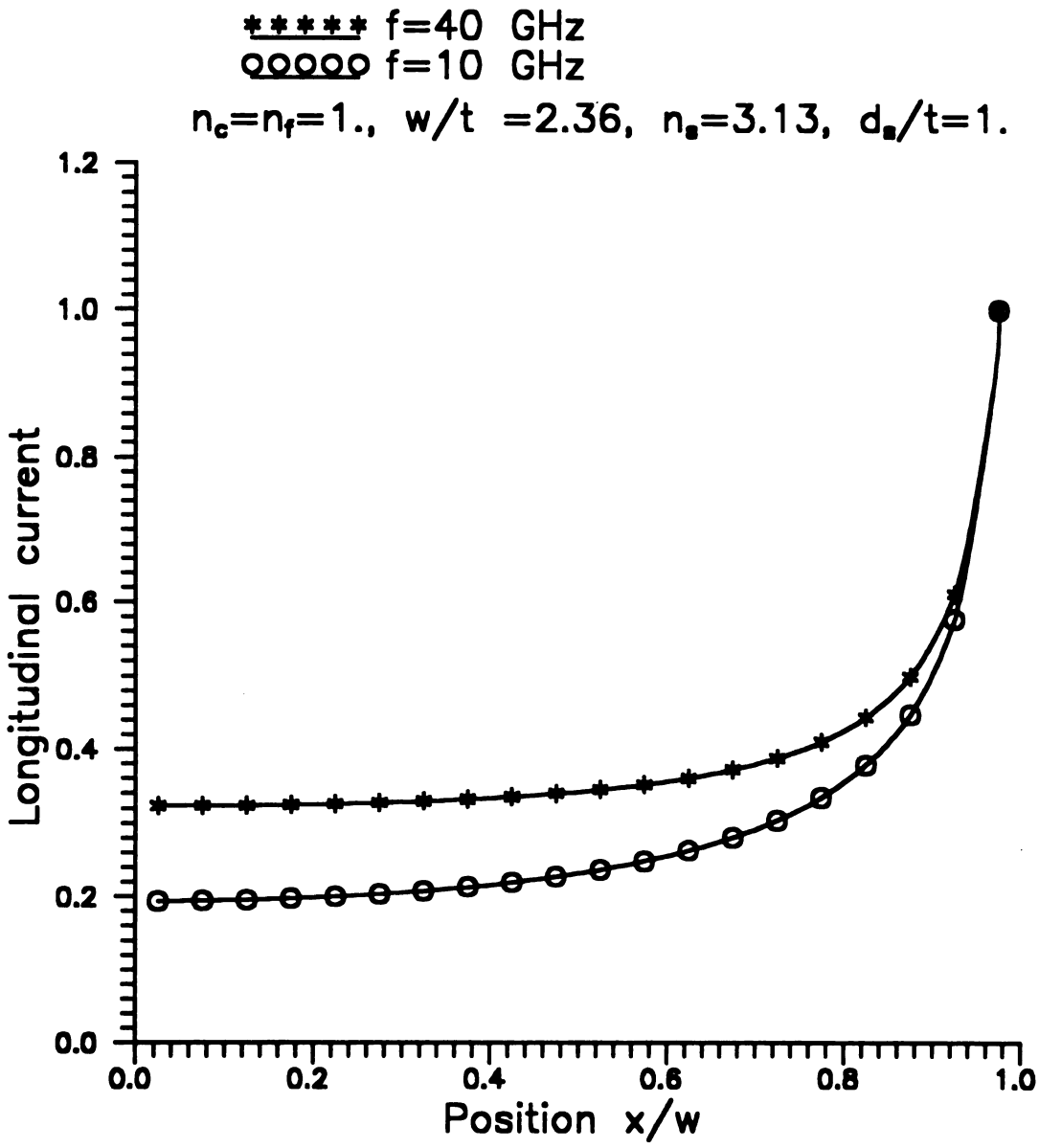

Figure 6.13: Longitudinal current distribution of the principal mode for the microstrip line with superstrate operating at two different frequencies.

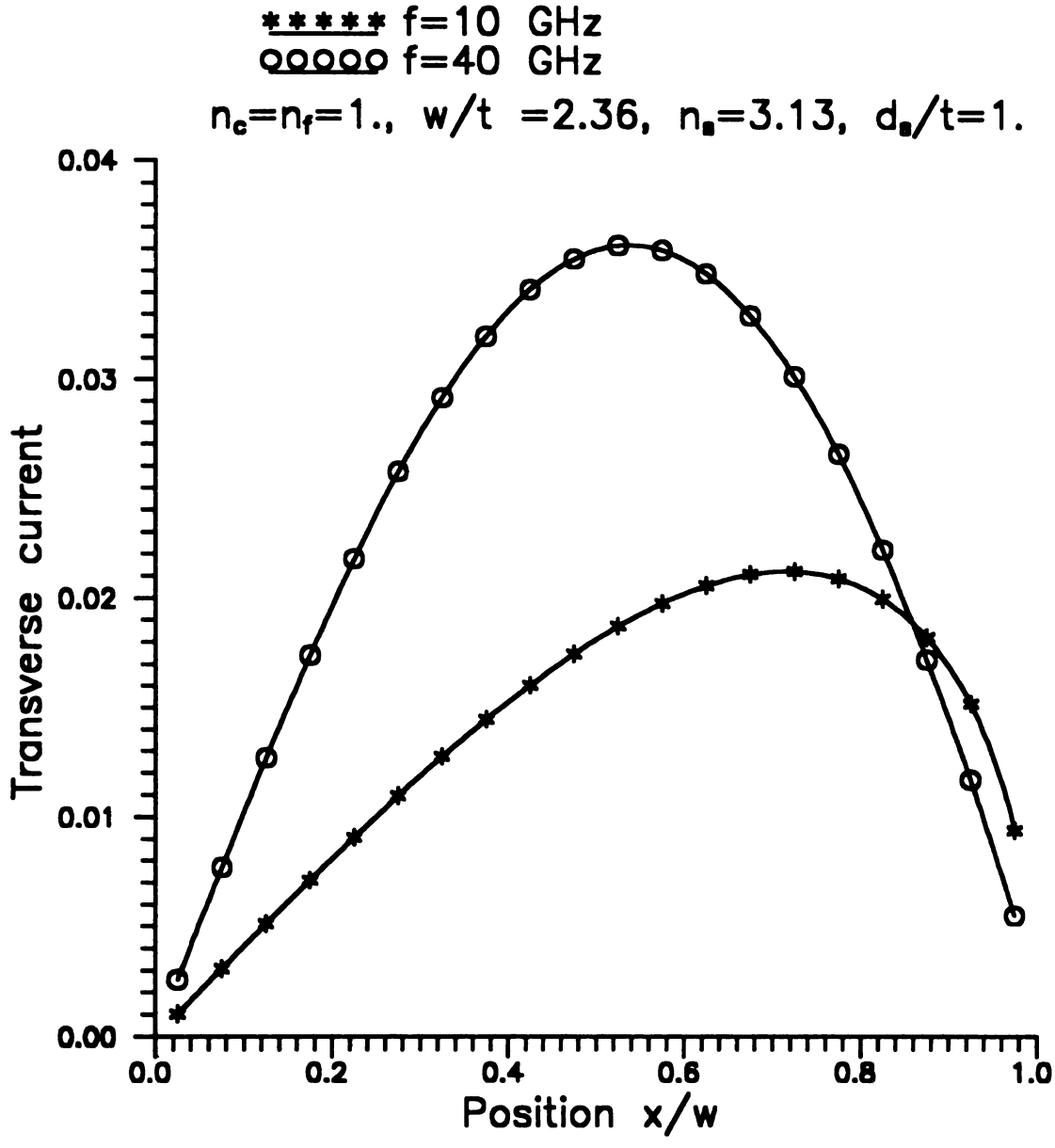

Figure 6.14: Transverse current distribution of the principal mode for the microstrip line with superstrate operating at two different frequencies.

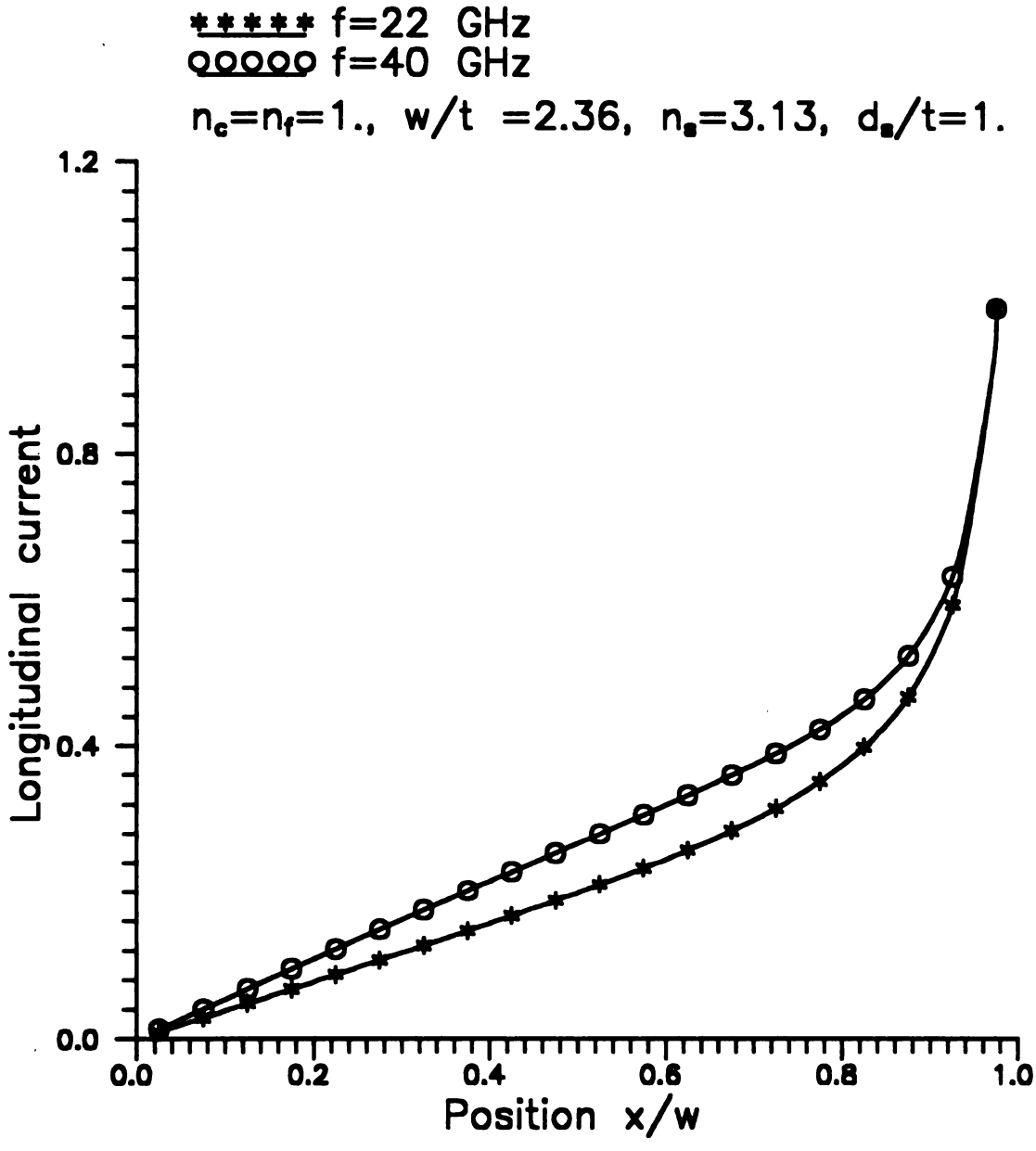

Figure 6.15: Longitudinal current distribution of the first higher-order mode for the microstrip line with superstrate operating at two different frequencies.

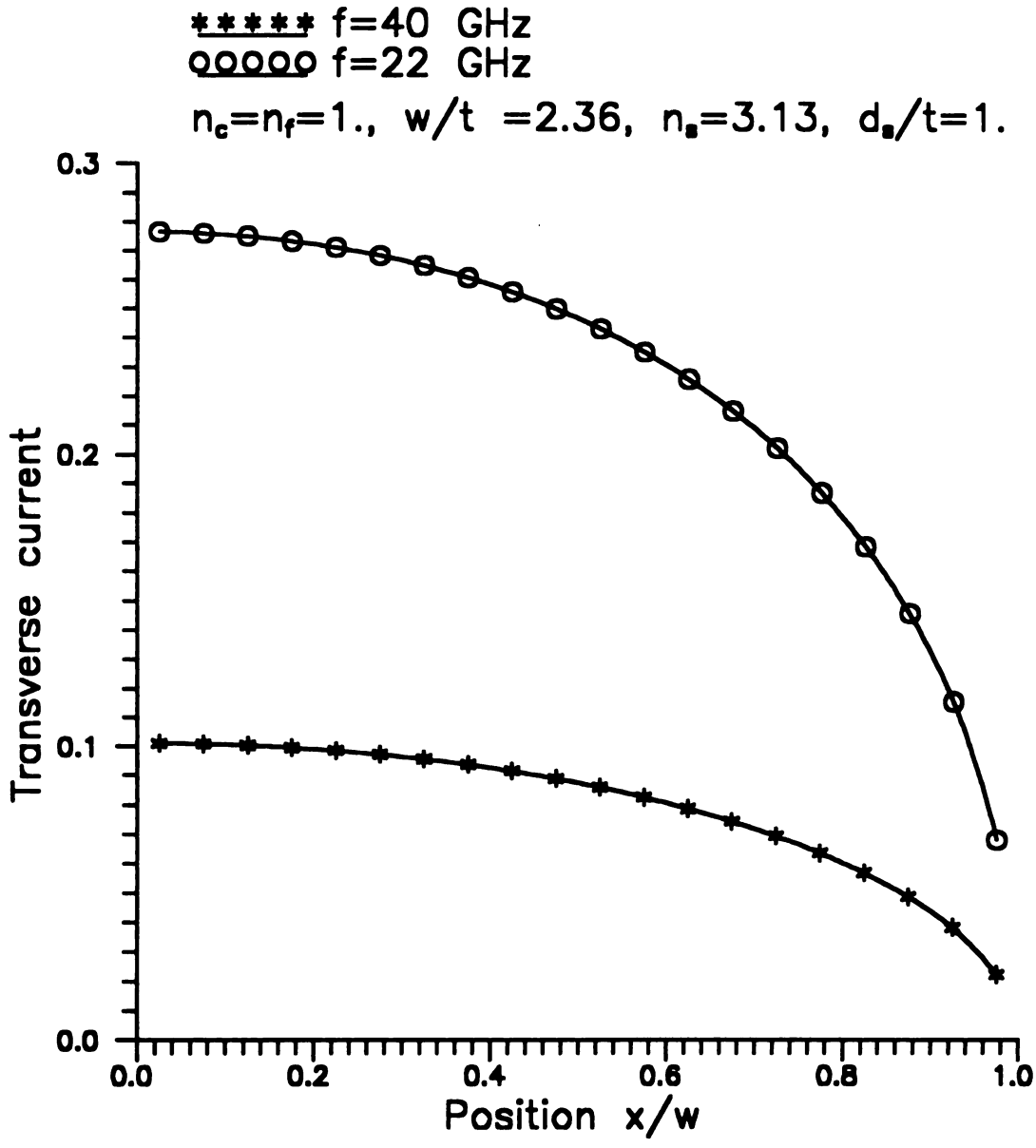

Figure 6.16: Transverse current distribution of the first higher-order mode for the microstrip line with superstrate operating at two different frequencies.

CHAPTER 7

CHARACTERISTIC IMPEDANCE OF MICROSTRIP TRANSMISSION LINE WITH SUPERSTRATE LAYER

7.1 INTRODUCTION

The dispersion characteristics of a microstrip with a superstrate layer were evaluated in chapter six. To completely analyze this microstrip structure, the characteristic impedance must be evaluated. We have seen in chapter five that the power-current method yields results very close to those of the voltage-current method. Since the latter method is much more convenient and is less analytically involved, we choose it to compute the characteristic impedance. We also have to note that the power-current method will be very difficult to exploit since the structure now involves additional layers.

7.2 FORMULATION OF THE PROBLEM

The voltage-current method developed in chapter five will be applied again in this chapter to obtain the characteristic impedance of the microstrip line with a superstrate layer. Consider the microstrip line of Fig. 6.3 with only the principal mode propagating along the $+z$ direction with propagation constant ζ_0. The characteristic impedance is defined by

$$Z = \frac{V_{av}}{I} \tag{1}$$

where the total longitudinal current I is given by

$$I = \int_{-w}^{w} k_z(x)\,dx \ . \tag{2}$$

The current density $k_z(x)$ is obtained in eqs (6.64) and (6.65) from the MOM solution to the integral equation. The average voltage V_{av} was defined in chapter five as follows

$$V_{av} = \frac{\int_{-w}^{w} v(x)\ k_z^*(x)\ dx}{\int_{-w}^{w} k_z^*(x)\ dx} \tag{3}$$

where the voltage is calculated by integrating the y component of electric field along the y-axis from the ground plane to the strip as follows

$$v(x) = \int_{gp}^{0} -e_{fy}(x,y)\,dy = -\int_{-t}^{0} e_{fy}(x,y)\,dy \ . \tag{4}$$

The spectral domain electric field in the substrate region is given as

$$\vec{e}_f(\vec{\rho}) = \frac{-j\eta_s}{k_s} \int_{-w}^{w} \bar{\bar{g}}_f^e(x,y|x',0;-\zeta_0)\cdot\vec{k}(\vec{\rho}')\,dx' \ . \tag{5}$$

Only the y-component of electric field is needed and is written as

$$e_{fy}(\vec{\rho}) = \int_{-w}^{w} \{g_{yx}^e(x,y|x',0;-\zeta_0)k_x(x') + g_{yz}^e(x,y|x',0;-\zeta_0)k_z(x')\}\,dx' \ . \tag{6}$$

With reference to Appendix B, the electric Green's dyad in the substrate region has the following scalar components

$$g^e_{\alpha\beta}(x,y|x',0;\zeta) = \frac{1}{2\pi}\int_{-\infty}^{\infty} L^e_{\alpha\beta}(\xi,\zeta,y)\,e^{j\xi(x-x')}d\xi \quad \text{... for } \alpha,\beta = x,y,z\ . \tag{7}$$

Only L^e_{yx} and L^e_{yz} are needed and are written as

$$\begin{aligned} L^e_{yx}(\xi,\zeta,y) &= j\xi N_s^{-2}\cosh p_f(y+t)\left(p_s(1+e^{-2p_s d_s}) + M_c^2 p_c(1-e^{-2p_s d_s})\right) \\ &\times\left\{\frac{(k_f^2+p_f^2)(N_s^2M_s^2-1)\left(p_s(1+e^{-2p_s d_s}) + N_c^2 p_c(1-e^{-2p_s d_s})\right)}{\cosh p_f t\, Z^e Z^h} + \frac{p_f}{\sinh p_f t\, Z^h}\right\} \\ &+ \frac{j\xi\cosh p_f(y+t)(k_f^2+p_f^2)(N_c^2M_c^2-1)4p_s^2M_s^2e^{-2p_s d_s}}{\cosh p_f t\, Z^e Z^h} \end{aligned} \tag{8}$$

$$\begin{aligned} L^e_{yz}(\xi,\zeta,y) &= j\zeta N_s^{-2}\cosh p_f(y+t)\left(p_s(1+e^{-2p_s d_s}) + M_c^2 p_c(1-e^{-2p_s d_s})\right) \\ &\times\left\{\frac{(k_f^2+p_f^2)(N_s^2M_s^2-1)\left(p_s(1+e^{-2p_s d_s}) + N_c^2 p_c(1-e^{-2p_s d_s})\right)}{\cosh p_f t\, Z^e Z^h} + \frac{p_f}{\sinh p_f t\, Z^h}\right\} \\ &+ \frac{j\zeta\cosh p_f(y+t)(k_f^2+p_f^2)(N_c^2M_c^2-1)4p_s^2M_s^2e^{-2p_s d_s}}{\cosh p_f t\, Z^e Z^h} \end{aligned} \tag{8}$$

Exploiting relation (7) in eq. (5) leads to

$$e_{fy}(\vec{\rho}) = \frac{-j\eta_s}{2\pi k_s}\int_{-w}^{w}\int_{-\infty}^{\infty}\{L^e_{yx}(\xi,-\zeta_0,y)k_x(x') + L^e_{yz}(\xi,-\zeta_0,y)k_z(x')\}\,e^{j\xi(x-x')}d\xi dx'\ . \tag{9}$$

Interchanging the spatial integration with the spectral one and recognizing that the spatial integration over the current can be interpreted as a Fourier transform on the variable x as follows

$$\begin{aligned} \int_{-w}^{w} k_x(x')e^{-j\xi x'}dx' &= \mathcal{F}\{k_x(x')\} = f_x(\xi) \\ \int_{-w}^{w} k_z(x')e^{-j\xi x'}dx &= \mathcal{F}\{k_z(x')\} = f_z(\xi) \end{aligned} \tag{10}$$

we have

$$e_{fy}(\vec{\rho}) = \frac{-j\eta_s}{2\pi k_s}\int_{-\infty}^{\infty}\{L_{yx}^{e}(\xi,-\zeta_0,y)f_x(\xi)+L_{yz}^{e}(\xi,-\zeta_0,y)f_z(\xi)\}e^{j\xi x}d\xi\ . \tag{11}$$

The current in eq. (10) is expressed in terms of Chebyshev polynomial series given by eqs. (6.64) and (6.65). Hence, the integral in eq. (10) can be evaluated in closed form. Referring to section 6.5, we have

$$f_\beta(\xi) = \int_{-w}^{w} k_\beta(x')e^{-j\xi x'}dx' = \sum_{n=1}^{N} a_{\beta n} f_{\beta n}(\xi) \quad \cdots \textit{for } \beta = x,z \tag{12}$$

where the $f_{\beta n}(\xi)$ are evaluated in terms of Bessel functions as follows

$$\begin{aligned} f_{zn}(\xi) &= (-1)^n \pi w J_{2n}(\xi w) \\ f_{xn}(\xi) &= -j(-1)^n \frac{\pi w}{2}\left[J_{2n+1}(\xi w)+\frac{1}{2}J_{2(n+1)+1}(\xi w)+\frac{1}{2}J_{2(n-1)+1}(\xi w)\right]. \end{aligned} \tag{13}$$

Exploiting the expression for the electric field given by eq. (9), the average voltage in relation (3) becomes

$$\begin{aligned} v_{av} &= \frac{-\int_{-w}^{w}\int_{-t}^{0} e_{fy}(x,y)k_z^{*}(x)dy\,dx}{\int_{-w}^{w} k_z^{*}dx} \\ &= \frac{j\eta_s}{2\pi k_s}\frac{\int_{-w}^{w}dx\int_{-t}^{0}dy\int_{-\infty}^{\infty}\{L_{yx}^{e}(\xi,0,-\zeta_0,y)f_x(\xi)+L_{yz}^{e}(\xi,-\zeta_0,y)f_z(\xi)\}e^{j\xi x}d\xi\,k_z^{*}(x)}{\int_{-w}^{w}k_z^{*}(x)dx}\ . \end{aligned} \tag{14}$$

Interchanging the first spatial integration with the spectral one and using the fact that

$$\int_{-w}^{w} k_z^{*}(x)e^{j\xi x}dx = f_z^{*}(\xi) \tag{15}$$

the average voltage becomes

$$V_{av} = \frac{j\eta_s}{2\pi k_s} \frac{\int_{-t}^{0} dy \int_{-\infty}^{\infty} \{ L_{yx}^e(\xi,-\zeta_0,y) f_x(\xi) f_z^*(\xi) + L_{yz}^e(\xi,-\zeta_0,y) f_z(\xi) f_z^*(\xi) \} d\xi}{\int_{-w}^{w} k_z^*(x)\, dx} . \quad (16)$$

Exploiting eqs. (2) and (16), relation (1) for the characteristic impedance yields

$$Z = \frac{j\eta_s}{2\pi k_s} \frac{\int_{-t}^{0} dy \int_{-\infty}^{\infty} \{ L_{yx}^e(\xi,-\zeta_0,y) f_x(\xi) f_z^*(\xi) + L_{yz}^e(\xi,-\zeta_0,y) f_z(\xi) f_z^*(\xi) \} d\xi}{\int_{-w}^{w} k_z(x)\, dx \int_{-w}^{w} k_z^*(x)\, dx} . \quad (17)$$

The spatial integration in eq. (17) can be performed analytically to yield

$$\begin{aligned} \int_{-t}^{0} L_{yz}^e(\xi,-\zeta_0,y)\, dy &= -j\zeta_0 L^e(\xi,-\zeta_0) \\ \int_{-t}^{0} L_{yx}^e(\xi,-\zeta_0,y)\, dy &= j\xi L^e(\xi,-\zeta_0) \end{aligned} \quad (18)$$

where

$$\begin{aligned} L^e(\xi,\zeta,y) = N_s^{-2} \left(p_s (1 + e^{-2p_s d_s}) + M_c^2 p_c (1 - e^{-2p_s d_s}) \right) \\ \times \left\{ \frac{(k_f^2 + p_f^2)(N_s^2 M_s^2 - 1) \left(p_s (1 + e^{-2p_s d_s}) + N_c^2 p_c (1 - e^{-2p_s d_s}) \right) \tanh p_f t}{p_f Z^e Z^h} + \frac{1}{Z^h} \right\} \\ + \frac{\tanh p_f t (k_f^2 + p_f^2)(N_c^2 M_c^2 - 1) 4 p_s^2 M_s^2 e^{-2p_s d_s}}{p_f Z^e Z^h} . \end{aligned} \quad (19)$$

Moreover, the principal mode is an even mode and therefore the longitudinal current is represented by Chebyshev polynomials of even order as follows

$$k_z(x) = \sum_{n=0}^{N} a_{zn} \frac{T_2 n(x/w)}{\sqrt{1-(x/w)^2}} \quad . \tag{20}$$

Exploiting the orthogonality of Chebyshev polynomials and eq. (20), expression (2) can be readily evaluated as in chapter six. We obtain

$$I = \pi w a_{z0} \tag{21}$$

where a_{z0} is the first expansion coefficient in the series for the z-component of current given in eq. (20).

Substituting eqs. (18) and (21) in eq. (17), the expression for the characteristic impedance is found as

$$Z = \frac{\eta_s}{2\pi^3 k_s w^2 |a_{z0}|^2} \int_{-\infty}^{\infty} \left[\zeta_0 L^e(\xi,-\zeta_0) f_z(\xi) f_z^*(\xi) - \xi L^e(\xi,-\zeta_0) f_x(\xi) f_z^*(\xi) \right] d\xi \quad . \tag{22}$$

It is found that the integrand in the above expression is an even function of ξ. Hence, the final form of characteristic impedance is

$$Z = \frac{\eta_s}{\pi^3 k_s w^2 |a_{z0}|^2} \int_{0}^{\infty} \left[\zeta_0 L^e(\xi,-\zeta_0) f_z(\xi) f_z^*(\xi) - \xi L^e(\xi,-\zeta_0) f_x(\xi) f_z^*(\xi) \right] d\xi \quad . \tag{23}$$

The spectral integration in eq. (23) is performed numerically.

7.3 NUMERICAL RESULTS

Numerical results are obtained for the typical configuration shown in Fig. 6.3 with various physical parameters. We first consider a microstrip line with parameters $2w = 3.0mm$, $t = 0.635mm$, $n_c = 1$ and $n_f = 3.13$. These are the same parameters used in Fig. 6.6, which illustrates the dispersion curve. Figure 7.1 shows the characteris-

tic impedance versus frequency for various superstrate permittivities and fixed superstrate height. It can be seen that as the superstrate permittivity becomes larger, the characteristic impedance gets smaller. This is as expected, since as the superstrate permittivity grows, the relative dominance of substrate and superstrate fields varies. In this case, the fields in the superstrate grow correspondingly giving rise to a decrease in the voltage in the substrate and hence the characteristic impedance decreases. We also have to note that this microstrip structure behaves like the conventional microstrip since the characteristic impedance increases with frequency.

Figure 7.2 illustrates the characteristic impedance versus frequency for a fixed superstrate permittivity and normalized superstrate height as parameter. It can be seen that as the superstrate thickness gets larger, the chararcteristic impedance slightly decreases. This can be explained by the fact that as the superstrate thickness grows, less electric field is concentrated underneath the strip and a decrease in the voltage and the characteristic impedance results.

Now, we turn our attention to the microstrip of Fig. 6.3, having air as substrate and cover. Figure 7.3 shows the characteristic impedance versus frequency with the superstrate refractive index as parameter. As the superstrate refractive index gets larger, the characteristic impedance decreases. Moreover, the characterstic impedance displays a significant change as a function of frequency for larger refractive indices (for $n_s = 2.5$ and $n_s = 3.13$). We also have to note that, for this particular structure, the characteristic impedance decreases with an increase in frequency. This is due to the fact that for this structure the relative substrate/superstrate fields are completely different from the conventional microstrip since the substrate does not

have the highest refractive index.

Figure 7.4 illustrates the characteristic impedance versus frequency with superstrate thickness as parameter. As the superstrate gets thicker, the characteristic impedance decreases. Moreover, this decrease is more pronounced than for the structure of Fig. 7.2. This can be explained by the fact that the field underneath the strip becomes smaller as the superstrate thickness increases. Consequently, the average voltage in the expression for the characteristic impedance (1) will decrease and so does the characteristic impedance.

7.4 SUMMARY

Two types of microstrip line with superstrate were analyzed. First, a microstrip line with substrate layer having the largest permittivity was analyzed. It was shown that the characteristic impedance for this structure does not deviate much from that of the conventional microstrip. Second, the results for a microstrip line having both the substrate and cover as free space displayed a tremendous change as its characteristic impedance showed a decrease with frequency. The voltage-current method was adopted in this analysis since it is less analytically involved than the power-current method.

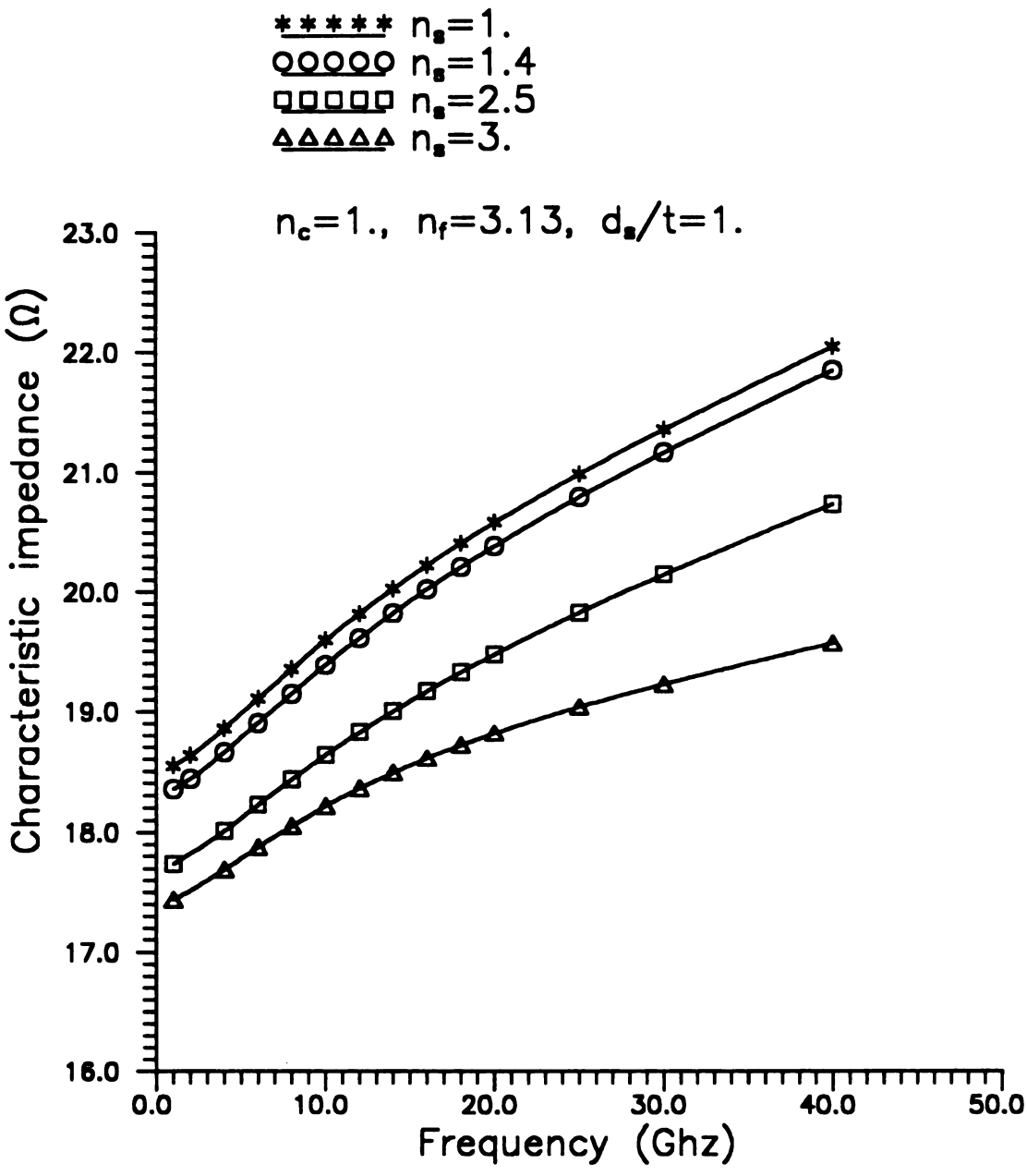

Figure 7.1: Characteristic impedance versus frequency for different superstrate refractive indices with w = 1.5 mm, t =0.635 mm, and ds /t = 1.

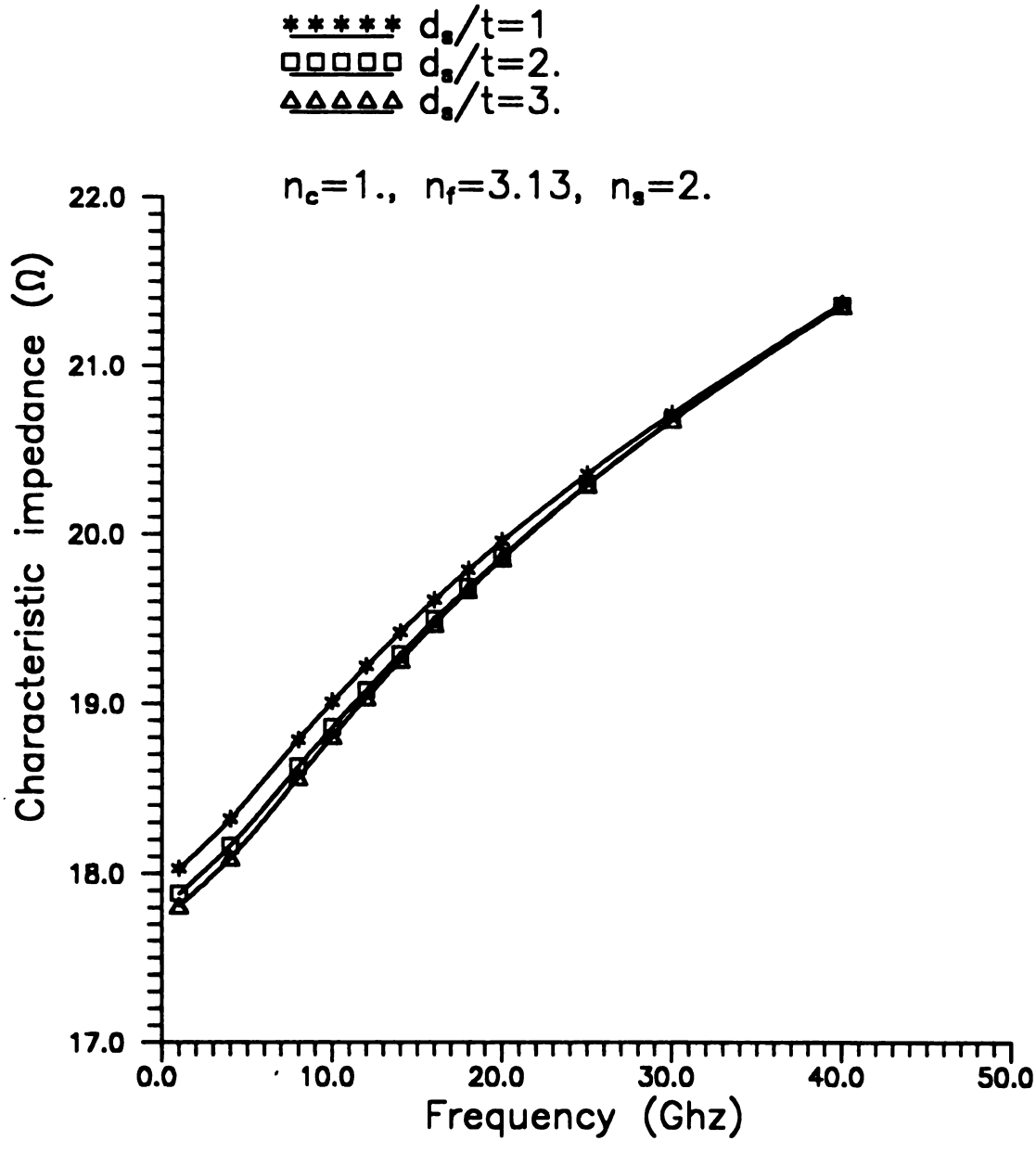

Figure 7.2: Characteristic impedance versus frequency for different superstrate height with w = 1.5 mm, t =0.635 mm, and n_s = 2.

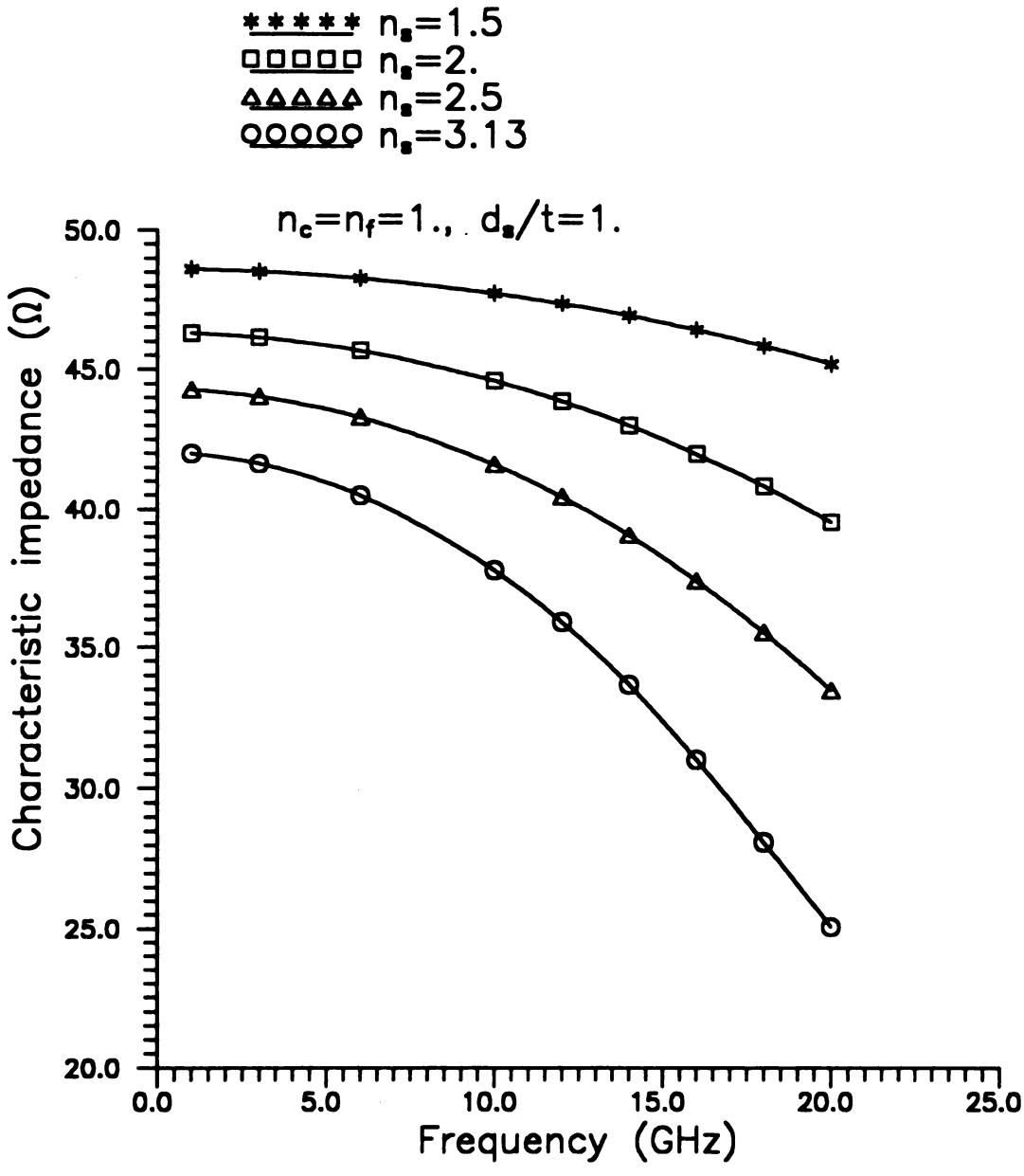

Figure 7.3: Characteristic impedance versus frequency for different superstrate refractive indices with w = 1.5 mm, t =0.635 mm, and ds /t = 1.

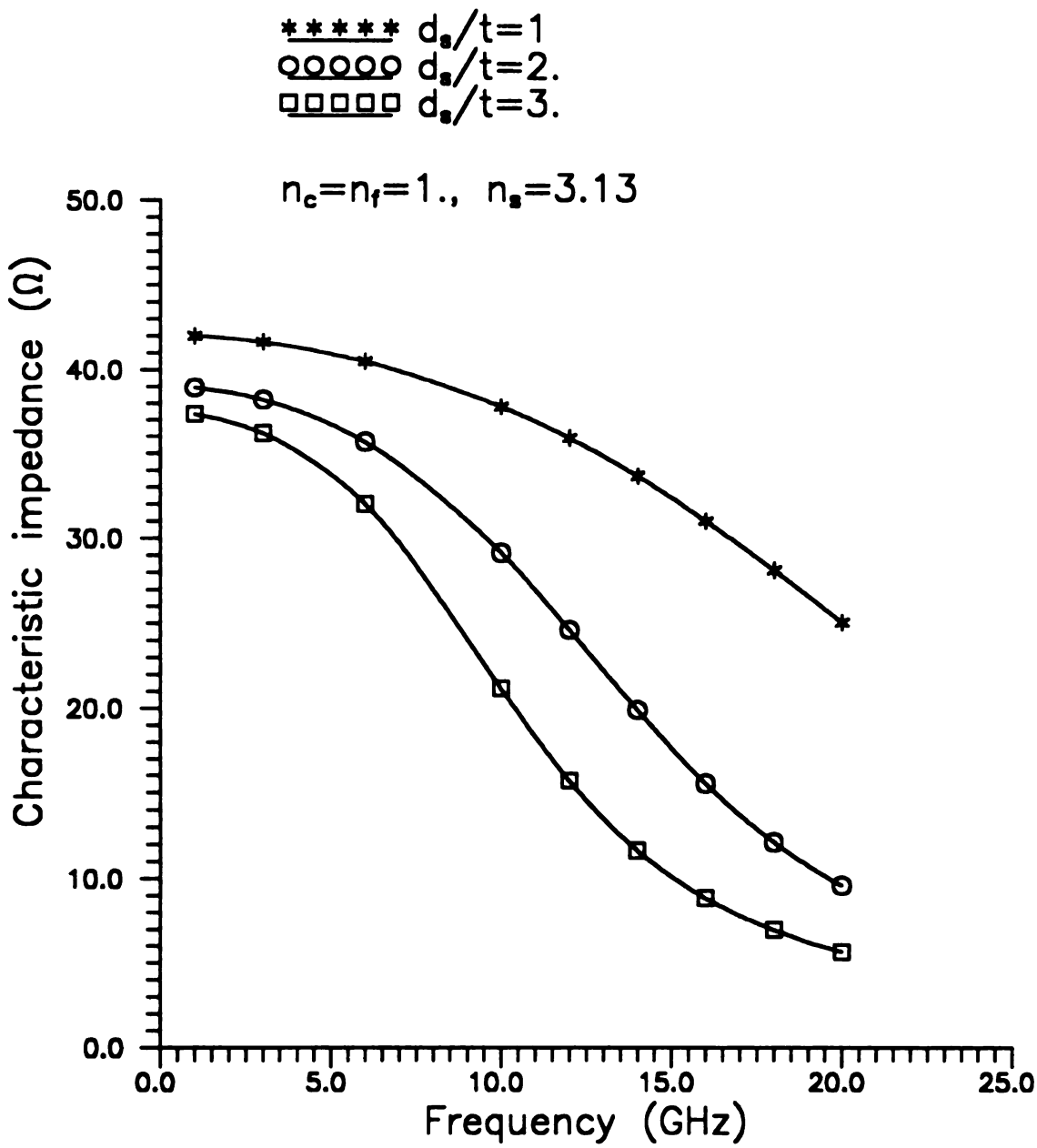

Figure 7.4: Characteristic impedance versus frequency for different superstrate height with w = 1.5 mm, t =0.635 mm, and n_s = 3.13.

CHAPTER 8

EM CHARACTERIZATION OF MATERIALS IN A MICROSTRIP SUPERSTRATE ENVIRONMENT

8.1 INTRODUCTION

In this chapter the dielectric (complex permittivity ϵ) and magnetic (complex permeability μ) characteristics are deduced for materials located in the superstrate of a four-layered conductor/substrate/superstrate/cover microstrip environment. A microstrip field applicator, providing a flexible broadband measurement methodology to accommodate material samples of various types, has been designed [53] and implemented for use with an automatic network analyzer.

The field applicator shown in Fig. 8.1 consists of a strip conductor located parallel to a conducting ground plate. Tapered transition regions connect the coaxial applicator terminals to the uniform strip region in which material samples are placed. The sample is located as a superstrate above the strip conductor. The transition regions, identified in Fig. 8.1 were designed to minimize ambient reflections. A method was devised to measure the scattering parameters of those transition regions between coaxial terminal ports and the front and back terminal planes of the sample region. Scattering parameters of the superstrate-loaded microstrip region are deembedded from measured S-parameters.

Measured scattering parameters of the sample region are processed to determine phase constant β_m and interfacial reflection coefficient Γ_m. Equating the analyt-

ical full-wave solutions for those quantities, available from previous chapters, to their measured values leads to a pair of complex transcendental equations $\beta(\epsilon,\mu,\omega) - \beta_m(\omega) = 0$ and $\Gamma(\epsilon,\mu,\omega) - \Gamma_m(\omega) = 0$, which are solved numerically for the desired constitutive parameters $\epsilon(\omega)$ and $\mu(\omega)$.

8.2 CHARACTERIZATION OF FIELD APPLICATOR: MEASUREMENT OF TRANSITION REGION S PARAMETERS

Using an equivalent two-port network of the system, as shown in Fig. 8.2, the scattering parameters of transition regions "a" and "b" and the sample region will be quantified. The reflected wave amplitudes are designated as b_i while a_i are the incident wave amplitudes.

8.2.1 Transition region "a"

Referring to Fig. 8.2, the scattering matrix [S] of transition region "a" relates the amplitudes of the reflected waves b_1, b_2 to the amplitudes of the incident waves a_1, a_2 as follows

$$\begin{bmatrix} b_1 \\ b_2 \end{bmatrix} = \begin{bmatrix} S_{11}^a & S_{12}^a \\ S_{21}^a & S_{22}^a \end{bmatrix} \begin{bmatrix} a_1 \\ a_2 \end{bmatrix} . \tag{1}$$

Solving for b_2 and using the fact that $a_2 = \Gamma_2 b_2$, we have

$$b_2 = \frac{S_{21}^a}{1 - S_{22}^a \Gamma_2} a_1 . \tag{2}$$

The reflection coefficient at terminal port 1 as given as

$$\Gamma_1 = \frac{b_1}{a_1} \ . \tag{3}$$

Solving for b_1 in eq. (1) in terms of a_1 and a_2 exploiting $a_2 = \Gamma_2 b_2$ and eq. (2), expression (3) becomes

$$\Gamma_1 = S_{11}^a + \frac{S_{12}^a S_{21}^a \Gamma_2}{1 - S_{22}^a \Gamma_2} \ . \tag{4}$$

Hence, to determine the scattering parameters for transition region "a", we need to measure Γ_1^{ci} (c for calibration, and $i = 1,2,3$) with port 2 terminated by three known terminations. A short placed at three known locations provides $\Gamma_2^{ci} = -\exp(-jk_0 l_i)$ with $l_1 = 0, l_2 = -l$ and $l_3 = l$. Applying expression (4) for three calibration measurements and solving simultaneously for the desired transition-region parameters subsequently leads to [53]

$$S_{11}^a = \Gamma_1^{c1} - \frac{S_{12}^a S_{21}^a \Gamma_1^{c1}}{1 - S_{22}^a \Gamma_2^{c1}} \tag{5}$$

with

$$S_{12}^a S_{21}^a = \left(\Gamma_1^{c2} - \Gamma_1^{c1}\right) \frac{\left(1 - S_{22}^a \Gamma_2^{c1}\right)\left(1 - S_{22}^a \Gamma_2^{c2}\right)}{\Gamma_2^{c2} - \Gamma_2^{c1}} \tag{6}$$

and

$$S_{22}^a = \frac{K^c - 1}{K^c \Gamma_2^{c3} - \Gamma_2^{c2}} \tag{7}$$

where the calibration constant K^c is defined as

$$K^c = \frac{\Gamma_1^{c3} - \Gamma_1^{c1}}{\Gamma_1^{c2} - \Gamma_1^{c1}} \frac{\Gamma_2^{c2} - \Gamma_2^{c1}}{\Gamma_2^{c3} - \Gamma_2^{c1}} \ . \tag{8}$$

Finally, with the scattering parameters $S^a_{\alpha\beta}$ known, the reflection coefficient at terminal port 2 is deduced from that measured at port 1 using eq. (4) as follows

$$\Gamma_2 = \frac{\Gamma_1 - S^a_{11}}{(\Gamma_1 - S^a_{11})S^a_{22} + S^a_{12}S^a_{21}} \quad . \tag{9}$$

8.2.2 Transition region "b"

Again, referring to Fig. 8.2, the scattering matrix of the sample region relates the amplitudes of the reflected waves to the incident waves as follows

$$\begin{bmatrix} b_3 \\ b_4 \end{bmatrix} = \begin{bmatrix} S^s_{11} & S^s_{12} \\ S^s_{21} & S^s_{22} \end{bmatrix} \begin{bmatrix} a_3 \\ a_4 \end{bmatrix} . \tag{10}$$

Solving for b_4 in terms of a_3 and a_4 and using the fact that $a_4 = \Gamma_4 b_4$, we have

$$b_4 = \frac{S^s_{21}}{1 - S^s_{22}\Gamma_4} a_3 \quad . \tag{11}$$

The reflection coefficient at terminal port 3 is given as

$$\Gamma_2 = \frac{a_2}{b_2} = \frac{b_3}{a_3} \quad . \tag{12}$$

Solving for b_3 in eq. (10) in terms of a_3 and a_4 and exploiting $a_4 = \Gamma_4 b_4$ and eq.(11), expression (12) becomes

$$\Gamma_2 = S^s_{11} + \frac{S^s_{12}S^s_{21}\Gamma_4}{1 - S^s_{22}\Gamma_4} \quad . \tag{13}$$

We have to note that since terminal port 6 is matched, we have

$$\Gamma_4 = S_{11}^b \ . \tag{14}$$

The transmission through the field applicator is described by

$$S_{21} = \frac{b_6}{a_1} = \frac{b_2}{a_1}\frac{b_4}{a_3}\frac{b_6}{a_5} = \frac{b_2}{a_1}\frac{b_4}{a_3}S_{21}^b \ . \tag{15}$$

Exploiting expressions (2), (11) and (14), eq. (15) becomes

$$S_{21} = \frac{S_{21}^a S_{21}^b}{1 - S_{22}^a \Gamma_2}\frac{S_{21}^s}{1 - S_{22}^s S_{11}^b} \ . \tag{16}$$

It can be seen from eq. (16) that we need to measure S_{11}^b and $S_{21}^a S_{21}^b$ [53]. First, to measure S_{11}^b we measure the reflection coefficient Γ_4 at terminal port 4 with the sample region "empty". We consequently obtain

$$\Gamma_4 = \frac{a_4}{b_4} = \frac{b_3}{a_3}\, e^{j2k_0 l_s} \ . \tag{17}$$

Using the fact that $\frac{b_3}{a_3} = \frac{a_2}{b_2} = \Gamma_2^e$, where the superscript e denotes that the sample region is "empty", and exploiting eq. (14) leads to

$$S_{11}^b = \Gamma_2^e\, e^{j2k_0 l_s} \ . \tag{18}$$

To measure $S_{21}^a S_{21}^b$ we use expression (16) with the sample region empty. In this case we have

$$\begin{aligned} S_{22}^s &= 0 \\ S_{21}^s &= e^{-jk_0 l_s} \ . \end{aligned} \tag{19}$$

Using eq. (19), expression (16) becomes

$$S_{21}^{e} = \frac{S_{21}^{a} S_{21}^{b}}{1 - S_{22}^{a} \Gamma_2^{e}} \, e^{-jk_0 l_s} \, . \tag{20}$$

Rearranging eq. (20) leads to

$$S_{21}^{a} S_{21}^{b} = S_{21}^{e} \left(1 - S_{22}^{a} \Gamma_2^{e}\right) e^{jk_0 l_s} \, . \tag{21}$$

This completes the necessary calibration of the two transition regions.

8.3 DE-EMBEDDING OF SAMPLE-REGION S PARAMETERS FROM MEASURED TERMINAL S PARAMETERS

We measure Γ_2^{t} and S_{21}^{t} under "test" conditions with sample present, to obtain

$$\Gamma_2 = S_{11}^{s} + \frac{S_{12}^{s} S_{21}^{s} S_{11}^{b}}{1 - S_{22}^{s} S_{11}^{b}} \tag{22}$$

$$S_{21}^{t} = \frac{S_{21}^{a} S_{21}^{b}}{1 - S_{22}^{a} \Gamma_2^{t}} \frac{S_{21}^{s}}{1 - S_{22}^{s} S_{11}^{b}} \, . \tag{23}$$

For the sample region, we have

$$\begin{aligned} S_{22}^{s} &= S_{11}^{s} \\ S_{12}^{s} &= S_{21}^{s} \, . \end{aligned} \tag{24}$$

Exploiting eqs. (24) in expressions (22) and (23) and rearranging leads to

$$\Gamma_2^{t} = S_{11}^{s} + \frac{\left(S_{21}^{s}\right)^2 S_{11}^{b}}{1 - S_{11}^{s} S_{11}^{b}} \tag{25}$$

$$\frac{S_{21}^{s}}{1 - S_{11}^{s} S_{11}^{b}} = \frac{1 - S_{22}^{a} \Gamma_2^{t}}{S_{21}^{a} S_{21}^{b}} S_{21}^{t} \, . \tag{26}$$

Expressions (25) and (26) can be solved analytically for S_{11}^s and S_{21}^s [53]. We have to note that the reflection coefficient at terminal port 2 is known form measured reflection coefficient at terminal port 1 as indicated by eq. (9). If we let

$$\begin{aligned} \Gamma_2^t &= P \\ \frac{1 - S_{22}^a \Gamma_2^t}{S_{21}^a S_{21}^b} S_{21}^t &= Q \end{aligned} \tag{27}$$

we can solve for S_{11}^s and S_{21}^s from eqs (25) and (26) as follows

$$\begin{aligned} S_{11}^s &= \frac{P - S_{11}^b Q^2}{1 - (S_{11}^b Q)^2} \\ S_{21}^s &= Q \frac{1 - S_{11}^b P}{1 - (S_{11}^b Q)^2} \end{aligned} \tag{28}$$

8.4 DETERMINATION OF MATERIAL CONSTITUTIVE PARAMETERS FROM MEASURED SAMPLE-REGION S PARAMETERS

The sample-region parameters are related to the measured S parameters as

$$\begin{aligned} S_{11}^s &= \frac{\Gamma(1 - T^2)}{1 - \Gamma^2 T^2} \\ S_{21}^s &= \frac{(1 - \Gamma^2) T}{1 - \Gamma^2 T^2} \end{aligned} \tag{29}$$

The interfacial reflection coefficient Γ and the transmission propagation factor T are defined as

$$\Gamma = \frac{Z_c^s - Z_c^e}{Z_c^s + Z_c^e} \tag{30}$$

$$T = e^{-j\beta l_s} \tag{31}$$

where $Z_c^{e,s}$ are the characteristic impedances of empty and sample regions and β is the propagation phase constant of the sample region. Expression (29) can be solved by the Nicholson-Ross-Wier (NRW) technique [54,55] for Γ and T to yield

$$\Gamma = K \pm \sqrt{K^2 - 1} \tag{32}$$

$$T = \frac{\left(S_{11}^s + S_{21}^s\right) - \Gamma}{1 - \left(S_{11}^s + S_{21}^s\right)\Gamma} \tag{33}$$

where

$$K = \frac{\left(S_{11}^s\right)^2 - \left(S_{21}^s\right)^2 + 1}{2S_{11}^s} \,. \tag{34}$$

Equating measured $\beta_m(\omega)$ and $\Gamma_m(\omega)$ to the corresponding theoretical values leads to a pair of equations which can be solved for complex ϵ and μ as follows

$$\begin{aligned} \beta(\epsilon,\mu,\omega) - \beta_m(\omega) &= 0 \\ \Gamma(\epsilon,\mu,\omega) - \Gamma_m(\omega) &= 0 \,. \end{aligned} \tag{35}$$

A full-wave theory for the microstrip phase constant and characteristic impedance was developed in chapters 6 and 7; it renders the above equations transcendental, and they must be solved numerically by a 2-D root search. The interfacial reflection coefficient is related to the characteristic impedance as follows

$$\Gamma = \frac{z_c - 1}{z_c + 1} \tag{36}$$

where z_c is the characteristic impedance normalized to that of the unloaded region.

8.5 NUMERICAL RESULTS

Measurements have been implemented for frequencies over the band of 300-2000 MHz. It was found that the reflection coefficient Γ is very small for this particular configuration and gets mixed with the noise. This is due to the fact that radiation exists and is not accounted for in this Nicholson-Ross-Wier (NRW) technique [54,55]. Hence, only results for the complex ϵ of a non-magnetic material have been obtained, and the root search was found to be stable. Figure 8.3 shows the real and imaginary part of the permittivity of a teflon sample. It can be seen that the real part of ϵ is around 2 as expected.

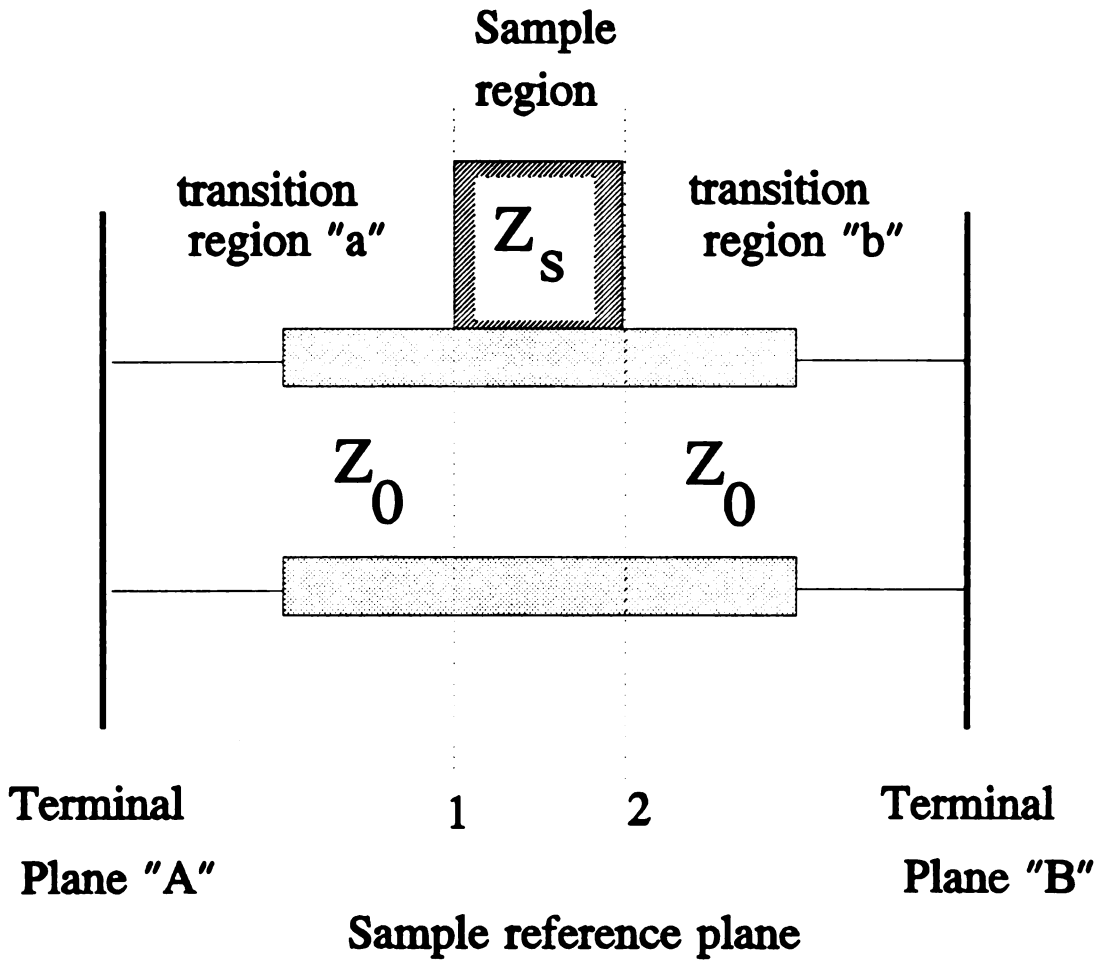

Figure 8.1: Transmission line field applicator with sample inserted in superstrate.

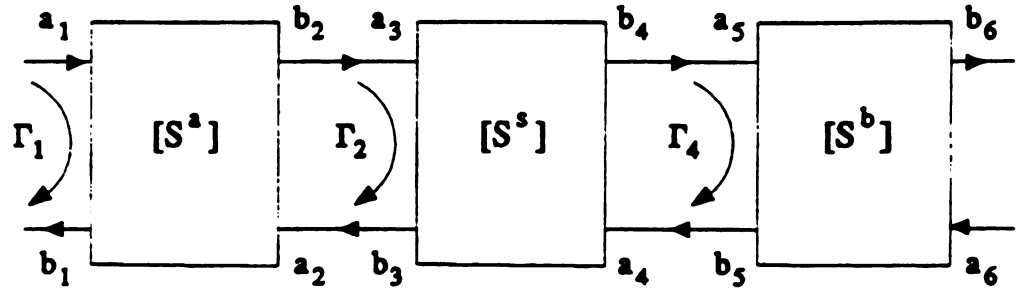

Figure 8.2: Equivalent two-port network.

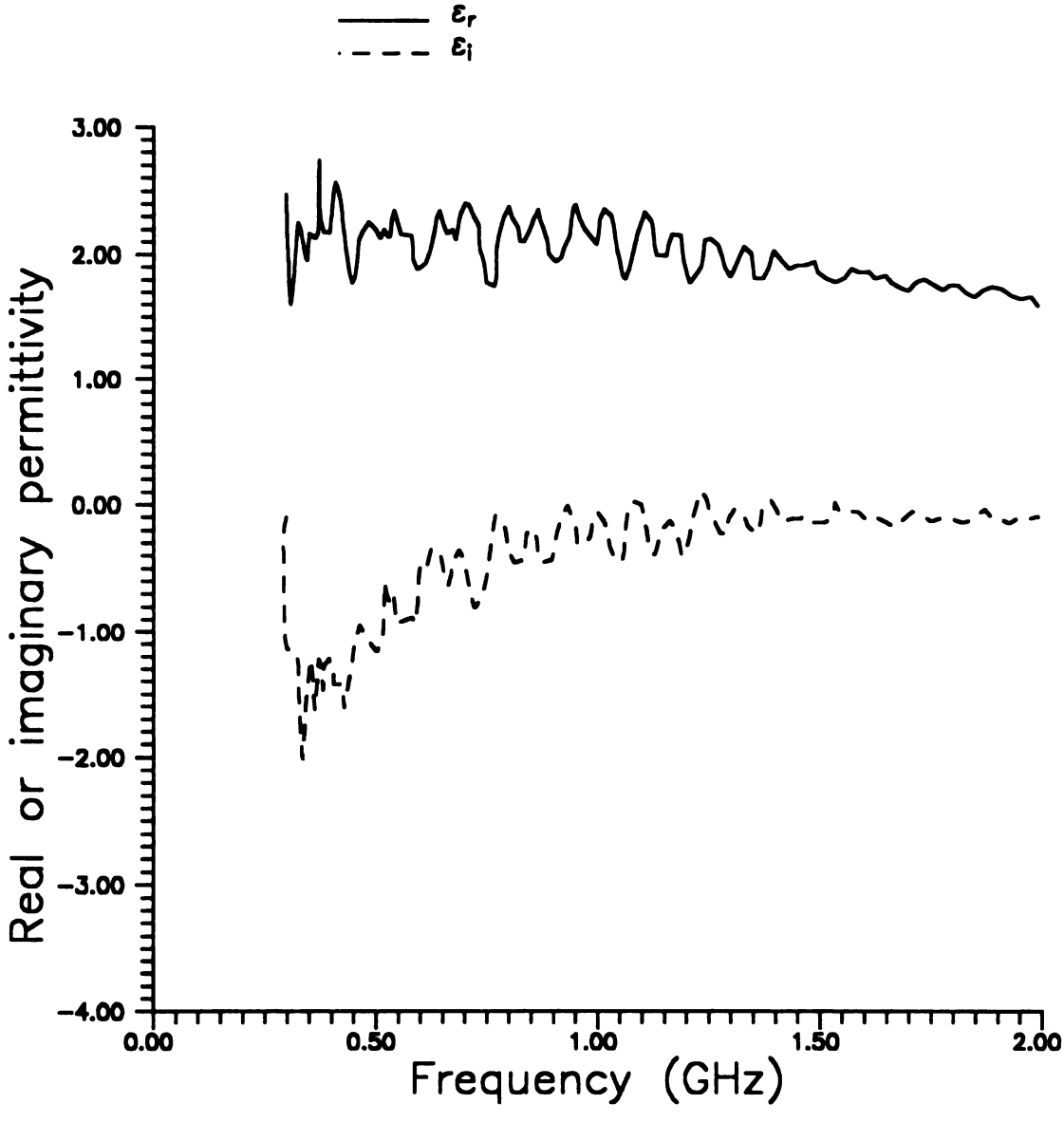

Figure 8.3: Frequency dependence of complex permittivity for teflon sample.

CHAPTER 9

SUMMARY AND CONCLUSIONS

This dissertation was devoted mostly to two main topics, namely, construction of dyadic Green's functions in planar layered media based upon wave matrices and the analysis of microstrip circuits with superstrate layer. The dyadic green's functions associated with a multi-layered environment were constructed in a systematic manner such that determining the Hertz potential in any region of a planar layered environment, maintained by general volume currents residing in any other layer, was rendered to multiplication of wave matrices. A rigorous full-wave integral operator formulation for the analysis of the electromagnetic properties of microstrip transmission line with a superstrate layer has been presented. Broad electromagnetic phenomena associated with this structure, including its dispersion characteristics, current distributions and characteristic impedance have been investigated via the rigorous full-wave integral equation approach.

Dyadic Green's functions for the EM field maintained by electric volume currents immersed in a planar layered environment were constructed in Chapter 3 through electric Hertz potentials. Spectral amplitudes in their Sommerfeld-integral representations were obtained using wave transmission and coupling matrices. Such Green's functions are appropriate for the analysis of contemporary integrated electronic and optical circuits operating at micro/mm/optical wavelengths, where the circuit components are located adjacent to a layered surround environment. This

systematic construction of EM Green's dyads for general volume currents removes any uncertainty regarding completeness of the field representation and naturally accommodates the source-point singularity.

In Chapter 4, the conventional microstrip transmission line was analyzed as an example of an integrated circuit located adjacent to a layered surround. The dyadic Green's functions associated with the layered background of the microstrip environment were constructed using wave matrices as discussed in Chapter 3. A Fourier transform-domain electric field integral equation (EFIE) description of general microstrip circuits was developed, and then applied to the conventional microstrip transmission line.

The complete propagation-mode spectrum of the microstrip line was identified. Numerical solutions to the homogeneous EFIE were implemented by the Galerkin's method of moments. Chebyshev polynomials weighted by square-root edge factors were utilized as basis functions in the current series expansion. Taking the edge behavior of the current into account explicitly enhances accuracy and accelerates the numerics. Moreover, by using Chebyshev polynomials only a few terms were required in the series to accurately represent the current.

A complete equivalent transmission-line representation for the open microstrip is obtained by evaluating its characteristic impedance. In fact, Chapter 5 presented a full-wave analysis for the characteristic impedance using both voltage-current and power-current definitions. These two methods were compared to each other. It was shown that the voltage-current method gives results very close to those of the more rigorous power-current method. The dependence of characteristic impedance upon frequency was a controversial issue since quite different functions of frequency have

been predicted. It was established in this chapter that, for the conventional microstrip, the characteristic impedance will always increase with frequency.

Chapter 6 presented a rigorous analysis of a microstrip transmission line with a superstrate layer. First, the dyadic Green's function associated with the layered conductor/substrate/superstrate/cover background environment was established. The EM fields in the substrate and superstrate regions were then evaluated. We have to note that this otherwise extensive effort was made relatively easy by using wave matrices as presented in Chapter 3.

A rigorous full-wave solution to the integral equation was pursued similar to the one in Chapter 4. The dispersion characteristics and current distributions of the guiding structure were analyzed for the principal and higher-order modes. It was found that the principal mode of the microstrip with superstrate never leaks. The microstrip line with superstrate behaves similarly to the conventional microstrip in the sense that the current distributions for the principal and higher-order modes behave in the same manner.

Chapter 7 completes the circuit modeling of the microstrip line with superstrate layer by determining its characteristic impedance. The voltage-current method was adopted in this analysis since it is less analytically involved than the power-current method; and, as was established in Chapter 5, the former method gives results very close to those of the latter method. Two types of microstrip line with superstrate were analyzed. First, a microstrip line with substrate layer having the largest permittivity was analyzed. It was shown that the characteristic impedance for this structure does not deviate much from that of the conventional microstrip. Second, the results for a microstrip line having both the substrate and cover as free

space displayed a tremendous change as its characteristic impedance showed a decrease with frequency.

Finally, the research in this dissertation has reflected some progress on the analysis and understanding of electromagnetic phenomena associated with microstrip structures with superstrate. There remain many topics which deserve further research effort in the future. In fact, Higher-order modes can be investigated in the leaky-wave (below cutoff) regime. Moreover, the analysis of microstrip line with superstrate in anisotropic media can be investigated. Furthermore, a full-wave theory for coupled microstrip transmission lines with superstrate can be studied based upon the analysis of a single microstrip line as presented in this dissertation.

APPENDIX A

CANONICAL TRANSFORM DOMAIN SOLUTION TO THE PLANAR INTERFACE REFLECTION PROBLEM

A.1 Single Interface

Consider the planar interface between medium (1) and medium (2) as shown in Fig. (A.1). The total transform-domain Hertz potential in medium (1) consists of an incident component augmented by a reflected part as

$$\tilde{\Pi}_{1,\alpha}(\vec{\lambda},y) = \tilde{\Pi}^{i}_{1,\alpha}(\vec{\lambda},y) + \tilde{\Pi}^{s}_{1,\alpha}(\vec{\lambda},y) \tag{A.1}$$

where $\alpha = x,y,z$.

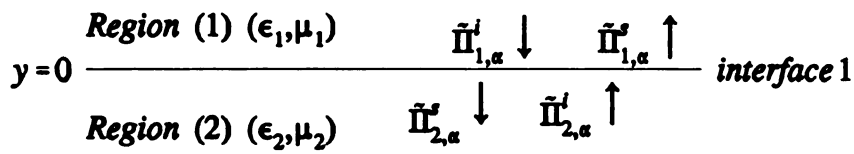

Figure A.1 Single interface

Similarly, the Hertz potential in medium (2) decomposes into an incident part and a reflected part as

$$\tilde{\Pi}_{2,\alpha}(\vec{\lambda},y) = \tilde{\Pi}^{i}_{2,\alpha}(\vec{\lambda},y) + \tilde{\Pi}^{s}_{2,\alpha}(\vec{\lambda},y) \ . \tag{A.2}$$

The incident and reflected components of Hertz potential in each layer satisfy the following

transform domain Helmoltz equation

$$\left(\frac{d^2}{dy^2} - p_l^2\right)\begin{Bmatrix}\tilde{\Pi}^i_{l,\alpha}(\vec{\lambda},y)\\ \tilde{\Pi}^s_{l,\alpha}(\vec{\lambda},y)\end{Bmatrix} = \begin{Bmatrix}\dfrac{-\tilde{J}_\alpha(\vec{\lambda},y)}{j\omega\epsilon_l}\\ 0\end{Bmatrix} \cdots l = 1,2\ . \tag{A.3}$$

Appropriate solutions to eq. (A.3) are

$$\begin{aligned}\tilde{\Pi}^i_{1,\alpha} &= a^-_{1,\alpha}(\vec{\lambda})e^{p_1 y}\\ \tilde{\Pi}^s_{1,\alpha} &= a^+_{1,\alpha}(\vec{\lambda})e^{-p_1 y}\\ \tilde{\Pi}^i_{2,\alpha} &= \tilde{a}^+_{2,\alpha}(\vec{\lambda})e^{-p_2 y}\\ \tilde{\Pi}^s_{2,\alpha} &= \tilde{a}^-_{2,\alpha}(\vec{\lambda})e^{p_2 y}\end{aligned} \tag{A.4}$$

where $a^{\pm}_{1,\alpha}(\vec{\lambda})$ and $\tilde{a}^{\pm}_{2,\alpha}(\vec{\lambda})$ are complex spectral amplitudes at the $y=0$ interface. $a^-_{1,\alpha}(\vec{\lambda})$ and $\tilde{a}^+_{2,\alpha}(\vec{\lambda})$ are regarded as known due to impressed currents while $a^+_{1,\alpha}(\vec{\lambda})$ and $\tilde{a}^-_{2,\alpha}(\vec{\lambda})$ are regarded as unknown and to be determined.

The total Hertz potentials in each region satisfy the following boundary conditions [50]

$$\left.\begin{aligned}\tilde{\Pi}_{1,\alpha}(\vec{\lambda},y) &= N_1^2 M_1^2\ \tilde{\Pi}_{2,\alpha}(\vec{\lambda},y)\\ \frac{\partial\tilde{\Pi}_{1,\alpha}(\vec{\lambda},y)}{\partial y} &= N_1^2\frac{\partial\tilde{\Pi}_{2,\alpha}(\vec{\lambda},y)}{\partial y}\end{aligned}\right\} \cdots \textit{for}\ \alpha = x,z \tag{A.5}$$

and

$$\begin{aligned}\tilde{\Pi}_{1,y}(\vec{\lambda},y) &= N_1^2\tilde{\Pi}_{2,y}(\vec{\lambda},y)\\ \left[\frac{\partial\tilde{\Pi}_{1,y}(\vec{\lambda},y)}{\partial y} - \frac{\partial\tilde{\Pi}_{2,y}(\vec{\lambda},y)}{\partial y}\right] &= -(M_1^2N_1^2-1)\left[j\xi\tilde{\Pi}_{2,x}(\vec{\lambda},y) + j\zeta\tilde{\Pi}_{2,z}(\vec{\lambda},y)\right].\end{aligned} \tag{A.6}$$

A.1.1 Scattering of Tangential Potential Components

Implementing boundary conditions (A.5) on tangential components of Hertz potentials at $y=0$ interface leads to

$$\begin{aligned} a_{1,\alpha}^{+} &= R_1^{t}\downarrow a_{1,\alpha}^{-} + T_1^{t}\uparrow \tilde{a}_{2,\alpha}^{+} \\ \tilde{a}_{2,\alpha}^{-} &= T_1^{t}\downarrow a_{1,\alpha}^{-} + R_1^{t}\uparrow a_{2,\alpha}^{+} \end{aligned} \tag{A.7}$$

where the tangential reflection coefficients at interface (1) associated with downward and upward travelling incident waves are defined, respectively, as

$$\left.\begin{aligned} R_1^{t}\downarrow &= \left.\frac{a_{1,\alpha}^{+}}{a_{1,\alpha}^{-}}\right|_{\tilde{a}_{2,\alpha}^{+}=0} \\ R_1^{t}\uparrow &= \left.\frac{\tilde{a}_{2,\alpha}^{-}}{\tilde{a}_{2,\alpha}^{+}}\right|_{a_{1,\alpha}^{-}=0} \end{aligned}\right\} \cdots \alpha = x,z \tag{A.8}$$

and are given as follows

$$\begin{aligned} R_1^{t}\downarrow &= \frac{M_1^2 p_1 - p_2}{M_1^2 p_1 + p_2} \\ R_1^{t}\uparrow &= -R_1^{t}\downarrow \ . \end{aligned} \tag{A.9}$$

The interfacial transmission coefficients at interface 1 are defined similarly and are given as

$$\begin{aligned} T_1^{t}\downarrow &= \left.\frac{\tilde{a}_{2,\alpha}^{-}}{a_{1,\alpha}^{-}}\right|_{\tilde{a}_{2,\alpha}=0} = \frac{2N_1^{-2}p_1}{M_1^2 p_1 + p_2} = N_1^{-2}M_1^{-2}(1+R_1^{t}\downarrow) \\ T_1^{t}\uparrow &= \left.\frac{a_{1,\alpha}^{+}}{\tilde{a}_{2,\alpha}^{+}}\right|_{\tilde{a}_{1,\alpha}^{-}=0} = \frac{2N_1^{2}M_1^{2}p_1}{M_1^2 p_1 + p_2} = N_1^{2}M_1^{2}(1+R_1^{t}\uparrow) \ . \end{aligned} \tag{A.10}$$

Solving for the wave amplitudes $a_{1\alpha}^{\pm}$ in medium (1) in terms of the wave amplitudes $\tilde{a}_{2\alpha}^{\pm}$ leads to

$$\begin{bmatrix} a_{1,\alpha}^{-} \\ a_{1,\alpha}^{+} \end{bmatrix} = \left[A_1^{f}\downarrow\right] \begin{bmatrix} \tilde{a}_{2,\alpha}^{-} \\ \tilde{a}_{2,\alpha}^{+} \end{bmatrix} \quad ; for\ \alpha = x,z \tag{A.11}$$

where we define the tangential wave-transmission chain matrix at interface (1) which chains region (2) wave amplitudes to those in region (1) as

$$\left[A_1^{f}\downarrow\right] = \frac{1}{T_1^{f}\downarrow} \begin{bmatrix} 1 & R_1^{f}\downarrow \\ R_1^{f}\downarrow & 1 \end{bmatrix}. \tag{A.12}$$

Note that the downgoing arrow in the notation for $\left[A_1^{f}\downarrow\right]$ illustrates the fact that the incident wave in region (1) is travelling in $-y$ direction. Similarly, the tangential wave-transmission matrix associated with upward travelling incident wave is

$$\left[A_1^{f}\uparrow\right] = \frac{1}{T_1^{f}\uparrow} \begin{bmatrix} 1 & R_1^{f}\uparrow \\ R_1^{f}\uparrow & 1 \end{bmatrix} \tag{A.13}$$

and where $\left[A_1^{f}\uparrow\right]$ is defined such that

$$\begin{bmatrix} \tilde{a}_{2,\alpha}^{+} \\ \tilde{a}_{2,\alpha}^{-} \end{bmatrix} = \left[A_1^{f}\uparrow\right] \begin{bmatrix} a_{1,\alpha}^{+} \\ a_{1,\alpha}^{-} \end{bmatrix} \quad ; for\ \alpha = x,z\ . \tag{A.14}$$

A.1.2 Scattering of Normal Potential Components

The tangential potential components were quantified independently above, and may therefore be regarded as available for this normal potential calculation. The boundary conditions on normal potential at the $y=0$ interface couple normal and tangential components as in eq. (A.6) leading to

$$\begin{aligned} a_{1,y}^{-} + a_{1,y}^{+} &= N_1^2(\tilde{a}_{2,y}^{+} + \tilde{a}_{2,y}^{-}) \\ p_1(a_{1,y}^{-} - a_{1,y}^{+}) + p_2(\tilde{a}_{2,y}^{+} - \tilde{a}_{2,y}^{-}) &= -(N_1^2M_1^2 - 1)\left[j\xi(\tilde{a}_{2,x}^{+} + \tilde{a}_{2,x}^{-}) + j\zeta(\tilde{a}_{2,z}^{+} + \tilde{a}_{2,z}^{-})\right]. \end{aligned} \tag{A.15}$$

Solving for the normal scattered wave amplitudes in both regions leads to

$$\begin{aligned} a_{1,y}^{+} &= R_1^{n\downarrow} a_{1,y}^{-} + T_1^{n\uparrow} \tilde{a}_{2,y}^{+} + c_1 F_t \\ \tilde{a}_{2,y}^{-} &= T_1^{n\downarrow} a_{1,y}^{-} + R_1^{n\uparrow} \tilde{a}_{2,y}^{+} + c_2 F_t \end{aligned} \tag{A.16}$$

where the normal reflection and transmission coefficients associated with either downward or upward travelling incident waves are defined, similarly to above, as follows

$$\begin{aligned} R_1^{n\downarrow} &= \left.\frac{a_{1,y}^{+}}{a_{1,y}^{-}}\right|_{\tilde{a}_{2,y}^{+}=F_t=0} \\ R_1^{n\uparrow} &= \left.\frac{\tilde{a}_{2,y}^{-}}{\tilde{a}_{2,y}^{+}}\right|_{a_{1,y}^{-}=F_t=0} \\ T_1^{n\uparrow} &= \left.\frac{a_{1,y}^{+}}{\tilde{a}_{2,y}^{+}}\right|_{a_{1,y}^{-}=F_t=0} \\ T_1^{n\downarrow} &= \left.\frac{\tilde{a}_{2,y}^{-}}{a_{1,y}^{-}}\right|_{\tilde{a}_{2,y}^{+}=F_t=0} \end{aligned} \tag{A.17}$$

and $F_t = (N_1^2M_1^2 - 1)\,[j\xi(\tilde{a}_{2,x}^{+} + \tilde{a}_{2,x}^{-}) + j\zeta(\tilde{a}_{2,z}^{+} + \tilde{a}_{2,z}^{-})]$, $c_1 = M_1^2/(N_1^2p_1 + p_2)$, $c_2 = 1/(N_1^2p_1 + p_2)$.

The normal interfacial reflection and transmission coefficients are given as

$$
\begin{aligned}
R_1^n\downarrow &= \frac{N_1^2 p_1 - p_2}{N_1^2 p_1 + p_2} = -R_1^n\uparrow \\
T_1^n\downarrow &= \frac{2p_1}{N_1^2 P_1 + p_2} = N_1^{-2}(1 + R_1^n\downarrow) \\
T_1^n\uparrow &= \frac{2N_1^2 p_2}{N_1^2 P_1 + p_2} = N_1^2(1 + R_1^n\uparrow).
\end{aligned}
\tag{A.18}
$$

Our goal is to be able to chain region (2) wave amplitudes to those in region (1) and vice versa. Hence, using equation (A.16), we solve for the normal wave amplitudes $a_{1,y}^{\pm}$ in region (1) in terms of those $\tilde{a}_{2,\alpha}^{\pm}$ ($\alpha = x,y,z$) in region (2) leading to

$$
\begin{aligned}
a_{1,y}^{-} &= \frac{-R_1^n\downarrow}{T_1^n\downarrow}\,\tilde{a}_{2,y}^{+} + \frac{1}{T_1^n\downarrow}\,\tilde{a}_{2,y}^{-} - c_2 F_t \\
a_{1,y}^{+} &= \frac{T_1^n\downarrow T_2^n\uparrow - R_1^n\downarrow R_1^n\uparrow}{T_1^n\downarrow}\,\tilde{a}_{2,y}^{+} + \frac{R_1^n\downarrow}{T_1^n\downarrow}\,\tilde{a}_{2,y}^{-} + \left(c_1 - \frac{R_1^n\downarrow c_2}{T_1^n\downarrow}\right)F_t .
\end{aligned}
\tag{A.19}
$$

Writing the above in matrix notation and after many simplifications, we have

$$
\begin{bmatrix} a_{1,y}^{-} \\ a_{1,y}^{+} \end{bmatrix} = \left[A_1^n\downarrow\right] \begin{bmatrix} \tilde{a}_{2,y}^{-} \\ \tilde{a}_{2,y}^{+} \end{bmatrix} + \left[C_1\downarrow\right] \left(j\xi \begin{bmatrix} \tilde{a}_{2,x}^{-} \\ \tilde{a}_{2,x}^{+} \end{bmatrix} + j\zeta \begin{bmatrix} \tilde{a}_{2,z}^{-} \\ \tilde{a}_{2,z}^{+} \end{bmatrix} \right). \tag{A.20}
$$

$\left[A_1^n\downarrow\right]$ is the normal wave matrix associated with downward travelling incident wave at interface (1) and is defined as

$$
\left[A_1^n\downarrow\right] = \frac{1}{T_1^n\downarrow} \begin{bmatrix} 1 & R_1^n\downarrow \\ R_1^n\downarrow & 1 \end{bmatrix}. \tag{A.21}
$$

$\left[C_1\downarrow\right]$ is the interfacial coupling matrix associated with downward travelling incident wave

and is given as

$$[C_1\downarrow] = \frac{N_1^2M_1^2-1}{2p_1}\begin{bmatrix}-1 & -1\\ 1 & 1\end{bmatrix}. \tag{A.22}$$

Similarly, for an incident wave travelling upward the normal wave amplitudes in region (2) are given in terms of wave amplitudes in region (1) as follows

$$\begin{bmatrix}\tilde{a}_{2,y}^{+}\\ \tilde{a}_{2,y}^{-}\end{bmatrix} = [A_1^{t}\uparrow]\begin{bmatrix}a_{1,y}^{+}\\ a_{1,y}^{-}\end{bmatrix} + [C_1\uparrow]\left(j\xi\begin{bmatrix}a_{1,x}^{+}\\ a_{1,x}^{-}\end{bmatrix} + j\zeta\begin{bmatrix}a_{1,z}^{+}\\ a_{1,z}^{-}\end{bmatrix}\right) \tag{A.23}$$

where

$$[A_1^{n}\uparrow] = \frac{1}{T_1^{n}\uparrow}\begin{bmatrix}1 & R_1^{n}\uparrow\\ R_1^{n}\uparrow & 1\end{bmatrix} \tag{A.24}$$

$$[C_1\uparrow] = \frac{1-N_1^{-2}M_1^{-2}}{2p_2}\begin{bmatrix}-1 & -1\\ 1 & 1\end{bmatrix}. \tag{A.25}$$

A.2 Effect of a Propagation Path Length

If region (2) has thickness t_2 as shown in Fig. (A.2), we now have two interfaces. To obtain the wave amplitudes in region (2) and at interface (2), the wave amplitudes at interface (1) are shifted downward as follows

$$\begin{aligned} a_{2,a}^{-} &= \tilde{a}_{2,a}^{-}e^{-p_2t_2}\\ a_{2,a}^{+} &= \tilde{a}_{2,a}^{+}e^{p_2t_2}\end{aligned} \tag{A.26}$$

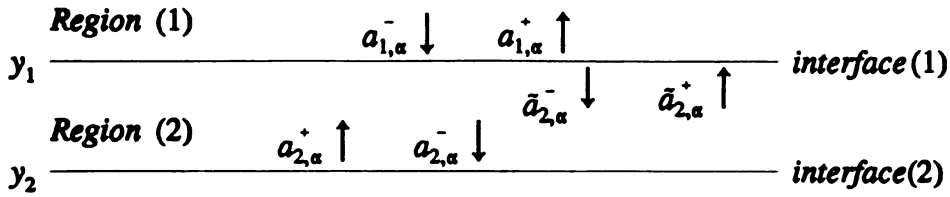

Figure A.2 Effect of a Propagation Path Length

A.2.1 Tangential potential components

The wave matrix formulation is modified to reference waves in region (2) to the location of interface (2) as follows

$$\begin{aligned}
\begin{bmatrix} a_{1,\alpha}^{-} \\ a_{1,\alpha}^{+} \end{bmatrix} &= \left[A_1^{f\downarrow}\right] \begin{bmatrix} \tilde{a}_{2,\alpha}^{-} \\ \tilde{a}_{2,\alpha}^{+} \end{bmatrix} \\
&= \left[A_1^{f\downarrow}\right] \begin{bmatrix} a_{2,\alpha}^{-} e^{p_2 t_2} \\ a_{2,\alpha}^{+} e^{-p_2 t_2} \end{bmatrix} \\
&= \left[A_1^{f\downarrow}\right] \begin{bmatrix} e^{p_2 t_2} & 0 \\ 0 & e^{-p_2 t_2} \end{bmatrix} \begin{bmatrix} a_{2,\alpha}^{-} \\ a_{2,\alpha}^{+} \end{bmatrix} \\
&= \left[A_1^{f\downarrow}\right] [\psi] \begin{bmatrix} a_{2,\alpha}^{-} \\ a_{2,\alpha}^{+} \end{bmatrix}
\end{aligned} \tag{A.27}$$

where

$$[\psi] = \begin{bmatrix} e^{p_2 t_2} & 0 \\ 0 & e^{-p_2 t_2} \end{bmatrix} \tag{A.28}$$

and the interfacial tangential transmission matrix at interface (1) is redefined as

$$\left[A_1^{t}\downarrow\right] = \frac{1}{T_1^{t}\downarrow}\begin{bmatrix} 1 & R_1^{t}\downarrow \\ R_1^{t}\downarrow & 1 \end{bmatrix}[\Psi]$$

$$\left[A_1^{t}\downarrow\right] = \frac{1}{T_1^{t}\downarrow}\begin{bmatrix} e^{p_2 t_2} & R_1^{t}\downarrow e^{-p_2 t_2} \\ R_1^{t}\downarrow e^{p_2 t_2} & e^{-p_2 t_2} \end{bmatrix}. \qquad \text{(A.29)}$$

A.2.2. Normal potential components

A similar modification of the wave matrix for normal potential components leads to

$$\begin{bmatrix} a_{1,y}^{-} \\ a_{1,y}^{+} \end{bmatrix} = \left[A_1^{n}\downarrow\right]\begin{bmatrix} a_{2,y}^{-} \\ a_{2,y}^{+} \end{bmatrix} + \left[C_1\downarrow\right]\left(j\xi \begin{bmatrix} a_{2,x}^{-} \\ a_{2,x}^{+} \end{bmatrix} + j\zeta \begin{bmatrix} a_{2,z}^{-} \\ a_{2,z}^{+} \end{bmatrix} \right) \qquad \text{(A.30)}$$

where the normal transmission and coupling matrices at interface (1) are redefined as

$$\left[A_1^{n}\downarrow\right] = \frac{1}{T_1^{n}\downarrow}\begin{bmatrix} e^{p_2 t_2} & R_1^{n}\downarrow e^{-p_2 t_2} \\ R_1^{n}\downarrow e^{p_2 t_2} & e^{-p_2 t_2} \end{bmatrix} \qquad \text{(A.31)}$$

$$\left[C_1\downarrow\right] = \frac{N_1^2 M_1^2 - 1}{2p_1}\begin{bmatrix} -e^{p_2 t_2} & -e^{-p_2 t_2} \\ e^{p_2 t_2} & e^{-p_2 t_2} \end{bmatrix}. \qquad \text{(A.32)}$$

APPENDIX B

ELECTRIC DYADIC GREEN'S FUNCTIONS

B.1 Fields in the Cover Region

In the cover layer of Fig . 4.2, the electric Green's dyad in the transform domain is identified in terms of Hertz potential Green's dyad as

$$\bar{\bar{g}}^e(\vec{\rho}\,|\,\vec{\rho}\,';\zeta) = PV(k_c^2+\tilde{\nabla}\tilde{\nabla}\cdot)\bar{\bar{g}}(\vec{\rho}\,|\,\vec{\rho}\,';\zeta) + \bar{\bar{L}}\delta(\vec{\rho}-\vec{\rho}\,') \tag{B.1}$$

where $\tilde{\nabla}=\nabla_t+\hat{z}\,j\zeta$ with $\nabla_t=\hat{x}\partial/\partial x+\hat{y}\partial/\partial y$ the transverse operator. The transform-domain Hertz potential Green's dyad is expressed as in eqs. (4.37) and (4.38) as follows

$$\bar{\bar{g}}(\vec{\rho}\,|\,\vec{\rho}\,';\zeta) = \bar{\bar{I}}g^p(\vec{\rho}\,|\,\vec{\rho}\,';\zeta) + \bar{\bar{g}}^s(\vec{\rho}\,|\,\vec{\rho}\,';\zeta) \tag{B.2}$$

where

$$\bar{\bar{g}}^s(\vec{\rho}\,|\,\vec{\rho}\,';\zeta) = (\hat{x}\hat{x}+\hat{z}\hat{z})g_t^s(\vec{\rho}\,|\,\vec{\rho}\,';\zeta) + \hat{y}\left(\nabla_T g_c^s(\vec{\rho}\,|\,\vec{\rho}\,';\zeta) + g_n^s(\vec{\rho}\,|\,\vec{\rho}\,';\zeta)\hat{y}\right). \tag{B.3}$$

Using eq. (B.2) and (B.3) in expression (B.1) leads to

$$\begin{aligned}\bar{\bar{g}}^e(\vec{\rho}\,|\,\vec{\rho}\,';\zeta) = {} & \hat{x}\hat{x}g_{xx}^e + \hat{y}\hat{y}g_{yy}^e + \hat{z}\hat{z}g_{zz}^e + \hat{x}\hat{y}g_{xy}^e + \hat{y}\hat{x}g_{yx}^e \\ & + \hat{x}\hat{z}g_{xz}^e + \hat{z}\hat{x}g_{zx}^e + \hat{y}\hat{z}g_{yz}^e + \hat{z}\hat{y}g_{zy}^e\end{aligned} \tag{B.4}$$

where $g_{\alpha\beta}^e$ ($\alpha,\beta = x,y,z$) are written in terms of Hertz potential Green's function components as follows

$$
\begin{aligned}
g^e_{xx} &= \left(k_c^2 + \frac{\partial^2}{\partial x^2}\right)(g_t + g^p) + \frac{\partial^2}{\partial x^2}\frac{\partial}{\partial y} g_c \\
g^e_{yx} &= \left(k_c^2 + \frac{\partial^2}{\partial y^2}\right)\frac{\partial}{\partial x} g_c + \frac{\partial}{\partial x}\frac{\partial}{\partial y}(g_t + g^p) \\
g^e_{zx} &= j\zeta \frac{\partial}{\partial x}(g_t + g^p) + j\zeta \frac{\partial}{\partial x}\frac{\partial}{\partial y} g_c \\
g^e_{xz} &= g^e_{zx} \\
g^e_{yz} &= \left(k_c^2 + \frac{\partial^2}{\partial y^2}\right) j\zeta g_c + j\zeta \frac{\partial}{\partial y}(g_t + g^p) \\
g^e_{zz} &= \left(k_c^2 + \zeta^2\right)(g_t + g^p) + \zeta^2 \frac{\partial}{\partial y} g_c \\
g^e_{yy} &= \left(k_c^2 + \frac{\partial^2}{\partial y^2}\right)(g_n + g^p) \\
g^e_{zy} &= j\zeta \frac{\partial}{\partial y}(g_n + g^p) \\
g^e_{xy} &= \frac{\partial}{\partial x}\frac{\partial}{\partial y}(g_n + g^p) \ .
\end{aligned}
\tag{B.5}
$$

Exploiting the Hertz potential Green's function components as in eq. (4.40) leads to

$$
g^e_{\alpha\beta}(x,y|x',0) = \frac{1}{2\pi}\int_{-\infty}^{\infty} C^e_{\alpha\beta}(\xi,\zeta)\, e^{j\xi(x-x')} e^{-p_0 y}\, d\xi \qquad \text{(B.6)}
$$

$$
\cdots \textit{for } \alpha, \beta = x,y,z
$$

where

$$
\begin{aligned}
C^e_{xx} &= \frac{(k_c^2-\xi^2)M_c^2}{Z^h} + \frac{p_c\xi^2(N_c^2M_c^2-1)}{Z^h(\lambda)Z^e(\lambda)} \\
C^e_{yx} &= \frac{-j\xi p_c M_c^2}{Z^h} + \frac{j\xi(k_c^2+p_c^2)(N_c^2M_c^2-1)}{Z^h(\lambda)Z^e(\lambda)} \\
C^e_{zx} &= C^e_{xz} = \frac{-\zeta\xi M_c^2}{Z^h} + \frac{p_c\xi\zeta(N_c^2M_c^2-1)}{Z^h(\lambda)Z^e(\lambda)} \\
C^e_{yz} &= \frac{-j\zeta p_c M_c^2}{Z^h} + \frac{j\zeta(k_c^2+p_c^2)(N_c^2M_c^2-1)}{Z^h(\lambda)Z^e(\lambda)} \\
C^e_{zz} &= \frac{(k_c^2-\zeta^2)M_c^2}{Z^h} + \frac{p_c\zeta^2(N_c^2M_c^2-1)}{Z^h(\lambda)Z^e(\lambda)} \\
C^e_{yy} &= \frac{M_c^2(k_c^2+p_c^2)}{Z^h} \\
C^e_{xy} &= \frac{-j\zeta p_c M_c^2}{Z^h} \\
C^e_{xy} &= \frac{-j\xi p_c M_c^2}{Z^h} .
\end{aligned}
\tag{B.7}
$$

B.2 Fields in the Film Region

In the film region of Fig. 4.2, the electric Green's dyad in the transform domain is identified in terms of Hertz potential Green's dyad as

$$
\bar{\bar{g}}^e(\vec{\rho}\,|\,\vec{\rho}\,';\zeta) = (k_f^2+\bar{\bar{\nabla}}\bar{\bar{\nabla}}\cdot)\bar{\bar{g}}(\vec{\rho}\,|\,\vec{\rho}\,';\zeta) \tag{B.8}
$$

where the Hertz potential Green's dyad has the same form as in eq. (B.3) and has the following components

$$
\begin{Bmatrix} g_t(\vec{\rho}\,|\,\vec{\rho}\,';\zeta) \\ g_n(\vec{\rho}\,|\,\vec{\rho}\,';\zeta) \\ g_c(\vec{\rho}\,|\,\vec{\rho}\,';\zeta) \end{Bmatrix} = \int_{-\infty}^{\infty} \begin{Bmatrix} B^t_{fc3}e^{p_f(y+t)} + B^t_{fc4}e^{-p_f(y+t)} \\ B^n_{fc3}e^{p_f(y+t)} + B^n_{fc4}e^{-p_f(y+t)} \\ B^c_{fc3}e^{p_f(y+t)} + B^c_{fc4}e^{-p_f(y+t)} \end{Bmatrix} \frac{e^{j\xi(x-x')}e^{-p_c(y')}}{4\pi p_c} d\xi \ . \tag{B.9}
$$

The B_{fc} coefficients are defined in eqs. (4.31), (4.32) and (4.33).

Exploiting eq. (B.3) in eq. (B.8) leads to

$$\begin{aligned}\bar{\bar{g}}^e(\vec{\rho}\,|\,\vec{\rho}\,';\zeta) = {} & \hat{x}\hat{x}g^e_{xx} + \hat{y}\hat{y}g^e_{yy} + \hat{z}\hat{z}g^e_{zz} + \hat{x}\hat{y}g^e_{xy} + \hat{y}\hat{x}g^e_{yx} \\ & + \hat{x}\hat{z}g^e_{xz} + \hat{z}\hat{x}g^e_{zx} + \hat{y}\hat{z}g^e_{yz} + \hat{z}\hat{y}g^e_{zy}\end{aligned} \tag{B.10}$$

where $g^e_{\alpha\beta}$ ($\alpha,\beta = x,y,z$) are written in terms of Hertz potential Green's function components given by eq. (B.9) as follows

$$\begin{aligned}
g^e_{xx} &= \left(k_c^2 + \frac{\partial^2}{\partial x^2}\right) g_t + \frac{\partial^2}{\partial x^2}\frac{\partial}{\partial y} g_c \\
g^e_{yx} &= \left(k_c^2 + \frac{\partial^2}{\partial y^2}\right)\frac{\partial}{\partial x} g_c + \frac{\partial}{\partial x}\frac{\partial}{\partial y} g_t \\
g^e_{zx} &= j\zeta\frac{\partial}{\partial x} g_t + j\zeta\frac{\partial}{\partial x}\frac{\partial}{\partial y} g_c \\
g^e_{xz} &= g^e_{zx} \\
g^e_{yz} &= \left(k_c^2 + \frac{\partial^2}{\partial y^2}\right) j\zeta g_c + j\zeta\frac{\partial}{\partial y} g_t \\
g^e_{zz} &= \left(k_c^2 + \zeta^2\right) g_t + \zeta^2\frac{\partial}{\partial y} g_c \\
g^e_{yy} &= \left(k_c^2 + \frac{\partial^2}{\partial y^2}\right) g_n \\
g^e_{zy} &= j\zeta\frac{\partial}{\partial y} g_n \\
g^e_{xy} &= \frac{\partial}{\partial x}\frac{\partial}{\partial y} g_n \,.
\end{aligned} \tag{B.11}$$

Exploiting eqs. (B.9) and (B.11) in (B.10) leads to

$$g^e_{\alpha\beta}(x,y\,|\,x',0) = \frac{1}{2\pi}\int_{-\infty}^{\infty} B^e_{\alpha\beta}(\xi,\zeta,y)\, e^{j\xi(x-x')}\, d\xi \qquad \text{... for } \alpha,\beta = x,y,z \tag{B.12}$$

where

$$B^e_{xx}(\xi,\zeta,y) = \frac{k_f^2-\xi^2}{N_c^2 Z^h(\lambda)} \frac{\sinh[p_f(y+t)]}{\sinh p_f t} - \frac{\xi^2 p_f (N_c^2 M_c^2 - 1)}{N_c^2 Z^h(\lambda) Z^e(\lambda)} \frac{\sinh[p_f(y+t)]}{\cosh p_f t}$$

$$B^e_{yx}(\xi,\zeta,y) = \frac{j\xi p_f}{N_c^2 Z^h(\lambda)} \frac{\cosh[p_f(y+t)]}{\sinh p_f t} + \frac{j\xi (k_f^2+p_f^2)(N_c^2 M_c^2 - 1)}{N_c^2 Z^h(\lambda) Z^e(\lambda)} \frac{\cosh[p_f(y+t)]}{\cosh p_f t}$$

$$B^e_{zx}(\xi,\zeta,y) = \frac{-\xi\zeta}{N_c^2 Z^h(\lambda)} \frac{\sinh[p_f(y+t)]}{\sinh p_f t} - \frac{\zeta\xi p_f (N_c^2 M_c^2 - 1)}{N_c^2 Z^h(\lambda) Z^e(\lambda)} \frac{\sinh[p_f(y+t)]}{\cosh p_f t}$$

$$B^e_{xz}(\xi,\zeta,y) = B^e_{zx}(\xi,\zeta,y)$$

$$B^e_{yz}(\xi,\zeta,y) = \frac{j\zeta p_f}{N_c^2 Z^h(\lambda)} \frac{\cosh[p_f(y+t)]}{\sinh p_f t} + \frac{j\zeta (k_f^2+p_f^2)(N_c^2 M_c^2 - 1)}{N_c^2 Z^h(\lambda) Z^e(\lambda)} \frac{\cosh[p_f(y+t)]}{\cosh p_f t}$$

$$B^e_{zz}(\xi,\zeta,y) = \frac{k_f^2-\zeta^2}{N_c^2 Z^h(\lambda)} \frac{\sinh[p_f(y+t)]}{\sinh p_f t} - \frac{\zeta^2 p_f (N_c^2 M_c^2 - 1)}{N_c^2 Z^h(\lambda) Z^e(\lambda)} \frac{\sinh[p_f(y+t)]}{\cosh p_f t}$$

$$B^e_{yy}(\xi,\zeta,y) = \frac{k_f^2+p_f^2}{Z^e(\lambda)} \frac{\cosh[p_f(y+t)]}{\cosh p_f t}$$

$$B^e_{zy}(\xi,\zeta,y) = \frac{j\zeta p_f}{Z^e(\lambda)} \frac{\sinh[p_f(y+t)]}{\sinh p_f t}$$

$$B^e_{xy}(\xi,\zeta,y) = \frac{j\xi p_f}{Z^e(\lambda)} \frac{\sinh[p_f(y+t)]}{\cosh p_f t} .$$

BIBLIOGRAPHY

BIBLIOGRAPHY

[1] Nyquist, D. P., and Yuan, Y., "Full-wave perturbation theory based upon electric field integral equations for coupled microstrip transmission lines," IEEE Trans. Microwave Theory Tech., vol. MTT-38, pp. 1576-1584, 1990.

[2] Sommerfeld, A., Partial Differential Equations in Physics, 1949, New York: Academic Press.

[3] Brekhovskikh, L. M., Waves in Layered Media, 1960, New York: Academic Press.

[4] Wait, J. R., Electromagnetic Waves in Stratified Media, Second Edition, 1970, New York, Pergamon press.

[5] Felsen, L. B. and N. Marcuvitz, radiation and Scattering of Electromagnetic Waves, 1973, New Jersey: Prentice Hall.

[6] Marcuse, D., Theory of Dielectric Optical Waveguides, New York, Academic Press, 1974.

[7] Kong, J. A., Theory of Electromagnetic Waves, New York, John Wiley and Sons, 1975.

[8] Kong, J. A., Electromagnetic Wave Theory, 1986, New York: Wiley Interscience.

[9] Chew, W. C., Fields and Waves in Inhomogeneous Media, 1990, New York: Van Nostrand Reinhold.

[10] C. H. Stoyer, "Electromagnetic fields of dipoles in stratified media," IEEE Trans. Antennas Propagat., vol. AP-25, pp. 547-552, July 1977.

[11] E. F. Kuester, D. C. Chang, and S.W. Plate, "Electromagnetic wave propagation along horizontal wire systems in or near a layered earth," Electromagn., vol 1, pp. 243-265, July-September 1981.

[12] Lee, J. K., and J. A. Kong, "Dyadic Green's functions for layered anisotropic media," Electromagnetics, vol. 3, pp. 111-130, 1983.

[13] Das, N. K., and D. M. Pozar, "A generalized spectral domain Green's function for multilayer dielectric substrates with application to multilayer transmission lines," 1987, IEEE Trans. Microwave Theory Tech., vol. MTT-

35, no. 3, pp. 326-335.

[14] J. R. Mosig, "Integral equation technique," in Numerical Techniques for Microwave and Millimeter-Wave Passive Structures (T. Itoh, ed.), pp. 133-213, New York: Wiley, 1989.

[15] K. A. Michalski and D. Zheng, "Electromagnetic scattering and radiation by surfaces of arbitrary shape in layered media, Part I: Theory, " IEEE Trans. Antennas Propagat., vol. 38, pp. 335-344, March 1990.

[16] Edwards, T. C., Foundations for Microstrip Circuit Design, John Wiley and Sons, New York, ... pp., 1981.

[17] Collin, R. E., Field Theory of Guided Waves, Second Edition, IEEE Press, New York, ... pp., 1991.

[18] Wheeler, H. A., "Transmission-line properties of parallel wide strips by a conformal mapping approximation," IEEE Trans. Microwave Theory Tech., vol. MTT-12, pp. 280-289, 1964.

[19] Wheeler, H. A., "Transmission-line properties of parallel strips separated by a dielectric sheet," IEEE Trans. Microwave Theory Tech., vol. MTT-13, pp. 172-185, 1965.

[20] Yamashita, E., "Variational method for the analysis of microstrip-like transmission lines," IEEE Trans. Microwave Theory Tech., vol. MTT-16, pp. 529-535, 1968.

[21] Owens, R. P., Aitken, J. E., and Edwards, T. C., "Quasi-static characteristics of microstrip on an anisotropic sapphire substrate," IEEE Trans. Microwave Theory Tech., vol. MTT-24, pp. 499-505, 1976.

[22] Denlinger, E. J., "A frequency dependent solution for microstrip transmission line, IEEE Trans. Microwave Theory Tech., vol. MTT-19, pp. 30-39, 1971.

[23] Getsinger, W. J., "Microstrip dispersion model," IEEE Trans. Microwave Theory Tech., vol. MTT-21, pp. 34-39, 1973.

[24] Haddad, G. I., and Krage, M. K., "Frequency-dependent characteristics of microstrip transmission lines," IEEE Trans. Microwave Theory Tech., vol. MTT-20, pp. 678-688, 1972.

[25] Itoh, T., and Mittra, R., "A new technique for the analysis of dispersion characteristics of microstrip lines," IEEE Trans. Microwave Theory Tech., vol. MTT-19, pp. 47-56, 1971.

[26] Itoh, T., and Mittra, R., "Spectral-domain approach for calculating the

dispersion characteristics of microstrip lines," IEEE Trans. Microwave Theory Tech., vol. MTT-21, pp. 496-499, 1973.

[27] Kuester, E. F., and Chang, D. C., "An appraisal of methods for computation of the dispersion characteristics of open microstrip," IEEE Trans. Microwave Theory Tech., vol. MTT-27, pp. 691-694, 1979.

[28] Jansen, R. H., "The spectral domain approach for microwave integrated circuits," IEEE Trans. Microwave Theory Tech., vol. MTT-33, pp. 1043-1056, 1985.

[29] Itoh, T., Planar Transmission Line Structures, IEEE Press, New York, 1987.

[30] Kobayashi, M., and E. Ando, "Dispersion characteristics of open microstrip lines," IEEE Trans. Microwave Theory Tech., vol. MTT-35, pp. 101-105, 1987.

[31] Alexopoulos, N. G., and Nakatani, A., "Toward a generalized algorithm for the modeling of the dispersive properties of integrated circuit structures on anisotropic substrates," IEEE Trans. Microwave Theory Tech., vol. MTT-33, pp. 1436-1441, 1985.

[32] Fache, N., and DeZutter, D., "Rigorous full-wave space-domain solution for dispersive microstrip lines," IEEE Trans. Microwave Theory Tech., vol. MTT-36, pp. 731-737, 1988.

[33] Kobayashi, M., and Iijima, T., "Frequency-dependent characteristics of current distributions on microstrip lines," IEEE Trans. Microwave Theory Tech., vol. MTT-37, pp. 799-801, 1989.

[34] Nyquist, D. P., "Deduction of EM phenomena in microstrip circuits from an integral-operator description of the system," Proc. URSI Triennial EM Theory Symp., pp. 535-537, Stockholm, Sweden, August 1989.

[35] Bianco, B., Panini, L., Parodi, M., and Ridella, S., "Some considerations about the frequency dependence of the characteristic impedance of uniform microstrips," IEEE Trans. Microwave Theory tech., vol. MTT-26, p. 162, 1978.

[36] Knorr, J. B., and Tufekcioglu, A., "Spectral-domain calculation of microstrip characteristic impedance," IEEE Trans. Microwave Theory tech., vol. MTT-23, pp. 725-728, 1975.

[37] Getsinger, W. J., "Measurement and modeling of the apparent characteristic impedance of microstrip," IEEE Trans. Microwave Theory tech., vol. MTT-31, pp. 624-632, 1983.

[38] Getsinger, W. J., "Microstrip characteristic impedance," IEEE Trans. Microwave Theory tech., vol. MTT-27, p. 293, 1979.

[39] Hashimoto, M., "A rigorous solution for dispersive microstrip," IEEE Trans. Microwave Theory tech., vol. MTT-33, pp. 1131-1137, 1985.

[40] Brews, J. R., "Characteristic impedance of microstrip lines," IEEE Trans. Microwave Theory tech., vol. MTT-35, pp. 30-34, 1987.

[41] Fache, N., and De Zutter, D., "Circuit parameters for single and coupled microstrip lines by a rigorous full-wave space-domain analysis," IEEE Trans. Microwave Theory tech., vol. MTT-37, pp. 421-425, 1989.

[42] Tripathi, V. K., and Lee, H., "Spectral-domain computation of characteristic impedances and multiport parameters of multiple coupled microstrip lines," IEEE Trans. Microwave Theory tech., vol. MTT-37, pp. 215-221, 1989.

[43] Livernois, T. G., and Katehi, P. B., "Characteristic impedance and electromagnetic field distribution in metal-insulator-semiconductor microstrip," IEEE Trans. Microwave Theory tech., vol. MTT-38, pp. 1740-1743, 1990.

[44] Fache, N., and De Zutter, D., "New high-frequency circuit model for coupled lossless and lossy waveguide structures," IEEE Trans. Microwave Theory tech., vol. MTT-38, pp. 252-259, 1990.

[45] Cheng, K. K. M., and Everard, J. K. A., "Accurate formulas for efficient calculation of the characteristic impedance of microstrip lines," IEEE Trans. Microwave Theory tech., vol. MTT-39, pp. 1658-1661, 1991.

[46] Slade, G. W., and Webb, K. J., "Computation of characteristic impedance for multiple microstrip transmission lines using a vector finite element method," IEEE Trans. Microwave Theory tech., vol. MTT-40, p. 34, 1992.

[47] Bagby, J. S., and D. P. Nyquist, "Dyadic Green's functions for integrated electronic and optical circuits," 1987, IEEE Trans. Microwave Theory Tech., vol. MTT-35, no. 2, pp. 206-210.

[48] Viola, M. S., and D. P. Nyquist, "An observation on the Sommerfeld-integral representation of the electric dyadic Green's function for layered media," 1988, IEEE Trans. Microwave Theory Tech., vol. MTT-36, no. 8, pp. 1289-1292.

[49] Yaghjian, A. D., "Electric dyadic Green's functions in the source region," 1980, Proc. IEEE, vol. 68, pp. 248-263.

[50] Yuan Yi, "Integral-operator analysis of layered media and integrated microstrip configurations", PHD Thesis, 1991.

[51] Nghiem, D., J. T. William, D. R. Jackson and A. A. Oliner, "Existence of a leaky dominant mode on microstrip line with an isotropic substrate: theory and measurement", 1993, IEEE MTT-S Digest, vol. 3, pp. 1291-1294.

[52] Tsuji, M., H. Shigesawa and A. A. Oliner, "Simultaneous propagation of both bound and leaky dominant modes on conductor-backed coplanar strips", 1993, IEEE MTT-S Digest, vol. 3, pp. 1295-1298.

[53] Hanson, G. W., J. M., Grimm and D. P., Nyquist, "An improved de-embedding technique for the measurement of the complex constitutive parameters of materials using a stripline field applicator," 1993, IEEE Trans. Instrumentation and measurement, vol. 42, pp. 740-745.

[54] Nicolson, A. M. and G. F. Ross, "Measurement of the intrinsic properties of materials by time-domain techniques," 1970, IEEE Trans. Instrumentation and measurement, vol. 19, pp. 377-382.

[55] Weir, W. B., "Automatic measurement of complex dielectric constant and permeability at microwave frequencies," 1974, Proc. IEEE, vol. 62, pp. 33-36.